

FINAL REPORT

AQRP Project 17 - 024 Improving the Modeling of Wildfire Impacts on Ozone and Particulate Matter for Texas Air Quality Planning

Revision 2.0

QA Requirements: Audits of Data Quality: 10% Required

Prepared by:
Chantelle Lonsdale, Chris Brodowski, and Matthew Alvarado
Atmospheric and Environmental Research, Inc. (AER)
131 Hartwell Ave.
Lexington, MA 02421
Correspondence to: malvarad@aer.com

Prepared for:
Texas Air Quality Research Program (AQRP)
The University of Texas at Austin
August 31, 2017

Document Change Record

Revision	Revision Date	Remarks
0.1	31 July 2017	Internal Version for Review
1.0	1 August 2017	Draft Submitted to TCEQ
1.1	27 August 2017	Revised Internal Draft
2.0	31 August 2017	Final Draft Submitted to TCEQ

Acknowledgements

The preparation of this report is based on work supported by the State of Texas through the Air Quality Research Program administered by The University of Texas at Austin by means of a Grant from the Texas Commission on Environmental Quality.

Executive Summary

Fires can have a large impact on ozone and particulate matter concentrations, and thus air quality, in Texas. Three-dimensional Eulerian models like CAMx take estimates of the primary emissions from biomass burning and unphysically “mix” them across large-scale grid boxes, leading to inaccurate chemical modeling and incorrect estimates of the impact of biomass burning on air quality. Plume-scale process models like AER’s Aerosol Simulation Program (ASP, Alvarado et al., 2015) allow us to examine the chemical and physical transformations of trace gases and aerosols within biomass burning plumes and to develop parameterizations for this aging process in coarser grid-scale models. Thus the first objective of this project was to improve our understanding of the impacts of local and out-of-state fires on air quality in Texas by implementing an improved ASP-based sub-grid scale parameterization of the formation of ozone and secondary organic aerosols in biomass burning plumes, derived from model runs of ASP coupled with the large-eddy simulation System for Atmospheric Modeling (SAM), into CAMx via the plume-in-grid (PiG) module. Our second objective was to use the Lagrangian trajectory-based modeling tool STILT-ASP to investigate the impact that long-range transport of wildfire smoke has on air quality in Texas. This project thus addressed two strategic topics of the AQRP program: “Improving the understanding of ozone and particulate matter (PM) formation [and] the interactions of ozone and PM precursors” and “Investigating global, international, and regional transport of pollutants using data and modeling analyses.”

We coupled the SAM and ASP models and made several improvements to the coupled SAM-ASP model in this project. For example, we reduced the number of model boxes that were used in the chemistry calculations in order to reduce the model run time without impacting the accuracy of the plume simulation, as this was necessary to allow us to do the 400 runs required to train the new parameterization. We also updated SAM-ASP to calculate the initial concentrations based on the mass emissions flux of the fire and emission factors for biomass burning species, rather than requiring the initial concentrations to be calculated outside of the model. This will allow SAM-ASP to better represent a wide range of fire sizes and intensities.

We evaluated the coupled SAM-ASP model by comparing the model results with measurements of the Williams Fire (Akagi et al., 2012) that was previously studied using the box model versions of ASP by Alvarado et al. (2015). Figure 1 shows the SAM-ASP calculated O₃ concentrations for the plume. The revised SAM-ASP model is able to correctly simulate the dilution of CO in the Williams Fire smoke plume, as well as the chemical loss of NO_x, HONO, and NH₃ and formation of PAN within the plume. The formation of O₃ in the model is underestimated (model value of $\Delta\text{O}_3/\Delta\text{CO}$ of 0.05 mol/mol at 4.5 hr downwind, rather than the measured value of 0.10 mol/mol). Thus we conclude that SAM-ASP does a reasonable job of simulating CO, HONO, PAN, and NO_x within biomass burning plumes, but currently underestimates the formation of O₃.

We then ran the coupled SAM-ASP model for 100 simulations (using Latin hypercube sampling) per fire fuel type (Savannah, Tropical Forest, Temperate Forest, and Boreal Forest) and developed a Gaussian Emulator Machine (GEM) to predict the normalized mean enhancement ratio (NMER, Akagi et al., 2011) of O₃, NO_x, PAN, and other species in terms of the fuel type, temperature, latitude, day of year, and starting hour of emission. We built separate GEM parameterizations for each fuel type as our initial test of the parameterization showed that including the different fuel types in a single GEM led to unrealistic results for O₃.

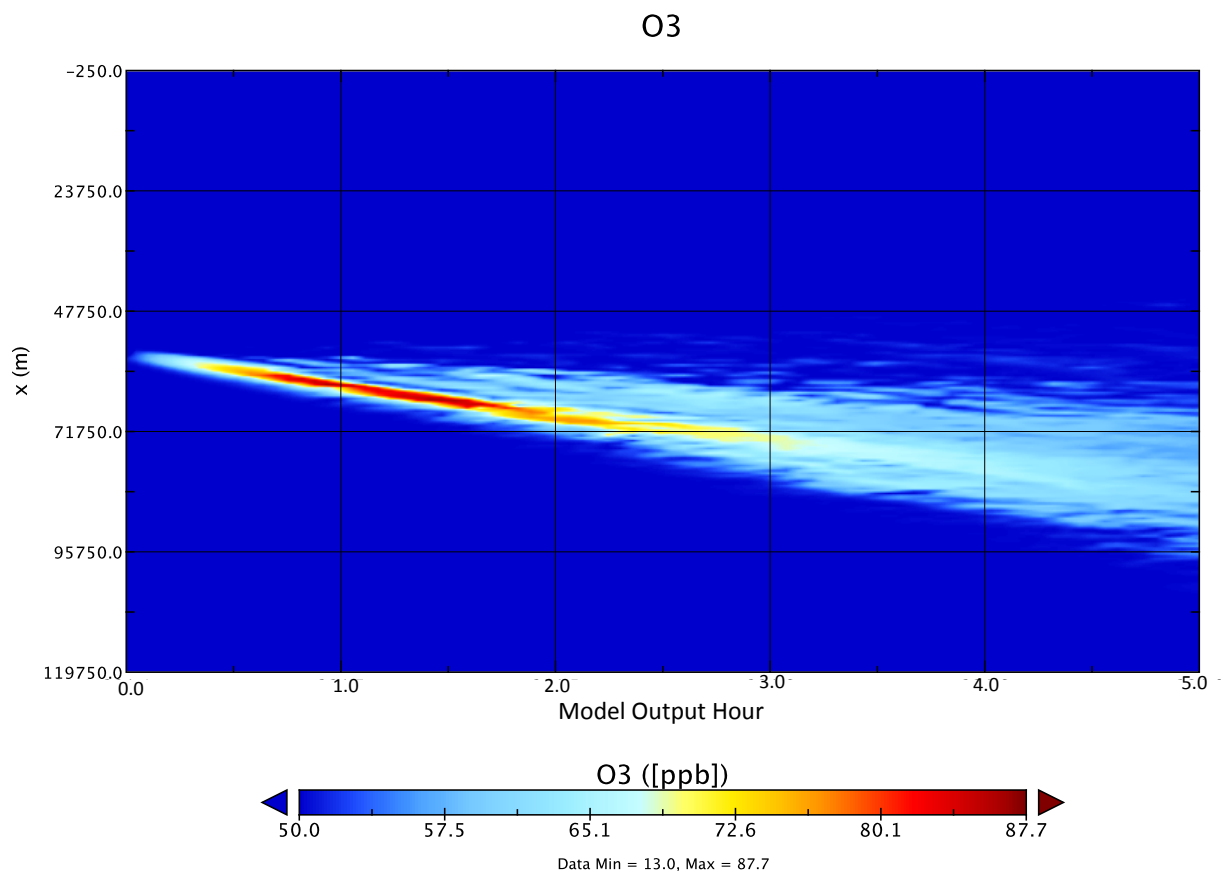


Figure 1. SAM-ASP simulated O₃ concentrations for the Williams Fire (Akagi et al., 2012) at 1.22 km altitude. The y axis is the horizontal dimension of the SAM-ASP Lagrangian wall.

However, our evaluation of the GEM parameterization showed that our current GEM training approach does not result in a parameterization of sufficient quality for use in regional air quality modeling. The GEM parameterization is able to represent the dependence of O₃ formation in the plume on fuel type, temperature, day of year, and latitude reasonably well, but the dependence on time of day is unrealistic, as the GEM prediction for the O₃ enhancement ratio ($\Delta\text{O}_3/\Delta\text{CO}$) is negative for plumes emitted at 14:00 local time in the summer, when these plumes should be forming O₃ up to the end of the simulation at 19:00 (7 PM) local time in the summer. Comparisons of the parameterization to the observations from the Williams Fire show that the GEM parameterization underestimates the measured $\Delta\text{O}_3/\Delta\text{CO}$ for these conditions (GEM value of 0.04 mol/mol, as opposed to measurements of 0.10 mol/mol), similar to the results of a custom SAM-ASP simulation for these conditions (0.05 mol/mol). The GEM predictions for NO_x and other NO_y species have more serious deficiencies, with the GEM parameterization overestimating the NO_x downwind in the Williams Fire, and GEM predictions of the formation of PAN and HNO₃ being inconsistent with the GEM predictions of the loss rate of NO_x. Further

work on the GEM parameterization training would be needed to identify the source of these errors and correct them.

Thus, rather than implement the GEM parameterization into CAMx, we instead implemented the parameterization of Lonsdale et al. (2015) into CAMx. This parameterization modifies the emissions of O₃, NO_y species, ethylene, and formaldehyde from fires based on a look-up-table (LUT) that is built from many runs of the ASP model within a simple Lagrangian parcel dispersion model. We added code to CAMx to read the FINN fire emission files directly and use them to initialize a biomass-burning-specific Plume-in-Grid (PiG) module. The downwind concentrations of O₃, NO_x, PAN, and other species transferred from the individual PiG puffs to the grid are determined by the parameterization based on the rate of CO transfer as well as fire and environmental conditions.

We used the modeling configuration from the 2012 CAMx modeling episode from TCEQ (May 16 – June 30, 2012) to evaluate the impact of the parameterization, as this episode and modeling configuration was used in the previous study of McDonald-Buller et al. (2015). The parameterization reduced the predicted impacts of fires on O₃ near the sources by ~30%, as expected.

For Task 2, we examined the 36-km CAMx boundary condition files (derived from the GEOS-Chem model) of the 2012 base case TCEQ modeling episode for potential episodes of biomass burning influence. Regions with CO concentration ≥ 120 ppbv along the southern boundary in May and June, which are sensitive to fires in Mexico and Central America, were simulated with STILT-ASP v2.0. The STILT-ASP v2.0 simulations show a lot of fine structure in the impacts of fires on CO along the boundaries that is not captured by the low-resolution boundary conditions from GEOS-Chem. In addition, the STILT-ASP v2.0 estimate of the $\Delta\text{O}_3/\Delta\text{CO}$ ratio during these events (mean of 0.15 mol/mol) is consistent with the review of Jaffe and Wigder (2012). However, the STILT-ASP v2.0 prediction of O₃ was high relative to GEOS-Chem (Figure 2), which appears to be due to an error in the simulation of the diurnal cycle of O₃ in STILT-ASP v2.0, especially at night. Predictions of NO_x and PAN were both much lower than the GEOS-Chem values, and this appears to be due to the chemistry of S/IVOCs used in ASP v2.1, which were derived from measurements of a biomass burning plume for the first 0-5 hours of aging (Alvarado et al., 2015). Thus the S/IVOC chemical mechanism of ASP v2.1 may need to be re-examined for the longer one to seven day runs of STILT-ASP v2.0.

We used STILT-ASP v2.0 to examine the impact of fires on CO, O₃, NO_x, and PM_{2.5} during three days where the Austin/Round Rock urban area was impacted by fires from Central Mexico and the Yucatan. On the day with the highest MDA8 O₃ (May 11), the model predictions of O₃, CO, and NO_x were all consistent with the observations, with O₃ slightly overestimated (MB of +3.6 ppbv, RMSE of 5.9 ppbv) and NO_x slightly overestimated (MB of +0.3 ppbv, RMSE of 1.9 ppbv). However, due to the loss of NO_x during S/IVOC chemistry as discussed above, the impact of fire emissions on O₃ was a decrease of 0.9 ppbv of the MDA8 O₃. PM_{2.5} was substantially overestimated, likely due to an underestimation of PM_{2.5} deposition. However, deposition should affect all aerosol sources relatively evenly, so the STILT-ASP v2.0 results can be used to estimate the relative fraction of PM_{2.5} at the receptor that is due to fires, which for this day was 12% (0.9 $\mu\text{g}/\text{m}^3$) averaged over the MDA8 period.

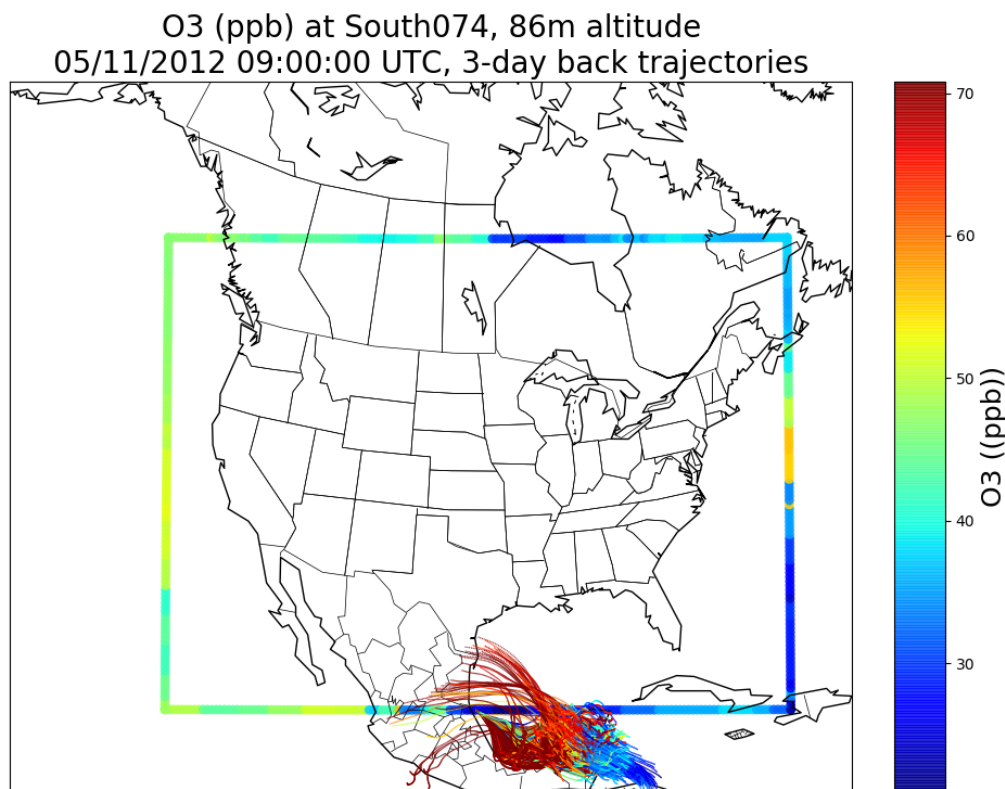


Figure 2. O₃ (ppbv) from a 3-day back trajectory run of STILT-ASP v2.0 for May 11, 2012 at 09:00 UTC (03:00 CST) fire-influenced box of the southern boundary of the CAMx modeling domain. The GEOS-Chem boundary conditions are also shown.

The results for the May 5 and May 25 Austin cases were very different, with STILT-ASP v2.0 strongly overestimating O₃ (MB = +40 ppbv) and underestimating NO_x (MB = -2.6 ppbv) on these days, with less severe overestimates of PM_{2.5}. The model suggests that fires had small but positive impacts on MDA8 O₃ on these days (0.2 and 0.3 ppbv, respectively), but noticeable impacts on the 8-hour average PM_{2.5} (2.6 and 4.0 $\mu\text{g}/\text{m}^3$, respectively).

In order to compare the STILT-ASP v2.0 predictions of the impacts of wildfires on O₃ and PM_{2.5} with the CAMx simulations of McDonald-Buller et al. (2015), we ran STILT-ASP for the CAMS 12 site in El Paso on two dates (June 4 and June 28) that were shown to have significant fire impacts on O₃ in McDonald-Buller et al. (2015). However, the STILT-ASP v2.0 estimates of the impacts of fires on CO were small (2-3 ppbv), likely due to the use of the FINN v1.5 emissions rather than the FINN v2.1 emissions used by McDonald-Buller et al. (2015). Furthermore, the STILT-ASP v2.0 estimate of the impact of fires on MDA8 O₃ on these days is small and negative (-0.1 to -0.4 ppbv), unlike the small but positive impacts predicted by CAMx with the biomass burning parameterization (2.1 and 1.2 ppbv), but this may be due to errors in the S/IVOC chemistry as discussed above.

We recommend that future work on assessing the impact of wildfires on air quality in Texas focus on: (a) the continued development of SAM-ASP using data from the upcoming NOAA FIREX campaign and other field campaigns; (b) exploring novel parameterization approaches, including further refinement of the implementation of the Lonsdale et al. (2015) parameterization within CAMx and exploring ways of revising the GEM training approach to enforce the conservation of NO_y species and improve the performance for periodic variables; and (c) the continued development of STILT-ASP, including the revision of the chemical mechanism of ASP v2.1 to better represent the long-term (1-7 day) chemistry of S/IVOCs and their impacts on NO_x and adjusting the deposition rate of aerosols within STILT-ASP v2.0 to better reflect ambient observations.

TABLE OF CONTENTS

Executive Summary	4
1 Introduction	17
1.1 Background	17
1.2 Project Objectives.....	17
1.3 Models Used in the Project.....	18
1.3.1 ASP.....	18
1.3.2 ASP-Based Sub-Grid Scale Biomass Burning Parameterization.....	20
1.3.3 SAM-ASP 2D Lagrangian Model	21
1.3.4 STILT-ASP Lagrangian Particle Chemical Transport Model.....	22
1.4 Report Outline	23
2 Toward an Improved Sub-grid Scale Parameterization of Biomass Burning ..	25
2.1 SAM-ASP Configuration	25
2.2 SAM-ASP Evaluation.....	26
2.3 Gaussian Emulation Machine (GEM) Development.....	30
2.4 GEM Parameterization Evaluation	32
2.4.1 Ozone	32
2.4.2 NO _y Species.....	36
2.5 Implementation of the Parameterization into CAMx	37
2.6 Evaluation of the Impact of Fires on O₃.....	39
3 Impact of Long-range Transport of BB Pollution on Texas Air Quality.....	43
3.1 Identifying Biomass Burning Impacts on the CAMx Boundaries.....	43
3.2 Examining CAMx Boundary Conditions with STILT-ASP.....	48
3.2.1 Impact of Fires on CO.....	48
3.2.2 Impact of Fires on O ₃ , NO _x , and PAN.....	48
3.3 Assessing Impact of Remote (out-of-domain) Fires on Texas Air Quality.....	61
3.3.1 May 11, 2012	61
3.3.1 May 5, 2012.....	66
3.3.2 May 25, 2012	69
3.4 Assessing the Impact of Close (in-domain) Fires on Texas Air Quality.....	72
3.4.1 June 4, 2012	72
3.4.2 June 28, 2012.....	75
4 Audits of Data Quality and Reconciliation with User Requirements	78
4.1 SAM-ASP and Parameterization Development.....	78
4.2 STILT-ASP Examination of the Impacts of Long-Range BB Transport.....	80
5 Conclusions.....	83
6 Recommendations for Further Study	85
7 References.....	86

List of Figures

FIGURE 1. SAM-ASP SIMULATED O ₃ CONCENTRATIONS FOR THE WILLIAMS FIRE (AKAGI ET AL., 2012) AT 1.22 KM ALTITUDE. THE Y AXIS IS THE HORIZONTAL DIMENSION OF THE SAM-ASP LAGRANGIAN WALL.....	5
FIGURE 2. O ₃ (PPBV) FROM A 3-DAY BACK TRAJECTORY RUN OF STILT-ASP v2.0 FOR MAY 11, 2012 AT 09:00 UTC (03:00 CST) FIRE-INFLUENCED BOX OF THE SOUTHERN BOUNDARY OF THE CAMx MODELING DOMAIN. THE GEOS-CHEM BOUNDARY CONDITIONS ARE ALSO SHOWN.	7
FIGURE 3. O ₃ (LEFT) AND PAN (RIGHT) MIXING RATIOS WITHIN THE WILLIAMS FIRE AS OBSERVED BY AKAGI ET AL. (2012) AND SIMULATED BY ASP. ASTERISKS ARE THE MEASURED MIXING RATIOS, WITH THE HORIZONTAL ERROR BARS SHOWING THE UNCERTAINTY IN THE ESTIMATED AGE AND THE VERTICAL ERROR BARS SHOWING THE UNCERTAINTY IN THE MEASUREMENT. RED, BLACK, AND GREEN ARE ASP RESULTS FOR THE SLOW, BEST-FIT (MEDIUM), AND FAST PLUME DILUTION RATES WITHIN A LAGRANGIAN PARCEL DISPERSION MODEL. DASHED LINES ARE FOR ABOVE-PLUME PHOTOLYSIS RATES, WHILE SOLID LINES ARE FOR THE MIDDLE OF THE PLUME, AND DOTTED LINES ARE FOR THE BOTTOM OF THE PLUME. REPRODUCED FROM ALVARADO ET AL. (2015).	18
FIGURE 4. ENHANCEMENT RATIO (G/G) OF ORGANIC AEROSOL (OA) TO CO ₂ VERSUS SMOKE AGE FOR THE WILLIAMS FIRE. THE RED CIRCLES ARE THE OBSERVED VALUES FROM AKAGI ET AL. (2012). BASED ON THE RESULTS OF ALVARADO ET AL. (2015).....	19
FIGURE 5. PARTITIONING OF NO _x SPECIES VERSUS TIME FOR SAVANNAH/GRASSLAND FIRES (LEFT) AND BOREAL FOREST FIRES (RIGHT). RESULTS ARE FOR A TEMPERATURE OF 285K, AN OVERHEAD O ₃ COLUMN OF 300 DU, A STARTING SZA OF 0° AND AN ENDING SZA OF 75°.....	20
FIGURE 6. SCHEMATIC SHOWING PHYSICAL STRUCTURE OF SAM-TOMAS MODEL. THE SAM-ASP MODEL WILL BE SIMILAR BUT WILL INCLUDE GAS- AND AEROSOL-PHASE CHEMISTRY RELEVANT TO OA CONDENSATION/EVAPORATION, BRC PRODUCTION AND LOSS, AND MIXING STATE CHANGES. REPRODUCED FROM SAKAMOTO ET AL. (2016).	21
FIGURE 7. OZONE MIXING RATIOS (PPB) ALONG THE 500 SEVEN-DAY STILT-ASP BACK-TRAJECTORIES CALCULATED TO FOR A SURFACE MONITOR IN SALT LAKE CITY.....	23
FIGURE 8. SAM-ASP SIMULATED CO CONCENTRATIONS FOR THE WILLIAMS FIRE (AKAGI ET AL., 2012) AT 1.22 KM ALTITUDE. THE Y AXIS IS THE HORIZONTAL DIMENSION OF THE SAM-ASP LAGRANGIAN WALL.....	27
FIGURE 9. AS IN FIGURE 8, BUT FOR O ₃	28
FIGURE 10. AS IN FIGURE 8, BUT FOR NO _x (NOTE THE LOG SCALE).....	29
FIGURE 11. SAM-ASP SIMULATION OF Δ CO, Δ O ₃ / Δ CO, Δ NO _x / Δ CO, Δ PAN/ Δ CO, Δ HONO/ Δ CO AND Δ NH ₃ / Δ CO FOR THE WILLIAMS FIRE (BLACK LINE) VERSUS OBSERVATIONS (BLUE DOTS).....	30
FIGURE 12. GEM CALCULATION OF THE MEAN O ₃ ENHANCEMENT RATIO (Δ O ₃ / Δ CO, MOL/MOL) FOR THE FULL RANGE OF LATITUDES AND DAYS OF THE YEAR, FIXED AT A TEMPERATURE OF 285 K, AND A MODEL START TIME OF 12:00 PM. THE LEFT COLUMN SHOWS ESTIMATES FROM 2 HOURS DOWNWIND, AND THE RIGHT COLUMN SHOWS ESTIMATES FROM 5 HOURS DOWNWIND OF THE SOURCE.	34
FIGURE 13. GEM CALCULATION OF THE MEAN O ₃ ENHANCEMENT RATIO (Δ O ₃ / Δ CO, MOL/MOL) FOR THE FULL RANGE OF TEMPERATURES (K) AND HOURS OF THE DAY, FIXED AT A LATITUDE OF 45° N, FOR THE SUMMER (TOP PLOT) AND WINTER (BOTTOM PLOT) SOLSTICES AT 3 HOURS DOWNWIND.	35
FIGURE 14. GEM CALCULATION OF THE MEAN O ₃ ENHANCEMENT RATIO (Δ O ₃ / Δ CO, MOL/MOL) FOR THE FULL RANGE OF LATITUDES AND DAYS OF THE YEAR, FIXED AT A TEMPERATURE OF 292 K, AND A MODEL START TIME OF 10:00 AM. THE STAR INDICATES THE APPROXIMATE CONDITIONS THAT MATCH THE WILLIAMS FIRE DESCRIBED IN ALVARADO ET AL., 2015.	36
FIGURE 15. GEM CALCULATION OF THE MEAN NO _x , PAN, HNO ₃ AND HONO ENHANCEMENT RATIO (PPB/PPB) FOR THE FULL RANGE OF LATITUDES AND DAYS OF THE YEAR, FIXED AT A TEMPERATURE OF 292 K, AND A MODEL START TIME OF 10:00 AM. THE STAR INDICATES THE APPROXIMATE CONDITIONS THAT MATCH THE WILLIAMS FIRE DESCRIBED IN ALVARADO ET AL. (2015).	37
FIGURE 16. DIFFERENCE IN O ₃ (PPBV) BETWEEN THE SUB-GRID PARAMETERIZED FIRE CASE AND THE “NO FIRE” CASE AT 17:00 CST ON JUNE 4, 2012.	40
FIGURE 17. DIFFERENCE IN O ₃ (PPBV) BETWEEN THE SUB-GRID PARAMETERIZED FIRE CASE AND THE “GRID FIRE” CASE AT 17:00 CST ON JUNE 4, 2012.	41
FIGURE 18. DIFFERENCE IN O ₃ (PPBV) BETWEEN THE SUB-GRID PARAMETERIZED FIRE CASE AND THE “NO FIRE” CASE AT 17:00 CST ON JUNE 28, 2012.	41

FIGURE 19. DIFFERENCE IN O ₃ (PPBV) BETWEEN THE SUB-GRID PARAMETERIZED FIRE CASE AND THE “GRID FIRE” CASE AT 17:00 CST ON JUNE 28, 2012.	42
FIGURE 20. NUMBER OF 3-HOUR OBSERVATIONS EXCEEDING 120 PPBV CO FOR EACH EDGE OF THE 36-KM GEOS-CHEM BOUNDARY GRID FOR MAY 2012.	44
FIGURE 21. NUMBER OF 3-HOUR OBSERVATIONS EXCEEDING 120 PPBV CO FOR EACH EDGE OF THE 36-KM GEOS-CHEM BOUNDARY GRID FOR JUNE 2012.	45
FIGURE 22. CO ALONG TWO 2-DAY STILT-ASP BACK-TRAJECTORY CALCULATIONS (500 LAGRANGIAN PARCELS EACH) OVERPLOTTED ON THE GEOS-CHEM BOUNDARY CONDITIONS FOR MAY 11, 2012 AT 09:00 UTC.	46
FIGURE 23. STILT 7-DAY BACK TRAJECTORY RUN (500 PARCELS) FOR MAY 5, 2012 FOR THE AUSTIN, TX SITE. NOTE THE SOUTHERLY FLOW, INDICATING THE POSSIBILITY THAT WILDFIRES IN MEXICO MAY IMPACT THE AUSTIN SITE.	47
FIGURE 24. (TOP PANEL) SIMULATED CO MIXING RATIOS (PPBV) FROM STILT-ASP v2.0 NO-CHEMISTRY 7-DAY BACK-TRAJECTORY RUN RESULTS WITH (RED LINE) AND WITHOUT (BLACK LINE) FINN FIRE EMISSIONS FOR MAY 11, 2012 AT 09:00 UTC (03:00 CST) AT 86 M ABOVE GROUND LEVEL ALONG THE SOUTHERN BOUNDARY OF THE CAMx 36 KM DOMAIN. THE BLUE LINE SHOWS THE GEOS-CHEM BOUNDARY CONDITION RESULTS. (BOTTOM PANEL) DIFFERENCE BETWEEN THE WITH-FIRE AND WITHOUT-FIRE EMISSIONS STILT-ASP SIMULATIONS.	50
FIGURE 25. AS IN FIGURE 20, BUT FOR MAY 24, 2012 AT 18:00 UTC (12:00 CST) AT 86 M ABOVE GROUND LEVEL.	51
FIGURE 26. AS IN FIGURE 20, BUT FOR JUNE 1, 2012 AT 18:00 UTC (12:00 CST) AT 86 M ABOVE GROUND LEVEL.	52
FIGURE 27. AS IN FIGURE 20, BUT FOR JUNE 2, 2012 AT 12:00 UTC (06:00 CST) AT 86 M ABOVE GROUND LEVEL.	53
FIGURE 28. STILT-ASP v2.0 CALCULATIONS OF O ₃ (PPBV) ALONG THE SOUTHERN CAMx DOMAIN BOUNDARY WITH FIRE EMISSIONS (ORANGE) AND WITHOUT FIRE EMISSIONS (GREY) FOR 09:00 UTC (03:00 CST) ON MAY 11, 2012 COMPARED WITH THE GEOS-CHEM DERIVED BOUNDARY CONDITION VALUES (GREEN).	54
FIGURE 29. STILT-ASP v2.0 CALCULATIONS OF CO (PPBV) ALONG THE SOUTHERN CAMx DOMAIN BOUNDARY WITH FIRE EMISSIONS (ORANGE) AND WITHOUT FIRE EMISSIONS (GREY) FOR 09:00 UTC (03:00 CST) ON MAY 11, 2012 COMPARED WITH THE GEOS-CHEM DERIVED BOUNDARY CONDITION VALUES (GREEN).	54
FIGURE 30. STILT-ASP v2.0 CALCULATIONS OF ΔO ₃ /ΔCO (MOL/MOL) ALONG THE SOUTHERN CAMx DOMAIN BOUNDARY FOR 09:00 UTC (03:00 CST) ON MAY 11, 2012.	55
FIGURE 31. STILT-ASP v2.0 CALCULATIONS OF O ₃ (PPBV) ALONG THE SOUTHERN CAMx DOMAIN BOUNDARY WITH FIRE EMISSIONS (ORANGE) AND WITHOUT FIRE EMISSIONS (GREY) FOR 09:00 UTC (03:00 CST) ON MAY 11, 2012 COMPARED WITH THE GEOS-CHEM DERIVED BOUNDARY CONDITION VALUES (GREEN).	55
FIGURE 32. STILT-ASP v2.0 CALCULATIONS OF PAN (PPBV) ALONG THE SOUTHERN CAMx DOMAIN BOUNDARY WITH FIRE EMISSIONS (ORANGE) AND WITHOUT FIRE EMISSIONS (GREY) FOR 09:00 UTC (03:00 CST) ON MAY 11, 2012 COMPARED WITH THE GEOS-CHEM DERIVED BOUNDARY CONDITION VALUES (GREEN).	56
FIGURE 33. CO (PPBV) FROM A 3-DAY BACK TRAJECTORY RUN OF STILT-ASP v2.0 FOR MAY 11, 2012 AT 09:00 UTC (03:00 CST) FOR THE 74 GRID BOX OF THE SOUTHERN BOUNDARY OF THE CAMx MODELING DOMAIN. THE GEOS-CHEM BOUNDARY CONDITIONS ARE ALSO SHOWN.	57
FIGURE 34. NO _x (PPBV) FROM A 3-DAY BACK TRAJECTORY RUN OF STILT-ASP v2.0 FOR MAY 11, 2012 AT 09:00 UTC (03:00 CST) FOR THE 74 GRID BOX OF THE SOUTHERN BOUNDARY OF THE CAMx MODELING DOMAIN. THE GEOS-CHEM BOUNDARY CONDITIONS ARE ALSO SHOWN.	57
FIGURE 35. PAN (PPBV) FROM A 3-DAY BACK TRAJECTORY RUN OF STILT-ASP v2.0 FOR MAY 11, 2012 AT 09:00 UTC (03:00 CST) FOR THE 74 GRID BOX OF THE SOUTHERN BOUNDARY OF THE CAMx MODELING DOMAIN. THE GEOS-CHEM BOUNDARY CONDITIONS ARE ALSO SHOWN.	58
FIGURE 36. O ₃ (PPBV) FROM A 3-DAY BACK TRAJECTORY RUN OF STILT-ASP v2.0 FOR MAY 11, 2012 AT 09:00 UTC (03:00 CST) FOR THE 74 GRID BOX OF THE SOUTHERN BOUNDARY OF THE CAMx MODELING DOMAIN. THE GEOS-CHEM BOUNDARY CONDITIONS ARE ALSO SHOWN.	58
FIGURE 37. STILT-ASP v2.0 CALCULATIONS OF O ₃ (PPBV) ALONG THE SOUTHERN CAMx DOMAIN BOUNDARY WITH FIRE EMISSIONS (ORANGE) AND WITHOUT FIRE EMISSIONS (GREY) FOR 18:00 UTC (12:00 CST) ON MAY 24, 2012 COMPARED WITH THE GEOS-CHEM DERIVED BOUNDARY CONDITION VALUES (GREEN).	59
FIGURE 38. STILT-ASP v2.0 CALCULATIONS OF CO (PPBV) ALONG THE SOUTHERN CAMx DOMAIN BOUNDARY WITH FIRE EMISSIONS (ORANGE) AND WITHOUT FIRE EMISSIONS (GREY) FOR 18:00 UTC (12:00 CST) ON MAY 24, 2012 COMPARED WITH THE GEOS-CHEM DERIVED BOUNDARY CONDITION VALUES (GREEN).	59
FIGURE 39. STILT-ASP v2.0 CALCULATIONS OF O ₃ (PPBV) ALONG THE SOUTHERN CAMx DOMAIN BOUNDARY WITH FIRE EMISSIONS (ORANGE) AND WITHOUT FIRE EMISSIONS (GREY) FOR 18:00 UTC (12:00 CST) ON MAY 24, 2012 COMPARED WITH THE GEOS-CHEM DERIVED BOUNDARY CONDITION VALUES (GREEN).	60

FIGURE 40. STILT-ASP v2.0 CALCULATIONS OF PAN (PPBV) ALONG THE SOUTHERN CAMx DOMAIN BOUNDARY WITH FIRE EMISSIONS (ORANGE) AND WITHOUT FIRE EMISSIONS (GREY) FOR 18:00 UTC (12:00 CST) ON MAY 24, 2012 COMPARED WITH THE GEOS-CHEM DERIVED BOUNDARY CONDITION VALUES (GREEN).....	60
FIGURE 41. STILT-ASP v2.0 ESTIMATES OF CO (PPBV) AT THE AUSTIN/ROUND ROCK CAMS 3 SITE WITH FIRE EMISSIONS (ORANGE) AND WITHOUT FIRE EMISSIONS (GREY) FOR 11:00-18:00 CST ON MAY 11, 2012. NOTE THAT THE CAMS 3 SITE MEASURED 100 ± 100 PPBV CO DURING THIS PERIOD.....	62
FIGURE 42. CO (PPBV) FROM A 7-DAY BACK TRAJECTORY RUN OF STILT-ASP v2.0 FOR MAY 11, 2012 AT 17:00 UTC (11:00 CST) FOR CAMS3 SITE AT AUSTIN/ROUND ROCK. THE GEOS-CHEM BOUNDARY CONDITIONS ARE ALSO SHOWN.....	63
FIGURE 43. STILT-ASP v2.0 ESTIMATES OF O ₃ (PPBV) AT THE AUSTIN/ROUND ROCK CAMS 3 SITE WITH FIRE EMISSIONS (ORANGE) AND WITHOUT FIRE EMISSIONS (GREY) FOR 11:00-18:00 CST ON MAY 11, 2012 COMPARED WITH OBSERVATIONS (BLUE).....	64
FIGURE 44. STILT-ASP v2.0 ESTIMATES OF NO _x (PPBV) AT THE AUSTIN/ROUND ROCK CAMS 3 SITE WITH FIRE EMISSIONS (ORANGE) AND WITHOUT FIRE EMISSIONS (GREY) FOR 11:00-18:00 CST ON MAY 11, 2012 COMPARED WITH OBSERVATIONS (BLUE).....	64
FIGURE 45. STILT-ASP v2.0 ESTIMATES OF PM _{2.5} (MG/M ³) AT THE AUSTIN/ROUND ROCK CAMS 3 SITE WITH FIRE EMISSIONS (ORANGE) AND WITHOUT FIRE EMISSIONS (GREY) FOR 11:00-18:00 CST ON MAY 11, 2012 COMPARED WITH OBSERVATIONS (BLUE).....	65
FIGURE 46. STILT-ASP v2.0 ESTIMATES OF CO (PPBV) AT THE AUSTIN/ROUND ROCK CAMS 3 SITE WITH FIRE EMISSIONS (ORANGE) AND WITHOUT FIRE EMISSIONS (GREY) FOR 11:00-18:00 CST ON MAY 5, 2012. NOTE THAT THE CAMS 3 SITE MEASURED 100 ± 100 PPBV CO DURING THIS PERIOD.....	66
FIGURE 47. STILT-ASP v2.0 ESTIMATES OF O ₃ (PPBV) AT THE AUSTIN/ROUND ROCK CAMS 3 SITE WITH FIRE EMISSIONS (ORANGE) AND WITHOUT FIRE EMISSIONS (GREY) FOR 11:00-18:00 CST ON MAY 5, 2012 COMPARED WITH OBSERVATIONS (BLUE).....	67
FIGURE 48. STILT-ASP v2.0 ESTIMATES OF NO _x (PPBV) AT THE AUSTIN/ROUND ROCK CAMS 3 SITE WITH FIRE EMISSIONS (ORANGE) AND WITHOUT FIRE EMISSIONS (GREY) FOR 11:00-18:00 CST ON MAY 5, 2012 COMPARED WITH OBSERVATIONS (BLUE).....	67
FIGURE 49. STILT-ASP v2.0 ESTIMATES OF PM _{2.5} (MG/M ³) AT THE AUSTIN/ROUND ROCK CAMS 3 SITE WITH FIRE EMISSIONS (ORANGE) AND WITHOUT FIRE EMISSIONS (GREY) FOR 11:00-18:00 CST ON MAY 5, 2012 COMPARED WITH OBSERVATIONS (BLUE).....	68
FIGURE 50. STILT-ASP v2.0 ESTIMATES OF CO (PPBV) AT THE AUSTIN/ROUND ROCK CAMS 3 SITE WITH FIRE EMISSIONS (ORANGE) AND WITHOUT FIRE EMISSIONS (GREY) FOR 10:00-17:00 CST ON MAY 25, 2012. NOTE THAT THE CAMS 3 SITE MEASURED 100 ± 100 PPBV CO DURING THIS PERIOD.....	69
FIGURE 51. STILT-ASP v2.0 ESTIMATES OF O ₃ (PPBV) AT THE AUSTIN/ROUND ROCK CAMS 3 SITE WITH FIRE EMISSIONS (ORANGE) AND WITHOUT FIRE EMISSIONS (GREY) FOR 10:00-17:00 CST ON MAY 25, 2012 COMPARED WITH OBSERVATIONS (BLUE).....	70
FIGURE 52. STILT-ASP v2.0 ESTIMATES OF NO _x (PPBV) AT THE AUSTIN/ROUND ROCK CAMS 3 SITE WITH FIRE EMISSIONS (ORANGE) AND WITHOUT FIRE EMISSIONS (GREY) FOR 10:00-17:00 CST ON MAY 25, 2012 COMPARED WITH OBSERVATIONS (BLUE).....	70
FIGURE 53. STILT-ASP v2.0 ESTIMATES OF PM _{2.5} (MG/M ³) AT THE AUSTIN/ROUND ROCK CAMS 3 SITE WITH FIRE EMISSIONS (ORANGE) AND WITHOUT FIRE EMISSIONS (GREY) FOR 10:00-17:00 CST ON MAY 25, 2012 COMPARED WITH OBSERVATIONS (BLUE).....	71
FIGURE 54. STILT-ASP v2.0 ESTIMATES OF CO (PPBV) AT THE EL PASO CAMS 12 SITE WITH FIRE EMISSIONS (ORANGE) AND WITHOUT FIRE EMISSIONS (GREY) FOR 11:00-18:00 MST ON JUNE 4, 2012 COMPARED WITH OBSERVATIONS (BLUE).73	
FIGURE 55. STILT-ASP v2.0 ESTIMATES OF O ₃ (PPBV) AT THE EL PASO CAMS 12 SITE WITH FIRE EMISSIONS (ORANGE) AND WITHOUT FIRE EMISSIONS (GREY) FOR 11:00-18:00 MST ON JUNE 4, 2012 COMPARED WITH OBSERVATIONS (BLUE).73	
FIGURE 56. STILT-ASP v2.0 ESTIMATES OF NO _x (PPBV) AT THE EL PASO CAMS 12 SITE WITH FIRE EMISSIONS (ORANGE) AND WITHOUT FIRE EMISSIONS (GREY) FOR 11:00-18:00 MST ON JUNE 4, 2012 COMPARED WITH OBSERVATIONS (BLUE).74	
FIGURE 57. STILT-ASP v2.0 ESTIMATES OF PM _{2.5} (MG M ⁻³) AT THE EL PASO CAMS 12 SITE WITH FIRE EMISSIONS (ORANGE) AND WITHOUT FIRE EMISSIONS (GREY) FOR 11:00-18:00 MST ON JUNE 4, 2012 COMPARED WITH OBSERVATIONS (BLUE).....	74
FIGURE 58. STILT-ASP v2.0 ESTIMATES OF CO (PPBV) AT THE EL PASO CAMS 12 SITE WITH FIRE EMISSIONS (ORANGE) AND WITHOUT FIRE EMISSIONS (GREY) FOR 11:00-18:00 MST ON JUNE 28, 2012 COMPARED WITH OBSERVATIONS (BLUE).	75

FIGURE 59. STILT-ASP v2.0 ESTIMATES OF O₃ (PPBV) AT THE EL PASO CAMS 12 SITE WITH FIRE EMISSIONS (ORANGE) AND WITHOUT FIRE EMISSIONS (GREY) FOR 11:00-18:00 MST ON JUNE 28, 2012 COMPARED WITH OBSERVATIONS (BLUE).
..... 76

FIGURE 60. STILT-ASP v2.0 ESTIMATES OF NO_x (PPBV) AT THE EL PASO CAMS 12 SITE WITH FIRE EMISSIONS (ORANGE) AND WITHOUT FIRE EMISSIONS (GREY) FOR 11:00-18:00 MST ON JUNE 28, 2012 COMPARED WITH OBSERVATIONS (BLUE).
..... 76

FIGURE 61. STILT-ASP v2.0 ESTIMATES OF PM_{2.5} (μg m⁻³) AT THE EL PASO CAMS 12 SITE WITH FIRE EMISSIONS (ORANGE) AND WITHOUT FIRE EMISSIONS (GREY) FOR 11:00-18:00 MST ON JUNE 28, 2012 COMPARED WITH OBSERVATIONS (BLUE).
..... 77

List of Tables

TABLE 1. VALUES USED IN THE SAM-ASP SIMULATIONS OF GEM TRAINING.....31
TABLE 2. SETUP FILES PRODUCED BY THE GEM PROGRAM FOR EACH APPLICATION OF MODEL PARAMETERS.....32

List of Acronyms

AER – Atmospheric and Environmental Research
AQRP – Air Quality Research Program
ASP – Aerosol Simulation Program
BB – Biomass Burning
CAMS – Continuous Ambient Monitoring Station
CAMx – Comprehensive Air quality Model with eXtensions
CMAQ – Community Multiscale Air Quality Model
DISCOVER-AQ – Deriving Information on Surface conditions from Column and Vertically Resolved Observations Relevant to Air Quality
EPA – Environmental Protection Agency
FINN – Fire INventory from NCAR
FIREX – Fire Influence on Regional and Global Environments Experiment
GEM - Gaussian Emulation Machine
GFED – Global Fire Emissions Database
HYSPLIT – Hybrid Single Particle Lagrangian Integrated Trajectory Model
MB – Mean Bias
MDA8 – Maximum Daily 8-hr Average
MEGAN – Model of Emissions of Gases and Aerosols from Nature
MOZART – Model for OZone and Related chemical Tracers
NAAQS – National Ambient Air Quality Standards
NARR – North American Regional Reanalysis
NCAR – National Center for Atmospheric Research
NEMR – Normalized Enhancement Mixing Ratio
NetCDF – Network Common Data Form
NOAA – National Oceanic and Atmospheric Administration
NO_x – Nitrogen Oxides (NO + NO₂)
OA – Organic Aerosol
PAN – PeroxyAcetyl Nitrate
PiG – Plume-in-Grid
PM_{2.5} – Particulate Matter with diameter below 2.5 microns
ppb – parts per billion
QAPP – Quality Assurance Project Plan
RH – Relative Humidity
RMSE – Root-Mean-Square Error

SAM – System for Atmospheric Modeling

S/IVOCs – Semi/Intermediate Volatility Organic Compounds

SOA – Secondary Organic Aerosol

STILT – Stochastic Time-Inverted Lagrangian Transport model

SZA – Solar Zenith Angle

TCEQ – Texas Commission on Environmental Quality

UTC – Coordinated Universal Time

VOC – Volatile Organic Compound

WRF – Weather Research and Forecasting model

1 Introduction

1.1 Background

The goal of this project was to use an advanced smoke plume chemistry model (AER's Aerosol Simulation Program, or ASP, Alvarado et al., 2015) to improve understanding of the formation of O₃ and PM_{2.5} in biomass burning plumes, and improve estimates of the impacts of in-state and out-of-state biomass burning on Texas air quality. Biomass burning (BB) is a major source of trace gases and aerosols that impact air quality. For example, in June 2012 the estimated median contribution of fires to maximum daily 8-hr average (MDA8) O₃ in Texas was 2 ppb, with maximum impacts of over 40 ppb (McDonald-Buller et al., 2015).

3D Eulerian chemical transport models like CAMx make estimates of the primary emissions from BB and unphysically “mix” them across large-scale grid boxes, which can lead to incorrect estimates of the impact of BB on air quality. For example, Baker (2015) found that the 3D Eulerian model CMAQ tended to overestimate the impact of BB on individual hourly ozone measurements at CASTNET monitoring sites near the fires by up to 40 ppb and underestimate it further downwind by up to 20 ppb. This behavior is consistent with an incorrect treatment of the sub-grid scale near-source O₃ and NO_y chemistry, where the model underestimates the loss of NO_x near the source due to formation of inorganic and organic nitrates, thus overestimating O₃ formation near the source (e.g., Alvarado et al., 2010). This same error leads to an underestimate of the amount of peroxy nitrates formed near the source, which then leads to an underestimate of O₃ formation downwind when the peroxy nitrates decompose, regenerating NO_x.

Plume-scale process models like AER's Aerosol Simulation Program (ASP, Section 1.3.1) allow us to examine the chemical and physical transformations of trace gases and aerosols within BB smoke plumes and to develop parameterizations for this aging process in coarser grid-scale models. For example, McDonald-Buller et al. (2015) used a subset of the ASP-based parameterization of Lonsdale et al. (2015) (Section 1.3.2) to adjust the chemistry of biomass burning in CAMx, and found that this approach reduced the median impact of BB on MDA8 O₃ in Texas by 0.3 ppb, or 15%.

1.2 Project Objectives

In this project, we worked to improve understanding of the impacts of local and out of state fires on air quality in Texas by: (a) implementing an improved version of the ASP-based sub-grid scale parameterization of the formation of O₃ and SOA in BB plumes into CAMx via the plume-in-grid (PiG) module (Section 2); and (b) using ASP within the Lagrangian particle dispersion model STILT (Section 1.3.4) to investigate the impact that long-range transport of BB smoke could have on the boundary conditions of the CAMx modeling for Texas, and thus on the simulated air quality (Section 3). We coupled ASP with the large eddy simulation model SAM (Khairoutdinov and Randall, 2003) to attempt to develop an improved parameterization. In order to minimize the computational expense, the PiG module is used to explicitly simulate only the CO emissions from individual fires. The downwind concentrations of O₃, NO_y species, ethylene, and formaldehyde are transferred from the individual plumes to the grid as determined by the parameterization based on fire and environmental conditions. We also used the STILT-ASP model to determine if the impacts of fires on the CAMx boundary conditions for CO, O₃, and NO_y species from GEOS-Chem have significant errors due to numerical diffusion or incorrect treatment of BB chemistry.

The objectives of this project were thus to:

1. Develop and evaluate an improved sub-grid scale parameterization of biomass burning for CAMx based on SAM-ASP.
2. Explore the impact of BB plumes on the boundary conditions used for CAMx and the resulting impact on Texas air quality with STILT-ASP.

1.3 Models Used in the Project

1.3.1 ASP

ASP (Alvarado and Prinn, 2009) simulates the gas-phase, aerosol-phase, and heterogeneous chemistry of young BB smoke plumes, including the formation of O_3 and secondary inorganic and organic aerosol. ASP uses a sectional aerosol size distribution and includes modules to calculate aerosol thermodynamics, gas-to-aerosol mass transfer (condensation/evaporation), coagulation of aerosols, and aerosol optical properties.

ASP has been extensively used to study the chemical and physical transformations of gases and aerosols within BB smoke plumes (e.g., Alvarado and Prinn, 2009; Alvarado et al., 2009, 2010). Recently, Alvarado et al. (2015) evaluated ASP simulations for a fire in California (Williams Fire, Akagi et al., 2012), as shown in Figure 3 and Figure 4. This study showed that ASP (all lines in Figure 3, blue line in Figure 4) could simulate most of the observations (e.g., OA, O_3 , NO_x , OH) using appropriate assumptions about the chemistry of the unidentified organic compounds.

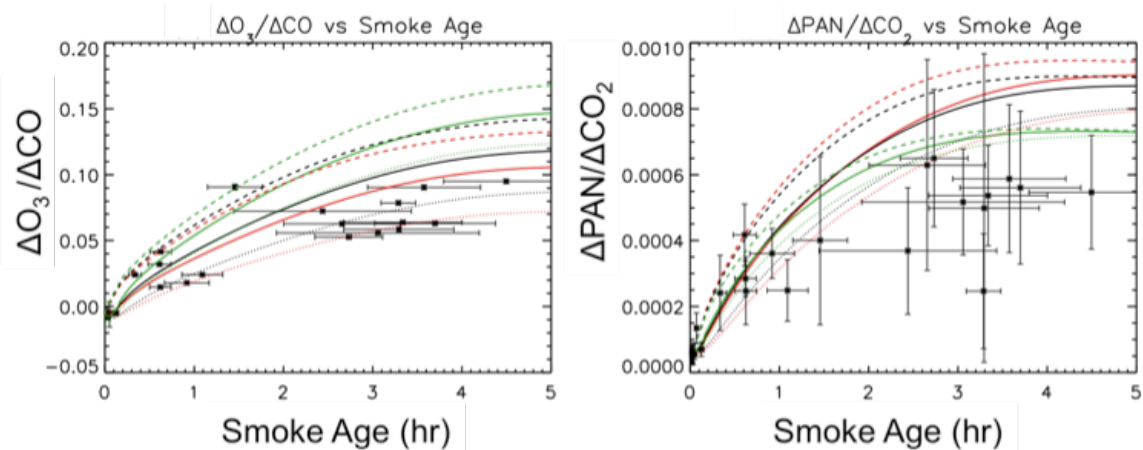


Figure 3. O_3 (left) and PAN (right) mixing ratios within the Williams Fire as observed by Akagi et al. (2012) and simulated by ASP. Asterisks are the measured mixing ratios, with the horizontal error bars showing the uncertainty in the estimated age and the vertical error bars showing the uncertainty in the measurement. Red, black, and green are ASP results for the slow, best-fit (medium), and fast plume dilution rates within a Lagrangian parcel dispersion model. Dashed lines are for above-plume photolysis rates, while solid lines are for the middle of the plume, and dotted lines are for the bottom of the plume. Reproduced from Alvarado et al. (2015).

The modules of the latest version of the ASP model (ASP v2.1) are briefly described below.

Gas-Phase Chemistry: All gas-phase chemistry for organic compounds containing four carbon atoms or fewer has been “unlumped,” i.e. the chemistry for each individual organic

compound is explicitly resolved following the Leeds Master Chemical Mechanism (MCM) v3.2 (e.g., Jenkin et al., 2003). The lumped chemistry for all other organic compounds in ASP has been updated to follow the Regional Atmospheric Chemistry Mechanism (RACM) v2 (Goliff et al., 2013). Heterogeneous reaction rates of gas-phase species are calculated based on the aerosol surface area as in Jacob (2000).

Aerosol Size Distribution, Thermodynamics, and Chemistry: The aerosol size distribution in ASP is represented using a moving-center sectional approach (Jacobson, 2005). The model can simulate an arbitrarily large number of size bins over an input particle range, or set with a single monodisperse diameter. The ASP SOA module is based on the semi-empirical Volatility Basis Set model of Robinson et al. (2007).

Gas-Particle Mass Transfer: Mass transfer between the gas and aerosol phases is calculated in ASP using a hybrid scheme where the flux-limited kinetic equations governing the condensation and evaporation of H_2SO_4 and organic species are integrated using a Gear algorithm, whereas NH_3 , HNO_3 , and HCl are assumed to be in equilibrium.

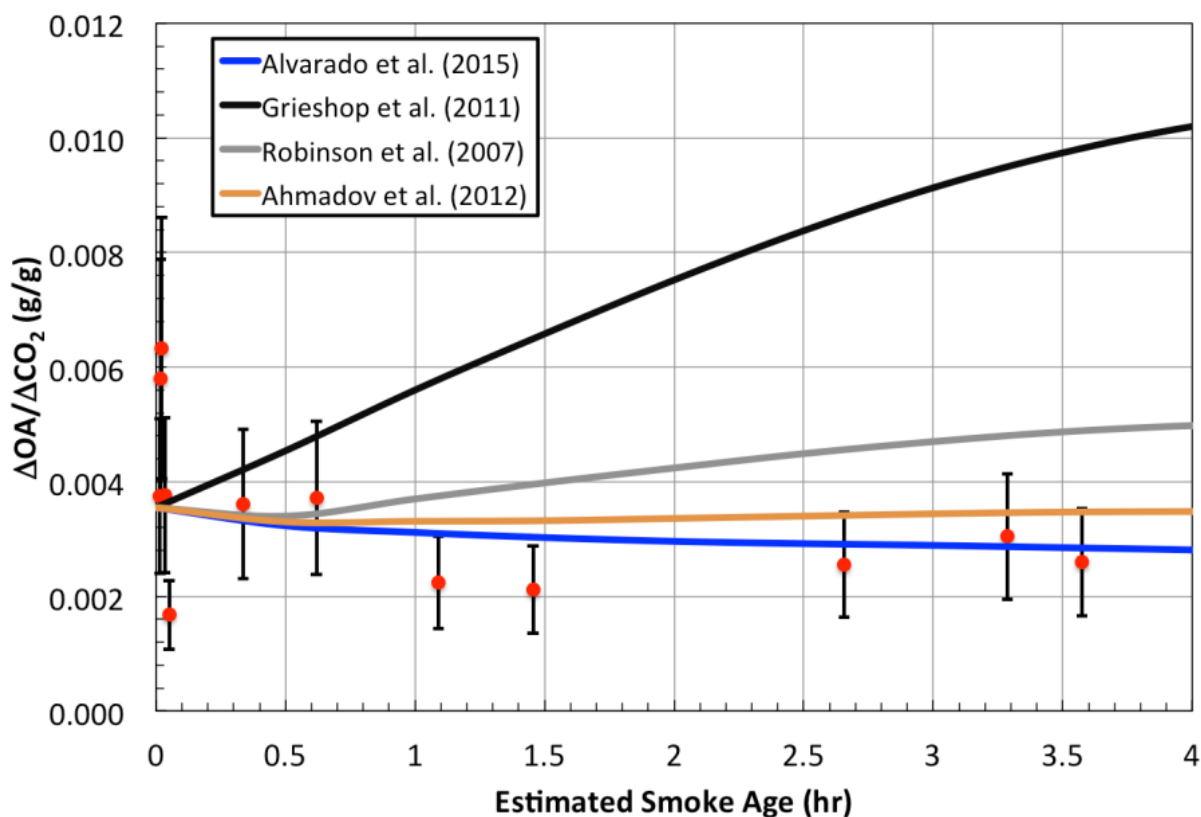


Figure 4. Enhancement ratio (g/g) of organic aerosol (OA) to CO_2 versus smoke age for the Williams Fire. The red circles are the observed values from Akagi et al. (2012). Based on the results of Alvarado et al. (2015).

1.3.2 ASP-Based Sub-Grid Scale Biomass Burning Parameterization

Our previous ASP-based sub-grid scale parameterization of biomass burning chemistry (Lonsdale et al., 2014, 2015) followed the approach used by Vinken et al. (2011) for implementing ship plume chemistry in GEOS-Chem. This approach modifies the emission from fires based on a look-up-table (LUT) that is built from many runs of the ASP model within a simple Lagrangian parcel dispersion model, as in Alvarado et al. (2015). In this project, we attempted to improve upon this previous work by running ASP within the large-eddy simulation model SAM (Section 1.3.3) and fitting the output using a Gaussian Emulator Machine (GEM, O'Hagan et al., 2006) as discussed in Section 2.3.

The Lonsdale et al. (2015) parameterization describes how the Normalized Enhancement Mixing Ratios (NEMRs, $\Delta X/\Delta CO$, Akagi et al., 2011) of different species within the plume vary for different values of the input parameters found to be most important in determining the plume chemistry: fuel type, starting and ending solar zenith angle (SZA), temperature, overhead O_3 column, and plume age. The parameterization calculates the NEMRs of O_3 , OA, ethylene, formaldehyde, and several NO_y species, including NO_x , PAN, ΣPN_s , ΣAN_s , $HNO_{3(g)}$, $NO_{3(p)}$, HONO, NO_3 , and N_2O_5 . Multiplying these NEMRs by the BB CO emissions gives the “effective” emissions of these compounds to the model grid after sub-grid scale processing. Figure 5 shows an example from the Lonsdale et al. (2015) parameterization of how NO_y partitioning can differ dramatically according to fuel type, from the relatively high NO_x savannah/grassland fire to the relatively low NO_x boreal forest fires, thus altering near-source and downwind production of O_3 from the fires.

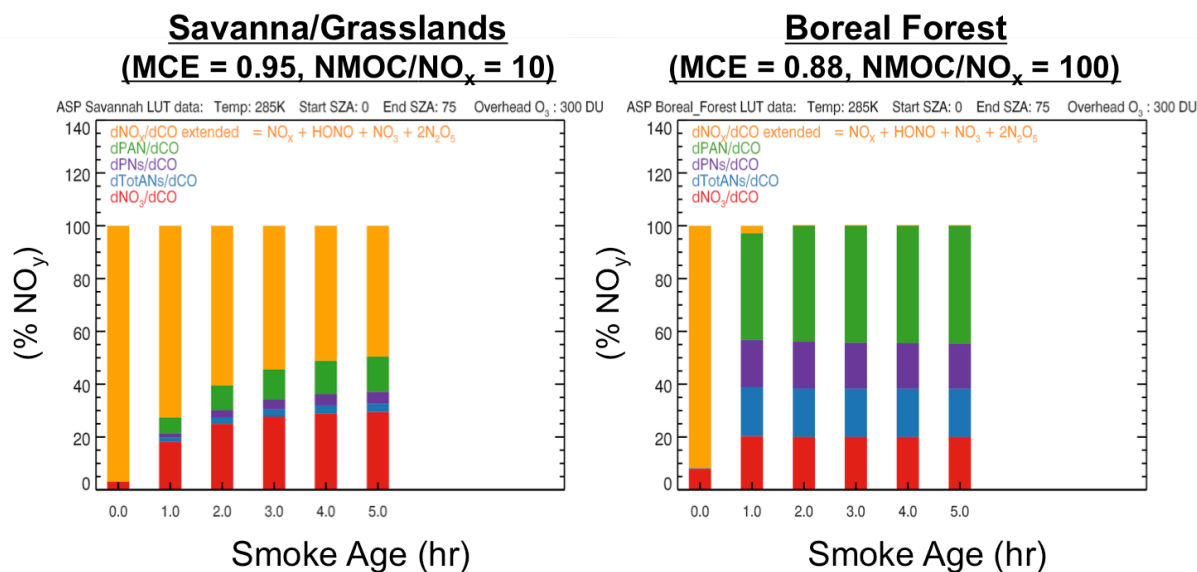


Figure 5. Partitioning of NO_y species versus time for Savannah/Grassland fires (left) and Boreal Forest fires (right). Results are for a temperature of 285K, an overhead O_3 column of 300 DU, a starting SZA of 0° and an ending SZA of 75° .

1.3.3 SAM-ASP 2D Lagrangian Model

In this project, we coupled ASP to the SAM model to develop an improved sub-grid scale parameterization of the impacts of biomass burning on air quality. The System for Atmospheric Modeling (SAM; Khairoutdinov and Randall, 2003) is a large-eddy simulation/cloud-resolving model that has been previously used to reproduce observed dispersion in coal-fired power-plant plumes (Lonsdale et al., 2012) and to study the coagulation of aerosols in biomass burning plumes (Sakamoto et al., 2016).

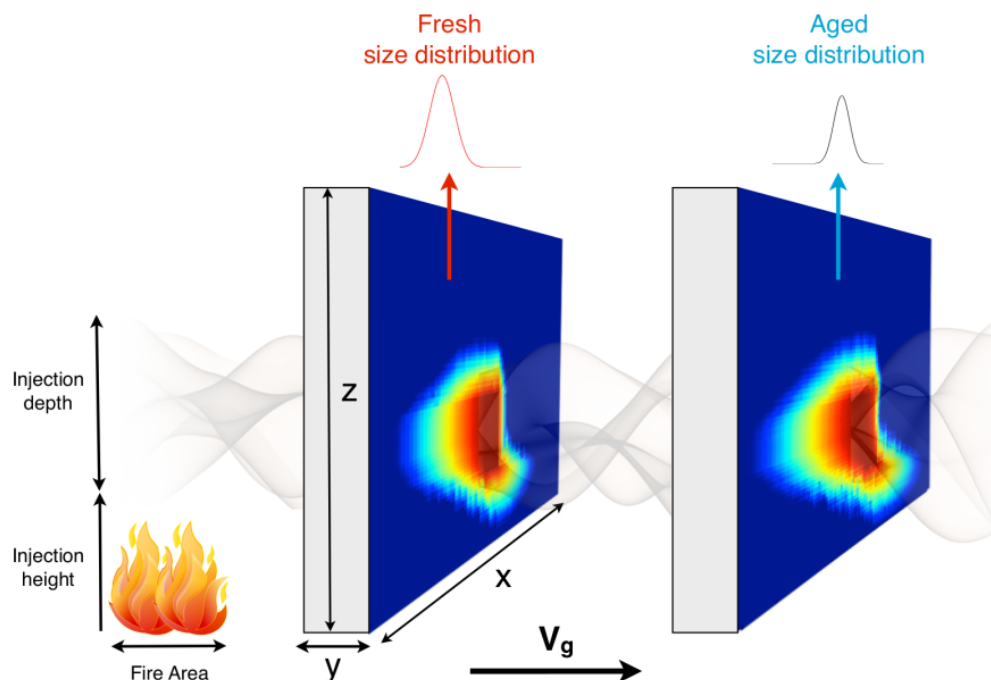


Figure 6. Schematic showing physical structure of SAM-TOMAS model. The SAM-ASP model will be similar but will include gas- and aerosol-phase chemistry relevant to OA condensation/evaporation, BrC production and loss, and mixing state changes. Reproduced from Sakamoto et al. (2016).

In this project, SAM was configured as a moving Lagrangian wall oriented normal to the mean wind in the layer of smoke injection (Figure 6). The coupling of SAM-ASP was performed similar to the coupling of SAM and TOMAS described in Lonsdale et al. (2012) and Stevens et al. (2012), and the coupling of ASP to the Cloud Resolving Model (CRM6) described in Alvarado et al. (2009). SAM was updated to transport over 600 chemical species calculated in ASP, as well as to calculate solar zenith angle and initialize gas phase concentrations based on SAM meteorological parameters. Photolysis rates are calculated using the Tropospheric Ultraviolet and Visible (TUV) radiation model, which generates off-line look-up tables of photolysis rates based on solar zenith angle and overhead O_3 columns. ASP is run as a subroutine for each time step in biomass-burning impacted grid cells in the SAM domain, with the SAM model supplying the temperature, pressure, air density, solar zenith angle, mass emissions flux, and initial gas concentrations to ASP. ASP then calculates the gas chemistry for each grid box,

with the updated gas concentrations returned to the SAM model for the calculation of advection, diffusion, and deposition. The plume does not currently come into contact with the ground, and so deposition was ignored in this project.

1.3.4 STILT-ASP Lagrangian Particle Chemical Transport Model

The STILT model (<http://www.stilt-model.org>; Lin et al., 2003) is a Lagrangian particle dispersion model derived from HYSPLIT but which includes additional modifications that improve the mass-conservation of the simulations and allow the use of customized WRF meteorological fields (Nehrkorn et al., 2010), which have been shown to improve the model performance when compared with tracer-release studies (e.g., Hegarty et al., 2013). STILT has been extensively used at AER in inverse modeling to improve emission estimates for greenhouse gases (e.g., McKain et al., 2012, 2015; Henderson et al., 2015).

STILT-Chem is an extension of STILT that includes gas-phase chemistry (Wen et al., 2013, 2014). While previous versions of STILT-Chem have used the CB4 chemical mechanism, in this project we will use a version of STILT-Chem that we have coupled with the gas and aerosol chemistry calculations of ASP (STILT-ASP) as part of projects funded by NSF and TCEQ (e.g., Alvarado et al., 2016, 2017; Lonsdale et al., 2016). Figure 7 shows an example back-trajectory run of STILT-ASP to estimate the impact of remote sources on O₃ measured at a monitoring site (receptor) in Salt Lake City. Each individual line is one of the 500 back-trajectories calculated from the STILT model. The average particle ozone mixing ratio (not shown) increases from ~55 ppb on the boundary of the model domain to a value of ~98 ppb at the receptor due to the influence of various emission sources.

We recently updated the emissions used within STILT-ASP and made other coding changes, resulting in STILT-ASP v2.0 (Alvarado et al., 2017). First, we updated the emission preprocessor to apply the more detailed ASP speciation to the FINN emissions directly. Emissions for individual species already included in the FINN MOZART4 files (i.e., NO, NO₂, HCHO) were unchanged, and other ASP species were included using a table of emission ratios we developed for each of the seven fire vegetation types included in the FINN inventory. Second, we used NARR meteorology to drive the MEGAN biogenic emission model to produce netCDF files of the hourly biogenic emissions for our period of interest, mapped to the RADM2 mechanism to ensure compatibility with the ASP chemical mechanism. Third, we added code to allow the model to read in CAMx-formatted area source emissions files for the national 36 km resolution domain, as well as the CAMx-formatted point source emission files from the TCEQ CAMx modeling episodes covering May to September of 2012.

The performance of STILT-ASP v2.0 was evaluated using selected surface observations from the 2013 Houston DISCOVER-AQ campaign (Alvarado et al., 2017). STILT-ASP v2.0 showed good average performance for O₃ at the five monitoring sites at the peak of the high O₃ episodes on Sept. 25-26, 2013, with a mean bias (MB) of -4 ppbv and a mean absolute error of 20 ppbv. However, errors in peak O₃ at individual sites could be up to 30 ppbv. NO_x had an average underestimate of 65% at these sites, while there was a significant positive bias in CO of 71 ppbv. For the two sites where NO₂/NO_x ratios could be calculated (Galveston and Seabrook Park), STILT-ASP v2.0 underestimates the NO₂/NO_x ratio (MB = -19%), suggesting that the model is not converting NO to NO₂ as rapidly as it is happening in the real atmosphere.

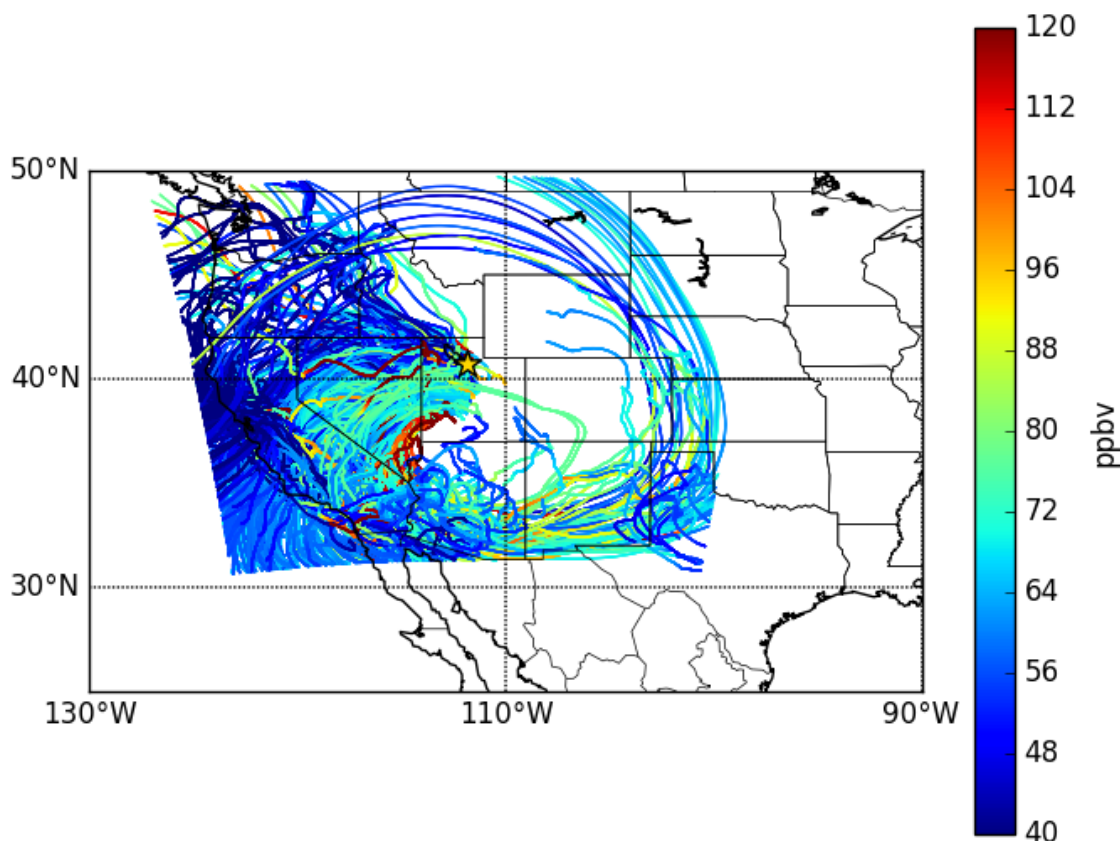


Figure 7. Ozone mixing ratios (ppb) along the 500 seven-day STILT-ASP back-trajectories calculated to for a surface monitor in Salt Lake City.

The source code of the STILT-ASP v2.0 model, as well as the necessary input files and preprocessors, are available for download from AER via email request to Dr. Alvarado (malvarad@aer.com). Model documentation includes a detailed User's Guide, a technical memo that describes the equations of the model in detail, and other documentation on the STILT and ASP models.

1.4 Report Outline

Section 2 describes the coupling the SAM and ASP models, the evaluation of the coupled SAM-ASP model, the development of a Gaussian Emulator Machine (GEM) based on the output of the SAM-ASP model, the evaluation of the GEM parameterization, and the implementation of the parameterization of Lonsdale et al. (2015) within the PiG module in CAMx and evaluation of the impacts on simulated O₃ from fires.

Section 3 describes our efforts to use the STILT-ASP model to evaluate the impacts of biomass burning plumes on the boundary of the TCEQ CAMx modeling domain for May and June of 2012 and to assess the impact of fires on O₃ and PM_{2.5} in Texas.

Section 4 describes the quality assurance steps that were performed in this project, including answers to the evaluation questions listed in the Quality Assurance Project Plan (QAPP). Section

5 summarizes the conclusions of our study, and our recommendations for further study are given in Section 6.

2 Toward an Improved Sub-grid Scale Parameterization of Biomass Burning

2.1 SAM-ASP Configuration

In this project, we used the coupled SAM-ASP model to perform gas-chemistry-only (no aerosol) simulations of biomass burning plumes. We used gas-chemistry-only runs, as adding aerosols to the SAM-ASP simulations significantly increases the run time and the impact of biomass burning on ozone is more uncertain and dependent on chemistry than the impact on PM_{2.5}. SAM-ASP was configured as a moving Lagrangian wall oriented normal to the mean wind in the layer of smoke injection (between 1200 and 1400 m) as depicted in Figure 6. The grid boxes in the moving wall have a 500 m x 500 m horizontal resolution with a 100 km total domain width and 40 m vertical resolution with a total vertical extent of 3 km. Large-scale meteorological forcing in SAM was taken from the North American Regional Reanalysis (NARR; Mesinger et al., 2006) meteorology.

During this project, we made several improvements to the coupled SAM-ASP model and corrected coding bugs as they were discovered. For example, when ASP v2.1 is run as a Lagrangian parcel model, it needs the initial concentrations within the plume specified. However, as SAM-ASP can simulate the dispersion of the smoke horizontally and vertically, we added the option to SAM-ASP to calculate the initial concentrations based on the mass emissions flux (kg burned/m²/s¹) and emission factors (g/kg burned) for biomass burning species (Akagi et al., 2011; Sakamoto et al., 2015). This will allow SAM-ASP to better represent a wide range of fire sizes and intensities.

We also found that the initial SAM-ASP simulations were too slow for the ~400 model runs needed to train the GEMs for the new parameterization (Section 2.3). Thus we explored different ways to reduce the computation time. For example, rather than calculating the chemistry in the “background” boxes outside of the main plume, we adjusted the model to only call ASP in the boxes that have been impacted by smoke, defined in this study as any grid box having a concentration of CO greater than 150 ppb (determined as the background concentrations based on the chaparral fire described in Alvarado et al., 2015). We explored varying this threshold in order to further decrease the run time of a simulation. For example, using 500 ppb of CO as the “in-plume” threshold was sufficient for the early part of the plume-simulated chemistry (< 1 hour). However, the rapid dilution of biomass burning plumes means that after ~ 1 hour, the outer edges of the plume drop below this concentration threshold, and thus the plume-average enhancement ratios begin to be biased if chemistry is not calculated for these boxes. In addition, using a threshold of 500 ppbv to define the “in-plume” boxes resulted in an apparent underestimation of the dilution rate of the plume, as this forced the “in-plume” concentration to stay above 500 ppbv throughout the simulation. Thus, a threshold of 150 ppbv CO was found to give the best balance between optimizing the model run time and giving accurate results for the first 5 hours of the plume aging.

We also uncovered and corrected an error in the calculation of the orientation direction for the Lagrangian wall, which is supposed to be normal to the mean wind of the model. By default, SAM used the mean wind direction from 900 mbar to the surface to determine the orientation of the wall. However, our assumed plume injection height in our SAM-ASP simulations of 1200 and 1400 m was above this height, and thus the orientation of the Lagrangian wall was not normal to the mean winds affecting the plume, but to the winds below the plume. This resulted in odd results for cases, such as the Williams Fire from Alvarado et al. (2015), where the wind

shear between the surface and the lower troposphere was significant. Thus, the model was corrected to calculate the mean wind direction for the layers of the plume, instead of surface layers.

2.2 SAM-ASP Evaluation

We evaluated the performance of the improved coupled SAM-ASP model developed in this project by comparing the results to observations from the Williams Fire made by Akagi et al. (2012), and previously simulated using ASP in a Lagrangian parcel model by Alvarado et al. (2015). The emission ratios for this simulation were taken from Alvarado et al. (2015), and included observed values for several gas-phase species measured by Akagi et al. (2012). Plume injection height was set to 1200 to 1400 m and background meteorology was taken from the NARR.

Figure 9 shows the calculated O₃ concentrations within the plume as the plume moves downwind. We can see that five hours downwind, the plume is approximately 25 km wide, and has an average O₃ concentration of approximately 60-70 ppbv, and absolute values up to 88 ppbv are seen in the center of the plume in the first two hours after emission. The plume moves slightly in the plane of the model as the winds at each level do not line up exactly with the mean wind across the plume. Figure 10 shows the rapid loss of NO_x in the plume (note the log color-bar scale) due to both dilution and chemical loss, but the in-plume NO_x concentrations are still ~3 ppb.

To compare our SAM-ASP simulation with the Akagi et al. (2012) observations, modeled NEMRs are calculated at each timestep of the model output. This is done by identifying the grid box in each 2D slice (in the z and x direction of the model) with the highest CO concentration, thus simulating an observation made near the plume center. The concentration of the species of interest (X) is then determined at that point, with the NEMR ($\Delta X/\Delta CO$) calculated in that grid box as:

$$\Delta X/\Delta CO = (X_{\text{in-plume}} - X_{\text{background}}) / (CO_{\text{in-plume}} - CO_{\text{background}}) .$$

Averaging the NEMR over the full horizontal domain of the model for the vertical level with the peak CO concentration gives similar results, so the above metric can be used to compare with aircraft observations of biomass burning plumes, which generally average over samples during a plume transect.

The in-plume CO enhancement ($\Delta CO = CO_{\text{in-plume}} - CO_{\text{background}}$, in ppbv) as well as the NEMRs for O₃, PAN, NO_x, HONO, and NH₃, are shown in Figure 11. We can see that the revised SAM-ASP model is able to correctly simulate the dilution of CO in the smoke plume, as well as the chemical loss of NO_x, HONO, and NH₃ and chemical formation of PAN within the plume. The formation of O₃ in the model is underestimated (model value of $\Delta O_3/\Delta CO$ of 0.05 mol/mol at 4.5 hr downwind, rather than the measured value of 0.10 mol/mol). This is in contrast to the results of the Lagrangian parcel model ASP study of Alvarado et al. (2015), where the parcel model somewhat overestimated the formation of O₃ ($\Delta O_3/\Delta CO$ of 0.12 mol/mol at 4.5 hr). Thus we conclude that SAM-ASP does a reasonable job of simulating CO, HONO, PAN, and NO_x within biomass burning plumes, but currently underestimates the formation of O₃.

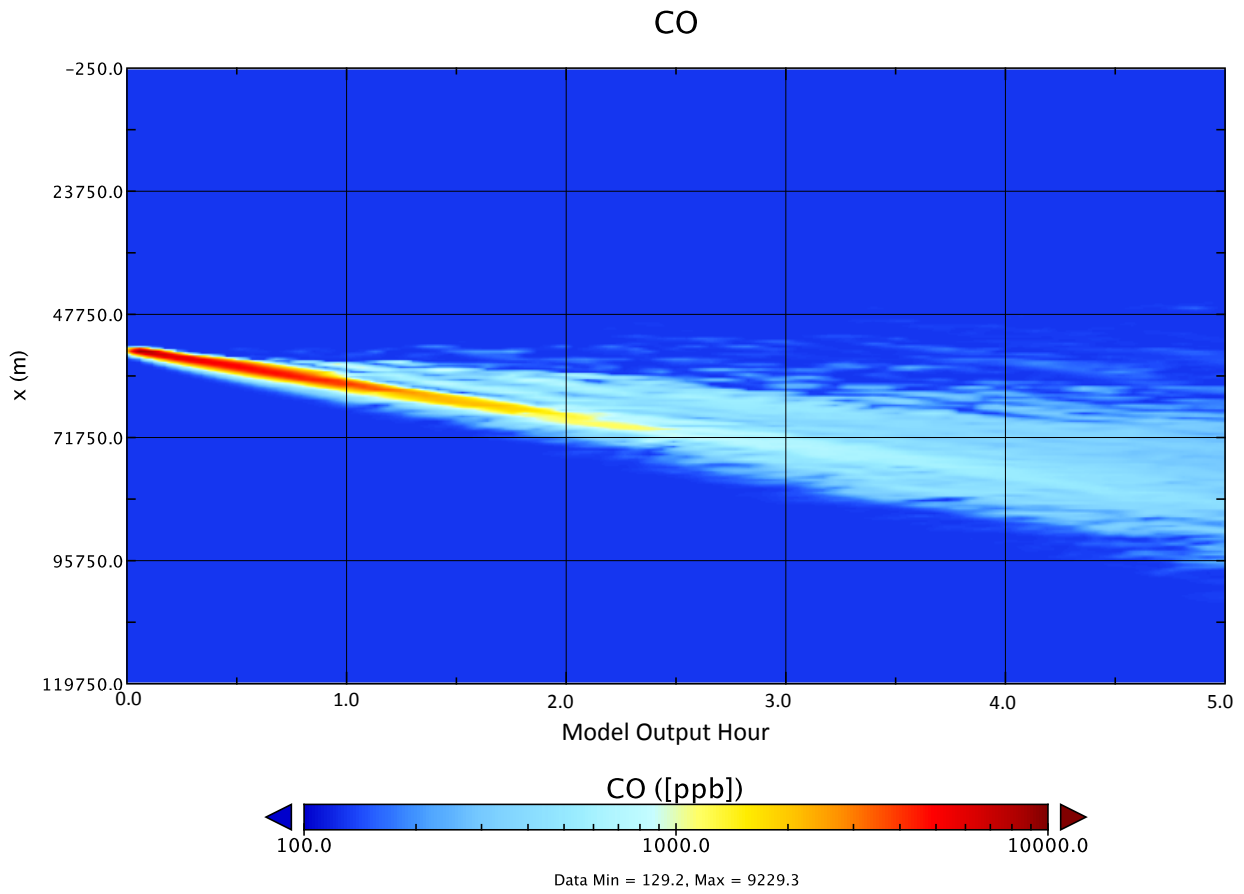


Figure 8. SAM-ASP simulated CO concentrations for the Williams Fire (Akagi et al., 2012) at 1.22 km altitude. The y axis is the horizontal dimension of the SAM-ASP Lagrangian wall.

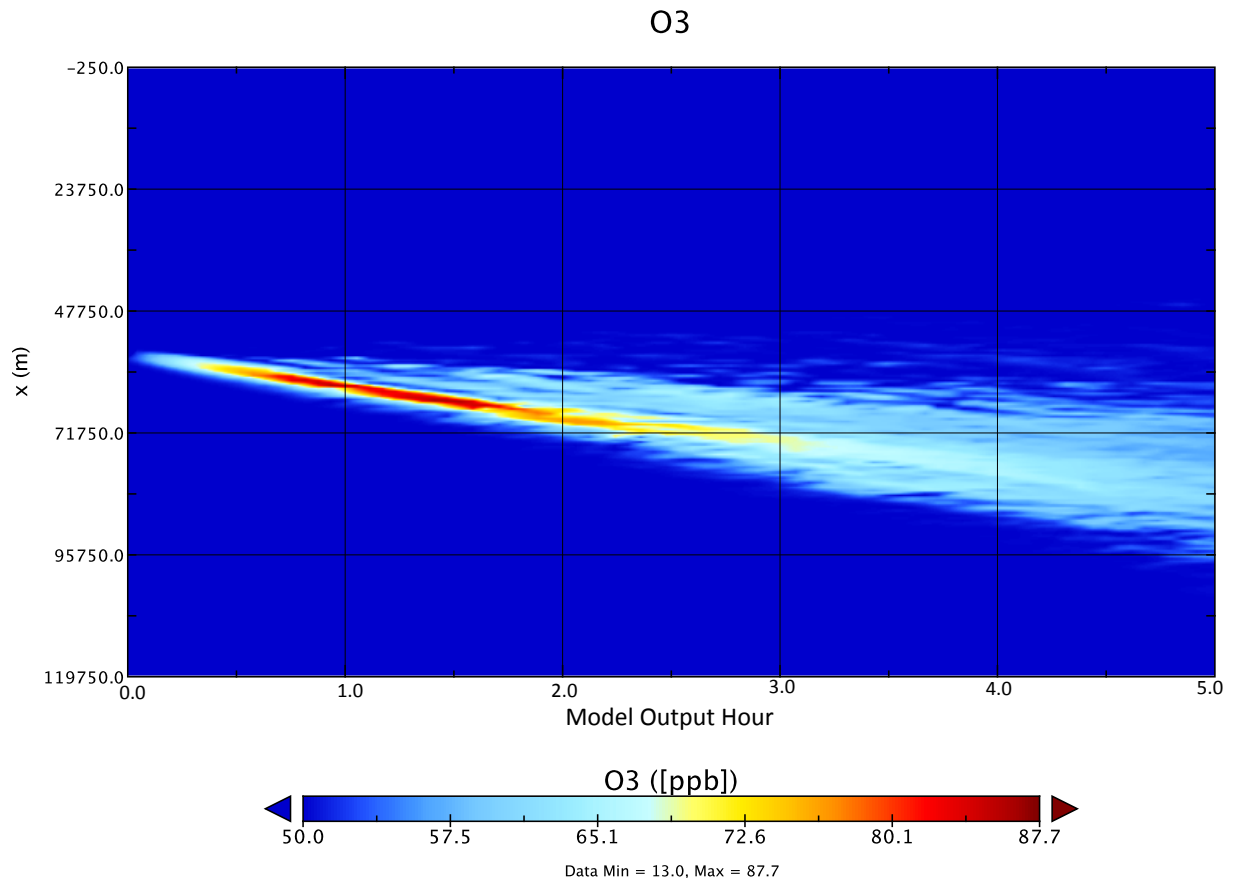


Figure 9. As in Figure 8, but for O₃.

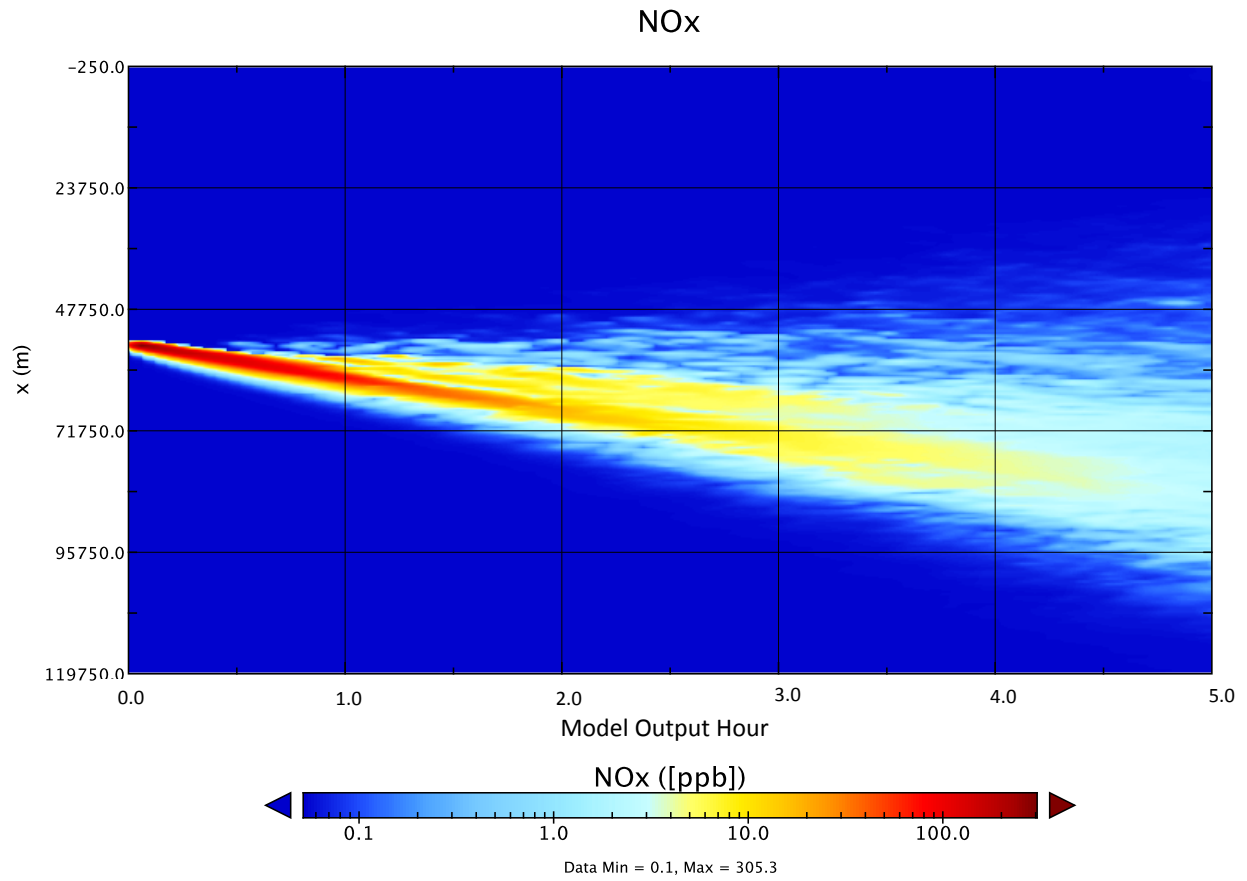


Figure 10. As in Figure 8, but for NO_x (note the log scale).

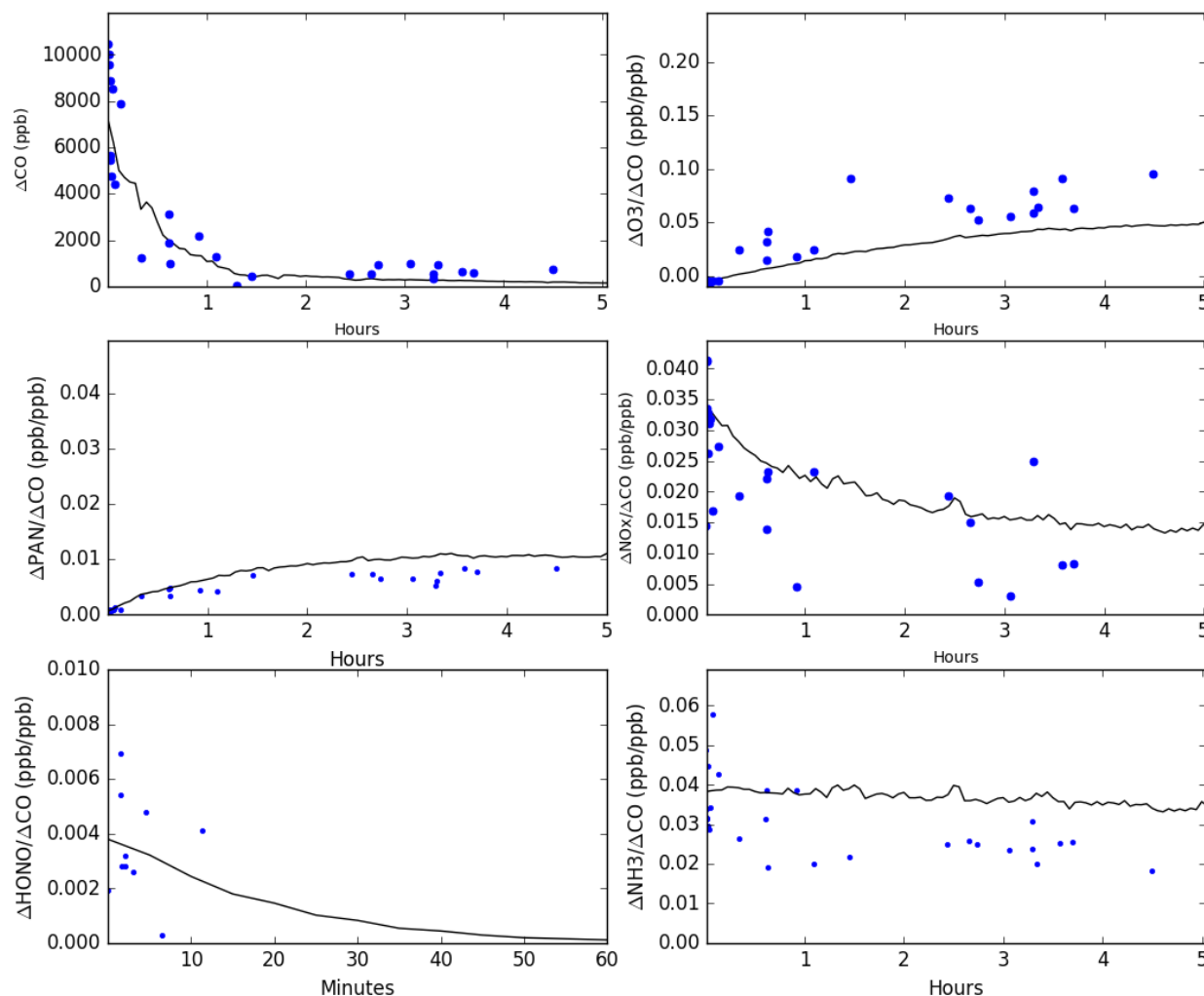


Figure 11. SAM-ASP simulation of ΔCO , $\Delta\text{O}_3/\Delta\text{CO}$, $\Delta\text{NO}_x/\Delta\text{CO}$, $\Delta\text{PAN}/\Delta\text{CO}$, $\Delta\text{HONO}/\Delta\text{CO}$ and $\Delta\text{NH}_3/\Delta\text{CO}$ for the Williams Fire (black line) versus observations (blue dots).

2.3 Gaussian Emulation Machine (GEM) Development

In this project, we ran SAM-ASP simulations for 400 different fire conditions and used the output to train a Gaussian Emulation Machine (GEM), which could then be used to simulate the SAM-ASP output for the enhancement ratios of O_3 , NO_x , HONO, HNO_3 , and PAN for many more conditions to develop a finely-resolved look-up table for implementation via the CAMx Plume-in-Grid module (Karamchandani et al., 2011; Section 2.5). As in the previous parameterization study of Lonsdale et al. (2015), we kept the wind speed, fire size, and injection height fixed, and in addition, used a constant mass emission flux, all based on the Williams Fire from Akagi et al. (2012). We also assumed clear-sky photolysis rates with an assumed land surface albedo of 0.10, again as in the Williams Fire.

Initially, we chose the following parameters to vary: fuel type (Savannah, Boreal, Temperate and Tropical Forest), temperature (K), overhead O_3 column (reported in Dobson Units, DU),

latitude ($^{\circ}$ N), day of year, and emission hour. The final three parameters are all used to calculate how the plume chemistry varies given the change of the solar zenith angle, and thus photolysis rates, after emission. Our initial GEM evaluation showed that the overhead O_3 parameter had very little impact on the model results, and thus it was not varied for our final parameterization runs, which used a fixed value of 300 DU. Emission ratios for each fuel type were taken from Akagi et al. (2011) and Andreae and Merlet (2001) and speciated for the ASP chemical mechanism.

We then used Latin-hypercube sampling to derive a statistically near-random sampling of these SAM-ASP model input parameters, which in principle dramatically reduces the number of SAM-ASP runs that are needed to develop a statistically reasonable parameterization. The values used for each input variable are given in Table 1. We found that the GEMs had difficulty representing periodic variables, like day of year, unless both endpoints (January 1, December 31) were included in the training: if they weren't, the January 1 GEM O_3 NEMR estimates did not match the December 31 estimates. Thus to try to ensure an accurate representation of the seasonal cycle's impact on the plume chemistry (via SZA), these days were included in the SAM-ASP runs used to form the GEM model training dataset.

Table 1. Values used in the SAM-ASP simulations of GEM training

Parameter	Range/Values
Fuel Type	Savannah, Boreal, Temperate, Tropical Forest
Temperature	275, 280, 285, 290, 295, and 300 K
Latitude	15, 30, 45, 60, and 75 $^{\circ}$ N
Day of Year	Solstices (06/21, 12/21), Equinoxes (03/20, 09/23), 01/01, 12/31
Emission Hour	Every hour, 01:00-23:00 local time

In order to develop the GEMs, we used the method and code of O'Hagan (2006), which is a Gaussian process emulator with a Bayesian-based statistical tool. The GEM treats the input and output parameters as indices to stochastic Gaussian functions, taking the mean and covariance values produced from the input/output parameters of the original simulation model, in our case SAM-ASP. We found that trying to include fuel type in the GEM, using proxies like the NO_x/VOC ratio in the emissions for the different fuel types, resulted in unphysical results for O_3 and other species. Thus we trained separate GEMs for each fuel type separately, varying the other input parameters in Table 1. For each fuel type, Latin hypercube sampling was used to select 100 combinations to represent the $6 \times 5 \times 6 \times 24 = 4320$ possible combinations of temperature, latitude, day of year, and emission hour.

For each application (i.e., an individual Latin-hypercube selection), the code of O'Hagan (2006) produces the setup files listed in Table 2. Additionally, an input file is required that contains a list of all possible combinations of inputs (i.e. Temperature \times Latitude \times Start Day \times Start Hour). The Bayesian tool (FORTRAN source code) then produces an estimate (the value of the emulator mean function) and a standard deviation of trace gas NEMRs (O_3 , NO_x , HONO, HNO_3 and PAN) for the full range of parameters listed in Table 1. The estimate and standard deviation can be computed using an approach of generating many random functions and applying Monte Carlo to each of these functions, with the Latin hypercube ensuring the least

amount of runs necessary. The sampled model run outputs, as determined by the Latin hypercube sampling, were fit to train each GEM run, based on the four input parameters (Temperature, Latitude, Start Day and Start Hour). As noted above, a separate GEM was trained for each fuel type (100 samples each), with separate GEMs trained based on the SAM-ASP model output at 1, 2, 3, 4 and 5 hours after emission.

The fitted GEMs can be used to generate look-up tables for the enhancement ratios of O₃, NO_x, HONO, HNO₃, PAN, and the radical CH₃CO₃ to CO on a much finer grid than that used to train the GEM parameterization. These look-up tables are saved as netCDF files, and cover day of year at a resolution of 1 day, starting hour at a resolution of 1 hour, temperature (from 275 K to 300 K) at a resolution of 1 K, and latitude (from 30 to 75 °N) at a resolution of 1 degree. The enhancement ratios are stored for 1, 2, 3, 4, and 5 hours after emission to capture the evolution of the enhancement ratios of these species with time. By including this fine-resolution output from the GEM in a netCDF file, it can be easily and quickly accessed by the CAMx model and can potentially be distributed for use in other models.

Table 2. Setup files produced by the GEM program for each application of model parameters

File Name	Description
emulator_ainv.txt	inverse correlation matrix
emulator_training_inputs.txt	training data inputs
emulator_mu_out.dat	estimated regression parameters
emulator_precision_out.dat	estimated GP prec = 1/variance
emulator_ainvh.txt	inverse correlation matrix times inverse Hessian
emulator_rough_out.dat	estimated function roughness
emulator_g.txt	inverse gain matrix
emulator_inv_hainvh.txt	$H.ainv.H^{-1}$
emulator_minmax.txt	max and mins of each input
emulator_scale.txt	mean and sd of output scaling

2.4 GEM Parameterization Evaluation

In order to evaluate the GEM parameterizations, we examined the finely-resolved netCDF output files described above to see if the dependence of O₃, NO_x, HONO, HNO₃ and PAN in this GEM output was consistent with our conceptual model of the chemical formation and loss of these species in biomass burning smoke plumes.

2.4.1 Ozone

Figure 12 shows the results from the GEM output of the O₃ NEMR for the full range of latitudes and start days, while temperature is held fixed at 285 K and the model start hour is held fixed at 12:00 pm local time, at two and five hours after emission. As expected, the Temperate Forest and Tropical Forest fuel types have a large enhancement of O₃ over the five-hour simulation, as these fuel types both have relatively high ratios of NO_x to VOCs, while the Boreal Forest type has little enhancement (< 0.02 ppb/ppb), due to the relatively low amount of NO_x

emitted. However, the relatively low O₃ NEMR for Savannah fires is surprising, as this fuel type has the highest NO_x to VOC ratio.

The dependence of the O₃ NEMR on latitude and time of day is consistent with the impact that these variables have on the solar zenith angle (SZA), and how the SZA affects photolysis rates, and thus ozone production, in the plume. The peak values are in the summer, as expected, and the enhancement ratio generally decreases with increasing latitude, although the GEM places the summer maximum fairly high north in the summer, possibly due to the longer period of daylight at high latitudes in the summer, but it could be an artifact of the fitting process.

Figure 13 shows O₃ enhancement ratios at three hours downwind for a fixed latitude (45 °N) and two fixed dates - the summer (top) and winter (bottom) solstices. The y-axis shows the full range of temperatures (275 K – 300 K) while the x-axis shows the hour of day. As expected, O₃ enhancement is higher in the summer solstice plot. The wintertime plot shows a net negative O₃ NEMR even three hours downwind, reflecting the higher SZAs and thus lower photolysis rates. In addition, in both plots the O₃ NEMR generally peaks at the highest temperature, as expected given the chemistry of O₃, with the ratio peaking at 0.02 mol/mol at three hours downwind.

However, the dependence of the ozone enhancement ratio on time of day does not appear to be correct in the GEM output. The summer plot peaks at about 10:30 local time (so that the plume aging covers the highest three-hour average SZA period), which makes sense, but the enhancement ratio goes negative for plumes starting at 14:00 local time, which should still be forming O₃ up to the end of the simulation at 19:00 (7 PM) local time in the summer. In addition, the secondary peak in the winter plot at 21:00 local time appears to be the result of a fitting artifact.

In order to evaluate the parameterization results against real data, O₃ NEMRs for the Savannah Fuel type are plotted in Figure 3 for all latitudes and days of the year, but for a temperature of 292 K, and a start time of 10:00 am local time. This is the closest parameterization selection to the Williams Fire (chaparral fire) described in Alvarado et al. (2015) (Figure 11), which burned on November 17, 2009, at 34° 41' 41" N latitude. It can be seen in Figure 11 that after 4.5 hours of model simulation, the ozone enhancement measured was approximately 0.10 mol/mol (top right panel). The star in Figure 14 roughly estimates the parameterization estimate for the matching Williams Fire conditions, giving a value of 0.04 ppb/ppb. This is only about half of the measured value, but is similar to the value of 0.05 ppb/ppb simulated in SAM-ASP for the Williams Fire (Figure 11). Thus, while the GEM gives plausible values for the O₃ NEMR, it tends to underestimate the observed ozone enhancement for the Williams Fire. Thus, our evaluation suggests that the GEMs show promise in their ability to be used to predict the changes in O₃ in biomass burning plumes during the first five hours of aging, but that there are issues with the dependence of the O₃ NEMR with respect to the time of emission, and to a lesser extent, latitude and fuel type, that would have to be addressed in future work before the GEM parameterization could be used in air quality models.

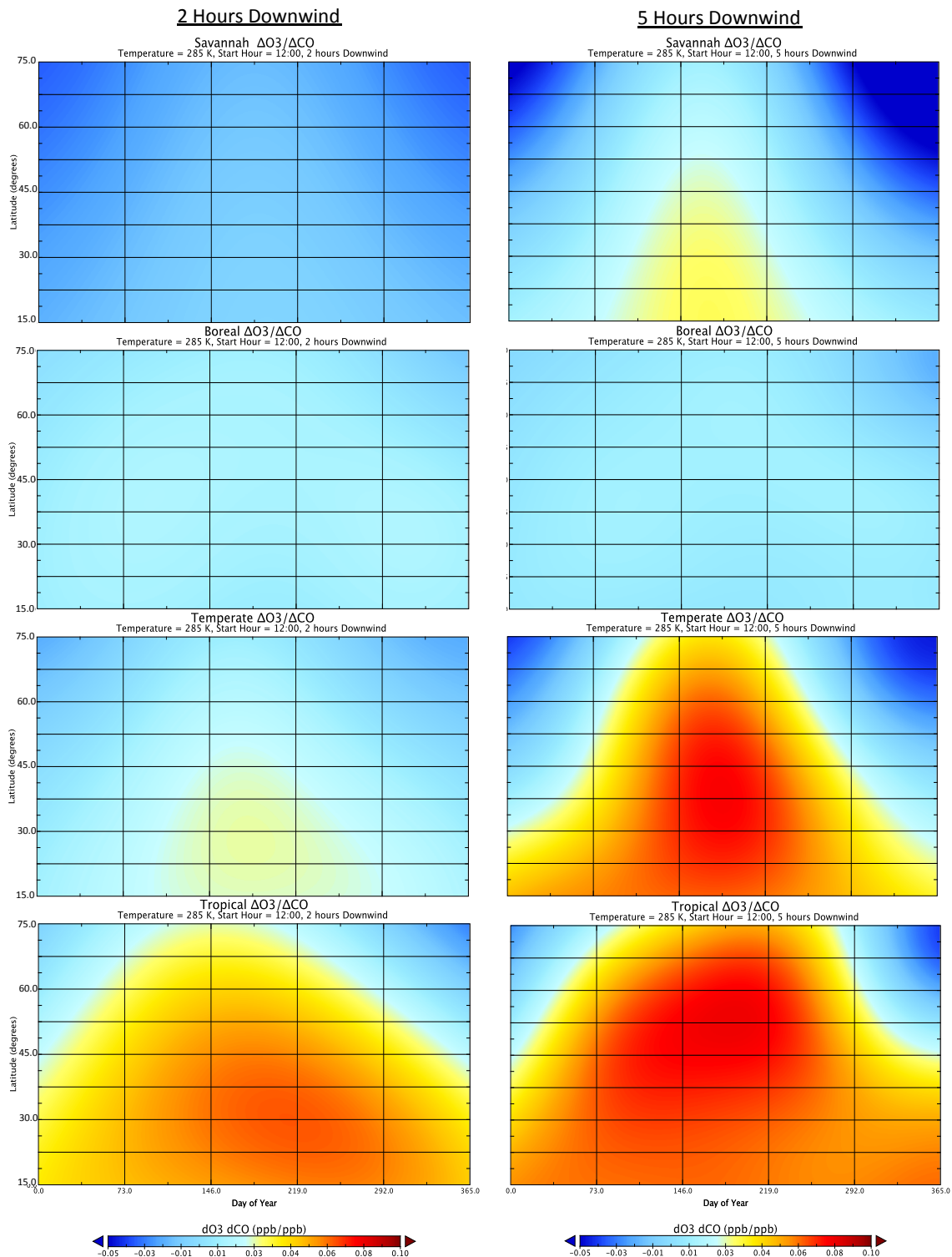


Figure 12. GEM calculation of the mean O₃ enhancement ratio ($\Delta O_3/\Delta CO$, mol/mol) for the full range of latitudes and days of the year, fixed at a temperature of 285 K, and a model start time of 12:00 pm. The left column shows estimates from 2 hours downwind, and the right column shows estimates from 5 hours downwind of the source.

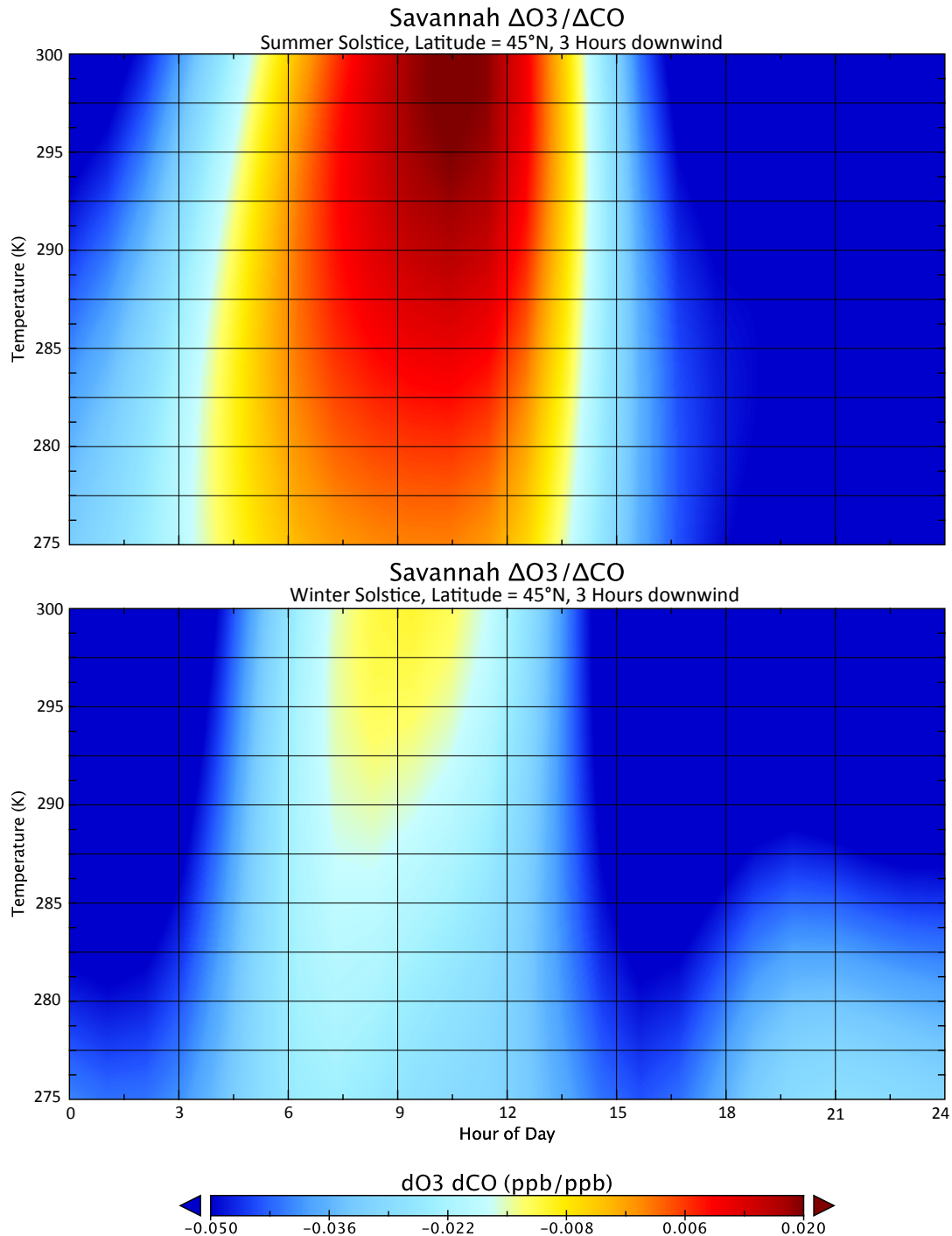


Figure 13. GEM calculation of the mean O₃ enhancement ratio ($\Delta O_3/\Delta CO$, mol/mol) for the full range of temperatures (K) and hours of the day, fixed at a latitude of 45° N, for the summer (top plot) and winter (bottom plot) solstices at 3 hours downwind.

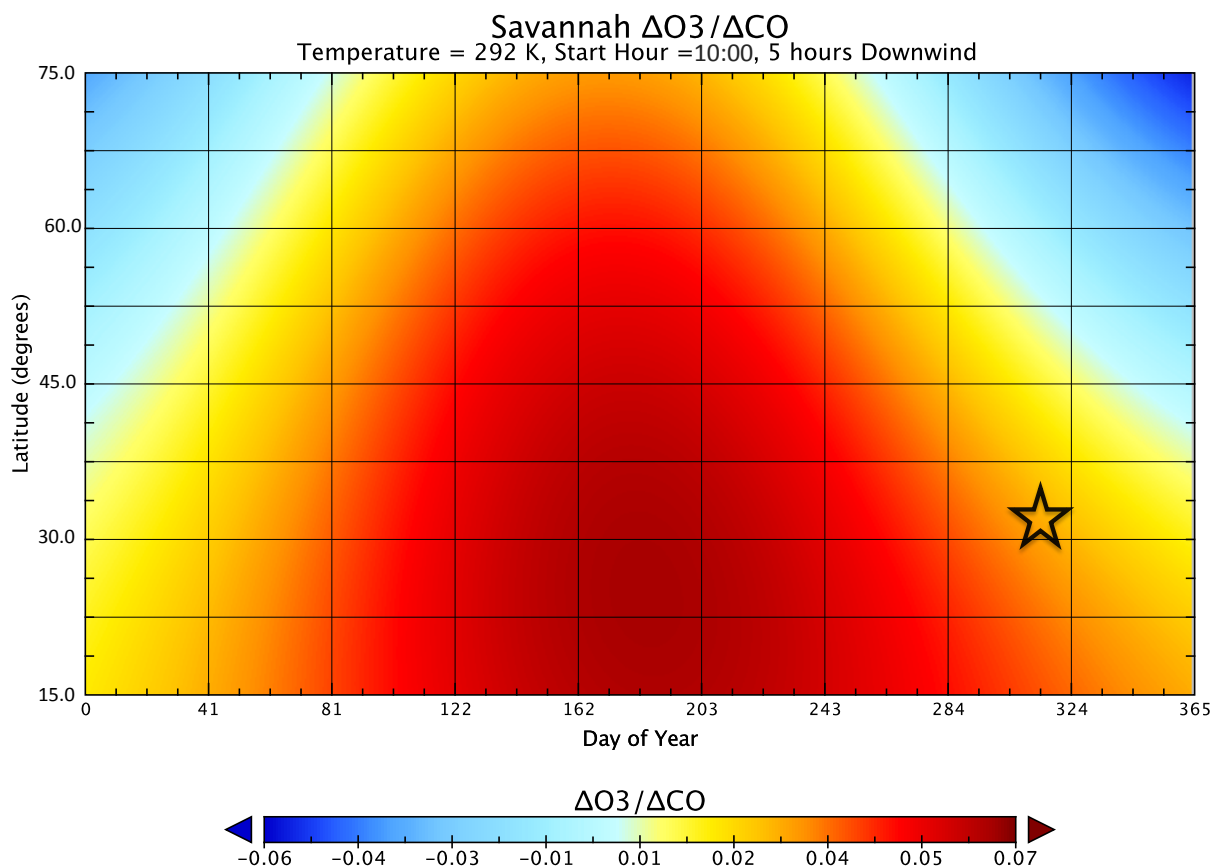


Figure 14. GEM calculation of the mean O_3 enhancement ratio ($\Delta O_3/\Delta CO$, mol/mol) for the full range of latitudes and days of the year, fixed at a temperature of 292 K, and a model start time of 10:00 am. The star indicates the approximate conditions that match the Williams Fire described in Alvarado et al., 2015.

2.4.2 NO_y Species

The NMERs of NO_x , PAN, HONO, and HNO_3 are plotted in Figure 15 for the same set of parameters as Figure 14, corresponding to the conditions of the Williams Fire. Comparing NO_x to the Williams Fire measurements presented in Figure 15, the GEM parameterization of NO_x NEMR of 0.023 mol/mol is at the upper end of the range of the measurements up to four hours downwind, but is lower than the value of 0.015 mol/mol predicted by the SAM-ASP model itself for the conditions of the Williams Fire. The parameterization also captures the near-zero HONO concentrations at five hours downwind.

However, the results for PAN and HNO_3 are inconsistent with the GEM predictions of the loss of NO_x , as well as with the results of the SAM-ASP model for the Williams Fire. The parameterization estimate for PAN and HNO_3 is extremely low. However, the loss of NO_x should always be accompanied by a growth in other NO_y species like PAN and HNO_3 , and so the GEM is not following the conservation of NO_y .

In addition, the dependence of all NO_y species on latitude and longitude does not match the conceptual model of the evolution of these species in the plumes. Values at the beginning and

end of the year for PAN and HNO₃ disagree substantially, and the NO_x NEMRs are not distributed symmetrically across the year, as we would expect for a species whose loss rate depends mainly on SZA and temperature. Thus our evaluation suggests that the GEMs are not of sufficient quality to be used to predict the changes in NO_y species downwind in biomass burning plumes during the first five hours of aging.

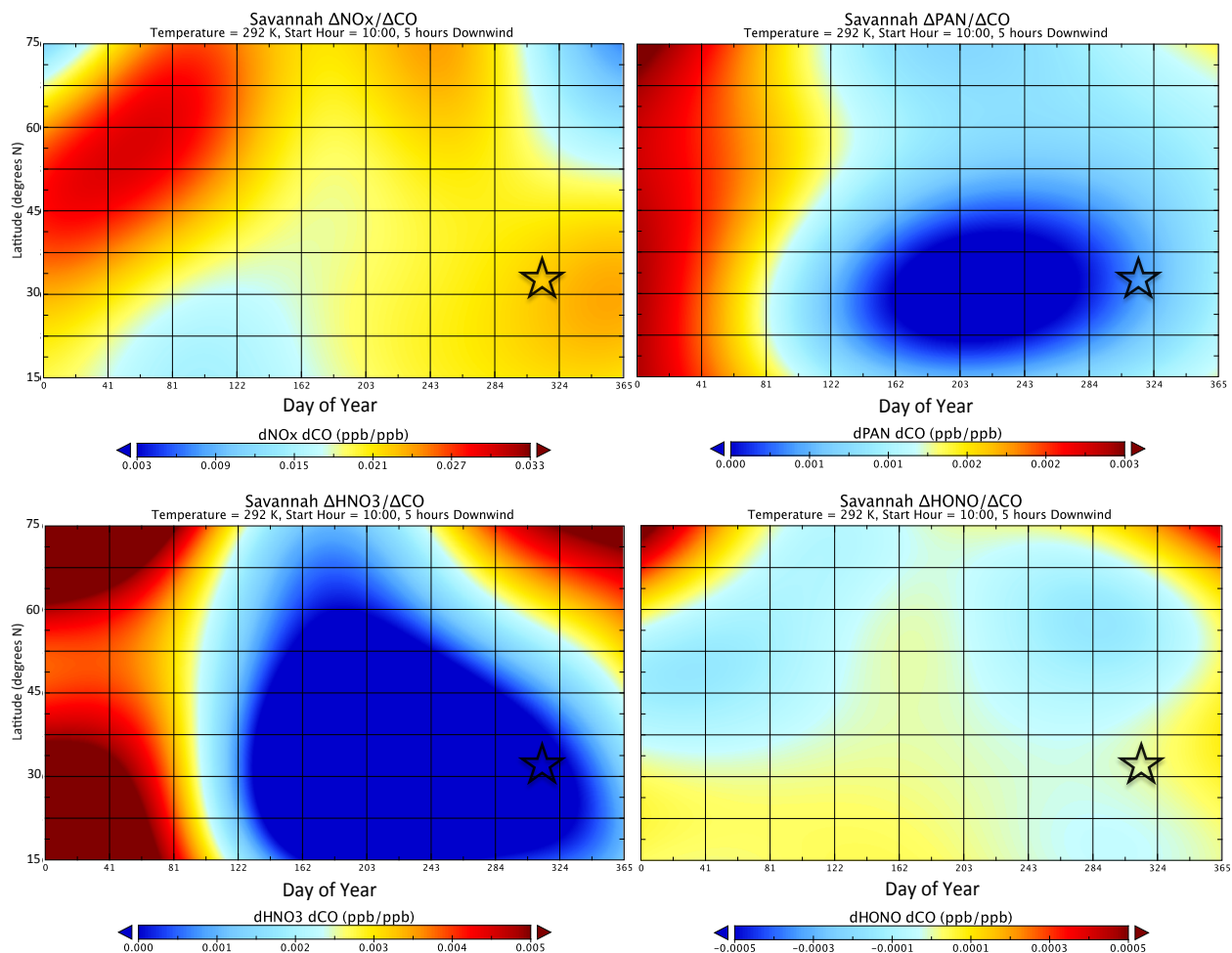


Figure 15. GEM calculation of the mean NO_x, PAN, HNO₃ and HONO enhancement ratio (ppb/ppb) for the full range of latitudes and days of the year, fixed at a temperature of 292 K, and a model start time of 10:00 am. The star indicates the approximate conditions that match the Williams Fire described in Alvarado et al. (2015).

2.5 Implementation of the Parameterization into CAMx

As noted in Section 2.4, we concluded that the current GEM parameterization was not yet of sufficient quality to be implemented into CAMx. Thus, we instead decided to implement the previous parameterization of Lonsdale et al. (2014, 2015), based on runs of ASP as a Lagrangian parcel model, into CAMx instead to assess the impact of the sub-grid scale chemistry on ozone. This work goes beyond the previous study of McDonald-Buller et al. (2015) in that McDonald-

Buller et al. (2015) did not use the full Lonsdale et al. (2014, 2015) parameterization (instead only using values at 1 hour downwind of the plume), and did not integrate the parameterization into the Plume-in-Grid module. However, note we are using the older, publically released v1.5 FINN emissions, rather than the v2.1 FINN emissions used in McDonald-Buller et al. (2015).

In order to implement the Lonsdale et al. (2015) parameterization into CAMx, we first used the initial parameterization runs to generate look-up tables for the enhancement ratios of the parameterized species (O_3 , NO_x , HONO, HNO_3 , PAN, other peroxy nitrates (PANX), alkyl nitrates (NTR), NO_3 , N_2O_5 , HCHO, C_2H_4 , CH_3CO_3 , and other acyl peroxy radicals (CXO_3)) to CO on a much finer grid than that used to train the GEM parameterization. These look-up tables are saved as netCDF files for each fuel type, and cover starting and ending (5 hr) SZA at a resolution of 1 degree, and temperature (from 275 K to 300 K) at a resolution of 1 K. The enhancement ratios are stored for 1, 2, 3, 4, and 5 hours after emission to capture the evolution of the enhancement ratios of these species with time.

In order to incorporate the parameterization results into the CAMx plume-in-grid (PiG) module (Karamchandani et al., 2011), we had to make several code changes and develop additional scripts. We developed a Python script to convert the FINN emissions, which are speciated using the MOZART-4 chemical mechanism, to the CB6r2 mechanism using the mapping given in McDonald-Buller et al. (2015). We then added code to CAMx to read in these emissions directly from the CB6r2-speciated CSV files. This allowed us to avoid significant EPS3 development work in our project, but this approach could be revised to use EPS3 output in the future if our parameterization is eventually implemented in the baseline CAMx model.

In order to simulate the fire plumes without disrupting the anthropogenic sources already using the PiG module, we created a duplicate of the necessary PiG subroutines that are only used for the fire sources. We adjusted the new version of the piginit.f file (finn_piginit.f) to initialize the puffs for the fire sources so that they track CO and the non-parameterized species but do not calculate any chemistry within the puff (except for CO), thereby minimizing the computational cost of including the fires in the PiG routine. In adding the fire emissions to the simulated puffs, we used the WRAP diurnal cycle for fire emissions, as in McDonald-Buller et al. (2015). However, for our tests in this project, we assumed that all fire puffs are emitted at a constant altitude of 1 km, a reasonably average height, so that we didn't have to derive a new plume-height algorithm – this simplification could be removed in future work. In effect, this approach leads to the fire emissions being evenly spread out over the lower 19 model layers (0-2500 m agl).

We added a subroutine to the finn_pigdrive.f file to use the netCDF output files from the GEM parameterization to get the correct enhancement ratios for the parameterized species from the Lonsdale et al. (2015) parameterization based on the fuel type, the SZA at puff creation, the SZA five hours later, and the current grid temperature. The netCDF results use a python-based spline interpolation in terms of the evenly spaced input parameters described above (temperature, starting and ending SZA).

We adjusted the finn_pigdrive.f file to calculate the mass “leaked” (i.e., loss of mass while the puff is still too small to be added to the computational grid) or “dumped” (i.e., adding all mass in the puff to the grid when it reaches sufficient size) to the grid of the parameterized species based on the PiG calculated mass transfer of CO to the grid and the enhancement ratios obtained from the new parameterization subroutine. The mass of other species leaked or dumped

to the grid are calculated based on their FINN molar emission ratios to CO. Note that this simplification assumes that we can neglect the evolution of even short-lived VOCs within the puff on the five-hour time scale simulated by the parameterization. For aldehydes, this might be a reasonable approximation as they are both destroyed and produced by chemistry within the biomass burning plume. However, for alkenes this may overestimate the concentrations of these VOCs from fires in the model, as they are not lost for the first five hours after emission. However, since O₃ production from biomass burning is generally NO_x-limited, and we include the most important aldehyde (HCHO) and alkene (C₂H₄) species, our approach that just parameterizes the O₃ and NO_y chemistry of the biomass burning plumes should give reasonable results for the impact of fires on biomass burning.

We added a flag to optionally dump the puff to the grid on the first time step, and we use this option to examine the difference in the estimated impacts of fires on O₃ when the fire emissions are added directly to the grid and when the parameterization is used. All fire puffs are forced to dump to the grid at the end of 5 hours to avoid going beyond the bounds of our parameterization, so after 5 hours all chemistry is done on the CAMx grid.

2.6 Evaluation of the Impact of Fires on O₃

We used the modeling configuration from the 2012 CAMx modeling episode from TCEQ (May 16 – June 30, 2012) to evaluate the impact of the parameterization, as this episode and modeling configuration was used in the previous study of McDonald-Buller et al. (2015). However, in our evaluation we only had time to examine results on the 36 km outer grid, and did not perform runs on the nested 12 km and 4 km grids. Model input files for this episode are publically available at <https://www.tceq.texas.gov/airquality/airmod/data/tx2012>. In order to avoid double-counting fire emissions, we used the monthly-average point source files from the 2012 “baseline” case, as these do not include fire emissions.

We then ran CAMx for this modeling episode under three emission scenarios: a baseline “no fire” run that did not include fire emissions, a “grid fire” run that added the fire emissions to the main computational grid right at emission, and a “sub-grid fire” run that used our SAM-ASP based GEM parameterization within the PiG module to simulate the sub-grid scale chemistry of the biomass burning plumes. The impact of fire emissions on O₃ is then calculated as the difference between the “no fire” runs and either the “grid fire” or “sub-grid fire” runs. As in McDonald-Buller et al. (2015), we focus on the days of June 4 (when northwestern Mexico exhibited high fire activity) and June 28 (when fire activity became more pronounced in the Rocky Mountains).

Figure 16 shows the predicted impact of fires on O₃ at 17:00 CST on June 4, 2012 when the sub-grid parameterization is used. As expected, the impacts are generally positive, and the maximum impacts of up to 17 ppbv are near the fire sources. Figure 17 shows the impacts of the sub-grid scale parameterization on these results relative to the “grid fire” case, where the emissions are immediately added to the 36 km resolution grid. We see that the parameterization decreases the O₃ formation by up to 7 ppbv near the fire source, as expected by the better representation of NO_x losses near the source, but can lead to small increases in O₃ of 1-2 ppbv downwind relative to the grid fire case.

The results on June 28 are similar, but smaller in magnitude, consistent with the results of McDonald-Buller et al. (2015). Figure 18 again shows the generally positive impacts of fires on O₃, and Figure 19 shows the parameterization generally decreases the impacts of fires on O₃.

Thus we expect the sub-grid parameterization will reduce the overestimate of fire impacts near the source seen in many Eulerian grid models, but further evaluation of the current parameterization and its implementation in CAMx are needed before it is ready to be used in air quality planning and analysis.

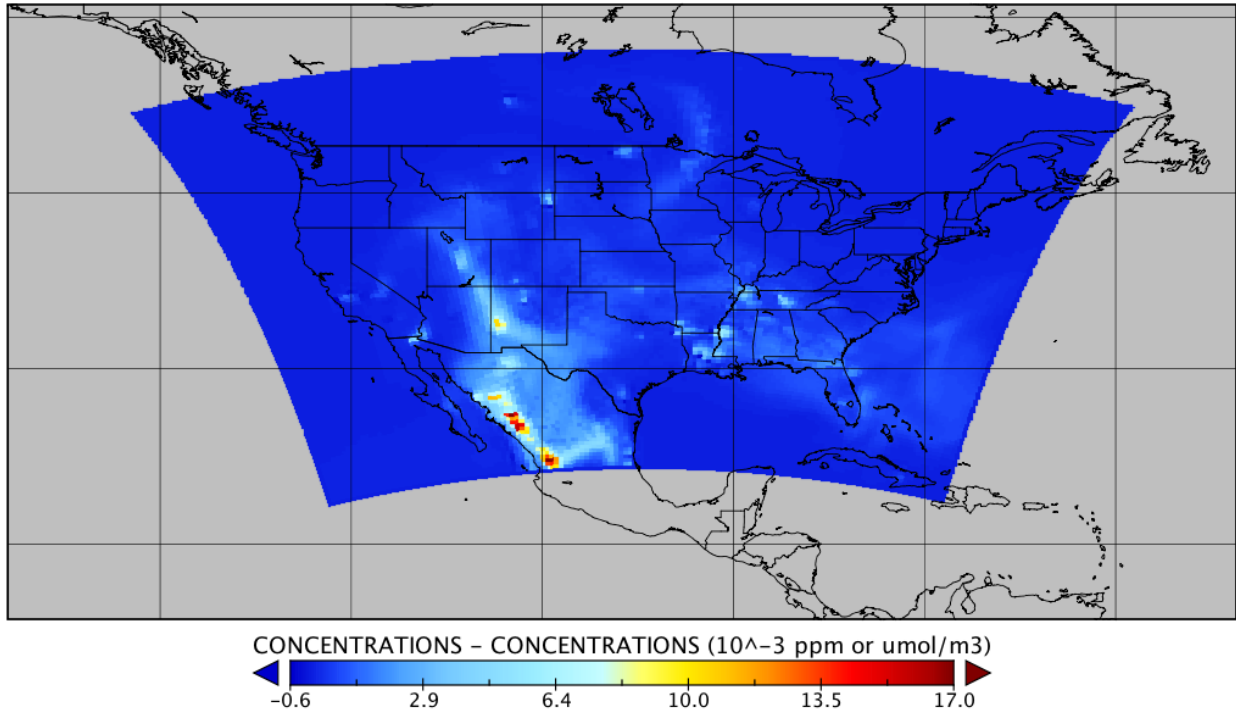


Figure 16. Difference in O_3 (ppbv) between the sub-grid parameterized fire case and the “no fire” case at 17:00 CST on June 4, 2012.

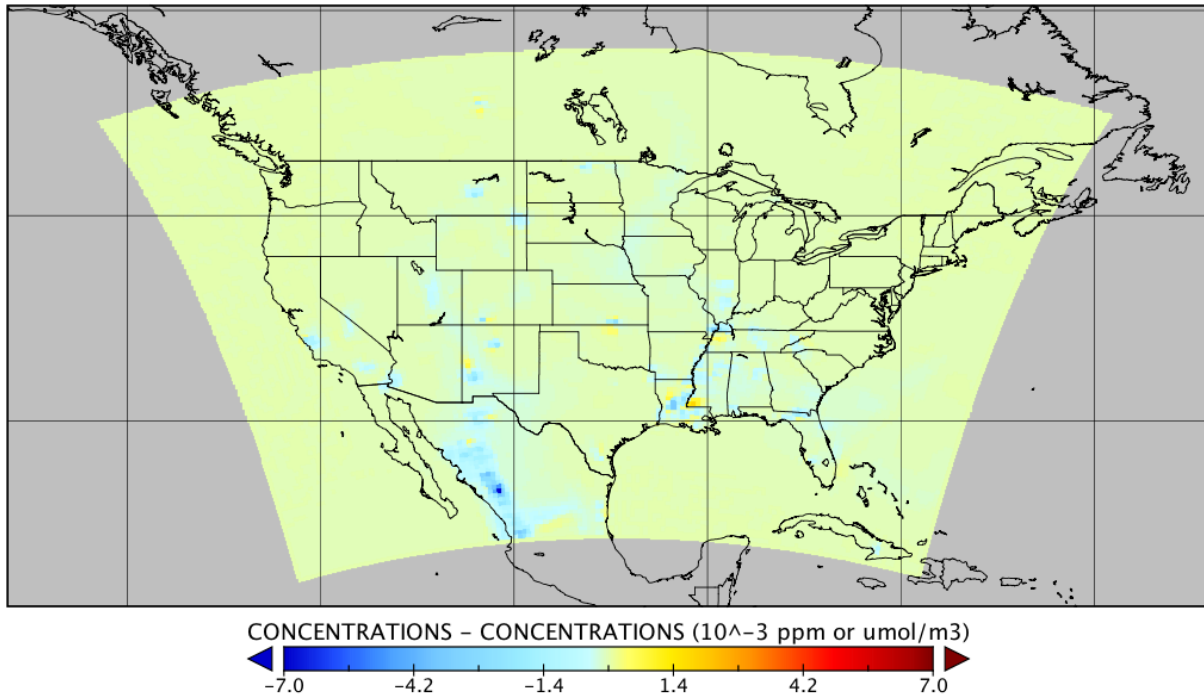


Figure 17. Difference in O_3 (ppbv) between the sub-grid parameterized fire case and the “grid fire” case at 17:00 CST on June 4, 2012.

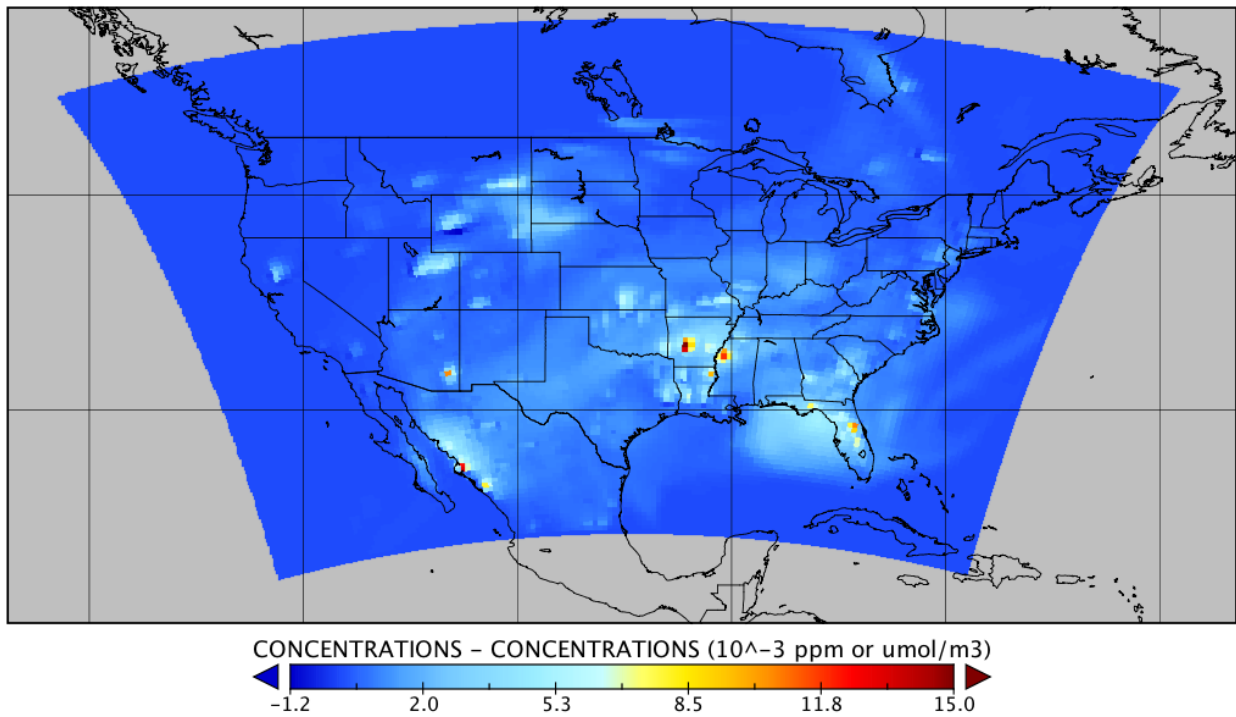


Figure 18. Difference in O_3 (ppbv) between the sub-grid parameterized fire case and the “no fire” case at 17:00 CST on June 28, 2012.

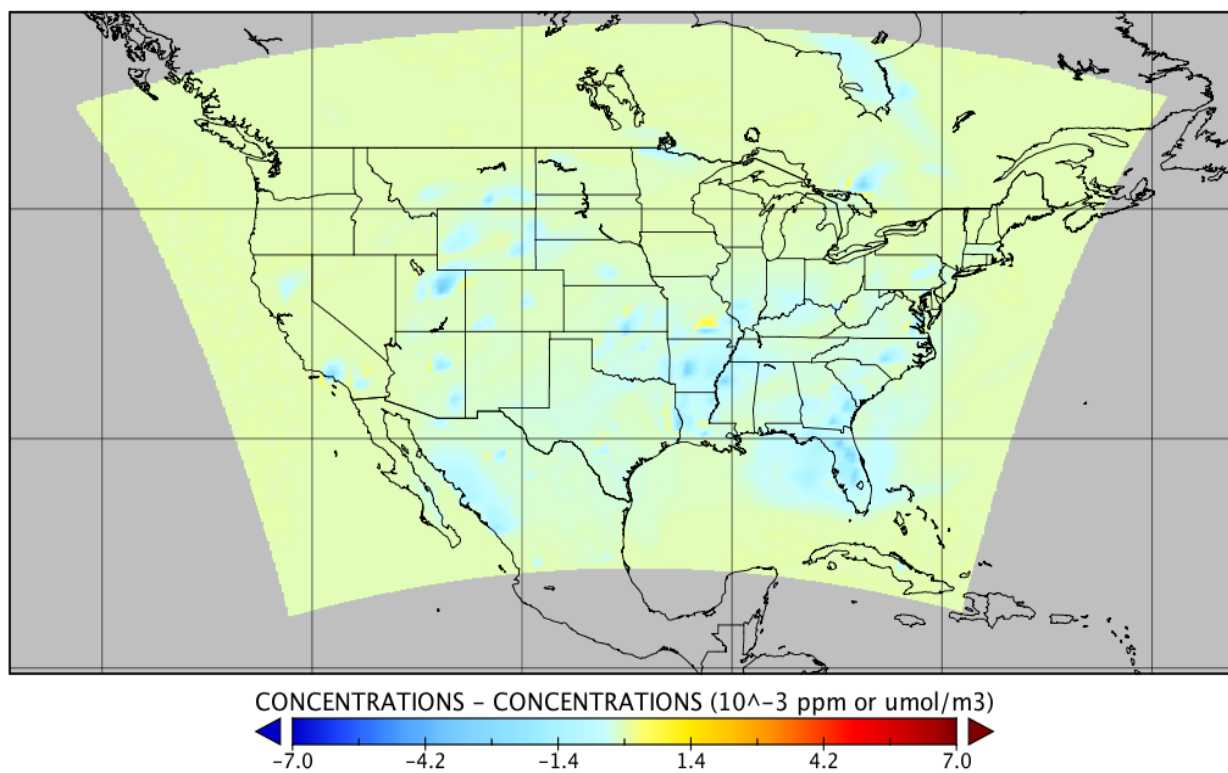


Figure 19. Difference in O₃ (ppbv) between the sub-grid parameterized fire case and the “grid fire” case at 17:00 CST on June 28, 2012.

3 Impact of Long-range Transport of BB Pollution on Texas Air Quality

One danger of using global 3D Eulerian chemical transport models like GEOS-Chem to estimate the impact of long-range transport of BB plumes is that the numerical diffusion in these models tends to reduce the plume concentrations, thus potentially altering the chemistry and leading to incorrect boundary conditions for regional air quality studies (e.g., Rastigejev et al., 2010). Lagrangian models, like STILT-ASP (Section 1.3.4), are not subject to this numerical diffusion and thus can be a useful check on the predictions of the 3D CTMs. In this task, we examined the CAMx boundary conditions produced from GEOS-Chem for the 2012 TCEQ CAMx modeling episode for periods where the boundaries of the North American (36 km) nest were impacted by biomass burning from outside the CAMx domain, mainly from fires in Mexico and Central America (Section 3.1). We ran the STILT-ASP model for a selected set of these “boundary” receptors that have a relatively high impact on Texas air quality to determine how this “Lagrangian” estimate of the impact of fires on the boundary conditions for CO, O₃, NO_y species, OA, etc., differs from the “Eulerian” estimate from GEOS-Chem (Section 0). We then used STILT-ASP to estimate the impact of out-of-domain (Section 3.3) and in-domain (Section 3.4) fires on air quality in Texas, in the second case comparing the STILT-ASP estimates with the CAMx-based estimates of McDonald-Buller et al. (2015).

3.1 Identifying Biomass Burning Impacts on the CAMx Boundaries

We analyzed the CO mixing ratios along the outer boundary of the 36-km CAMx/GEOS-Chem model grid for the May and June 2012 TCEQ modeling episodes (as in Figure 22). Regions with CO concentration ≥ 120 ppbv were reduced to those episodes likely to be due to biomass burning emissions entering the domain. This was first done by examining each edge of the boundary grid and calculating the total number of three-hour observations exceeding the 120 ppbv threshold for each day. Figure 20 shows the example results for May 2012, while Figure 21 shows the results for June 2012.

While our original plan was to look at the impact of inter-hemispheric transport of fires, there is little evidence of biomass burning from Asia impacting the western edge of the CAMx domain in May and June of 2012. In addition, the high CO values along the eastern boundaries of the domain are generally due to outflow of pollution from the continental US, and not from biomass burning transport into the domain. The northern boundary spikes may be due to biomass burning in the Canadian boreal forest, but these remote fires likely have less of an impact on Texas air quality than closer fires in Mexico and Central America.

We focused on the southern boundary spikes that are likely due to biomass burning in Mexico and Central America. Several days (May 2, 3, 5, 6, 11, and 24, as well as June 1, 2, 3, 4, and 30) were selected for further investigation. Note that this does not include the June 4 and June 28 fire events discussed in Section 3.4 and in McDonald-Buller et al. (2015), as these events were due to fires within the CAMx domain (northwestern Mexico and the Rocky Mountains, respectively), not fires outside of the domain.

We then used the STILT-ASP model to confirm that these periods were likely affected by biomass burning outside of the CAMx domain. For example, a STILT-ASP 2-day back-trajectory for one receptor along the southern CAMx boundary on May 11, 2012 is shown in Figure 22, along with one receptor along the eastern boundary. This shows that the fire CO along the southern boundary in this case is a result of smoke from fires in the Yucatan Peninsula being

transported to the southern boundary of the CAMx domain. This is in contrast to the high CO observed on the eastern boundary of the CAMx domain, which appears to be a result of anthropogenic outflow from the continental US rather than biomass burning. After this analysis, we selected a set of four periods that were analyzed to compare the GEOS-Chem derived boundary conditions with the STILT-ASP simulations (Section 0): May 11 at 09:00 UTC (03:00 CST), May 24 at 18:00 UTC (12:00 CST), June 1 at 18:00 UTC (12:00 CST), and June 2 at 12:00 UTC (06:00 CST).

In order to determine whether or not the identified remote wildfires were likely to have impacted Texas air quality, the STILT model was then run for a selection of cases in order to determine the one-week air flow history for the city of Austin (e.g., Figure 23). This evaluation suggested that May 5, May 11, and May 25 were days where biomass burning from outside the domain appeared to have a significant impact on both the CAMx boundary conditions and Texas air quality, and these were selected for further analysis using STILT-ASP (Section 3.3). In addition, we ran STILT-ASP for the city of El Paso on the two dates identified in McDonald-Buller et al. (2015) as having significant impacts on Texas O₃ from in-domain: June 4 and June 28.

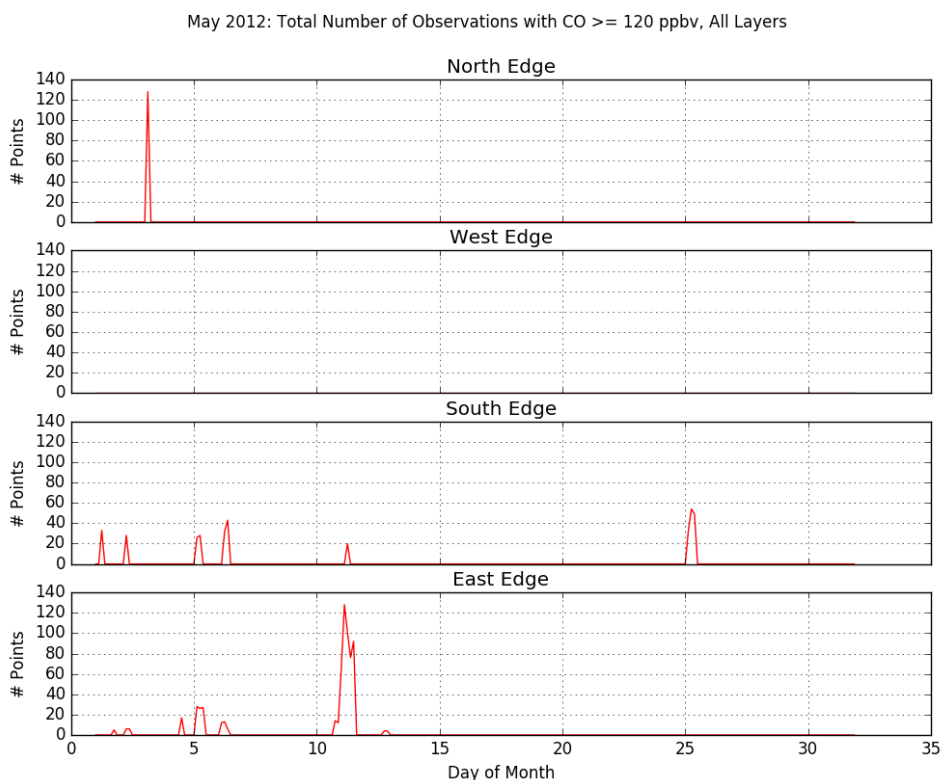


Figure 20. Number of 3-hour observations exceeding 120 ppbv CO for each edge of the 36-km GEOS-Chem boundary grid for May 2012.

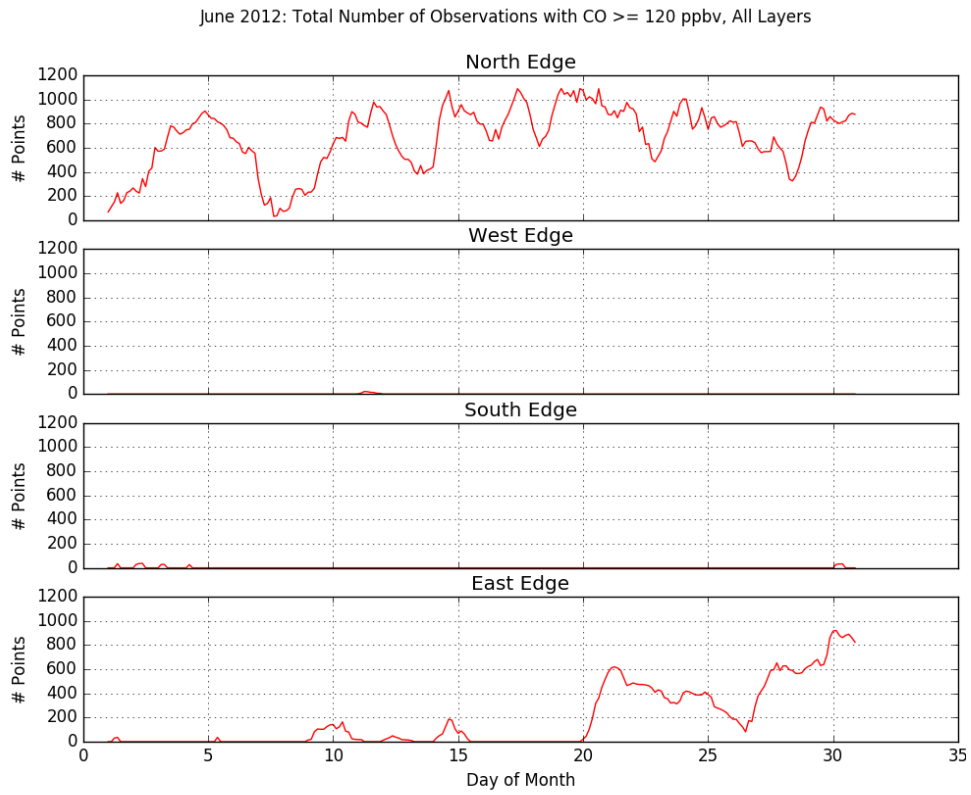


Figure 21. Number of 3-hour observations exceeding 120 ppbv CO for each edge of the 36-km GEOS-Chem boundary grid for June 2012.

CO (ppbv) along STILT-ASP Trajectories and GEOS-Chem Boundary Grid
(May 11, 2012, 86 m altitude, 09:00:00 UTC)

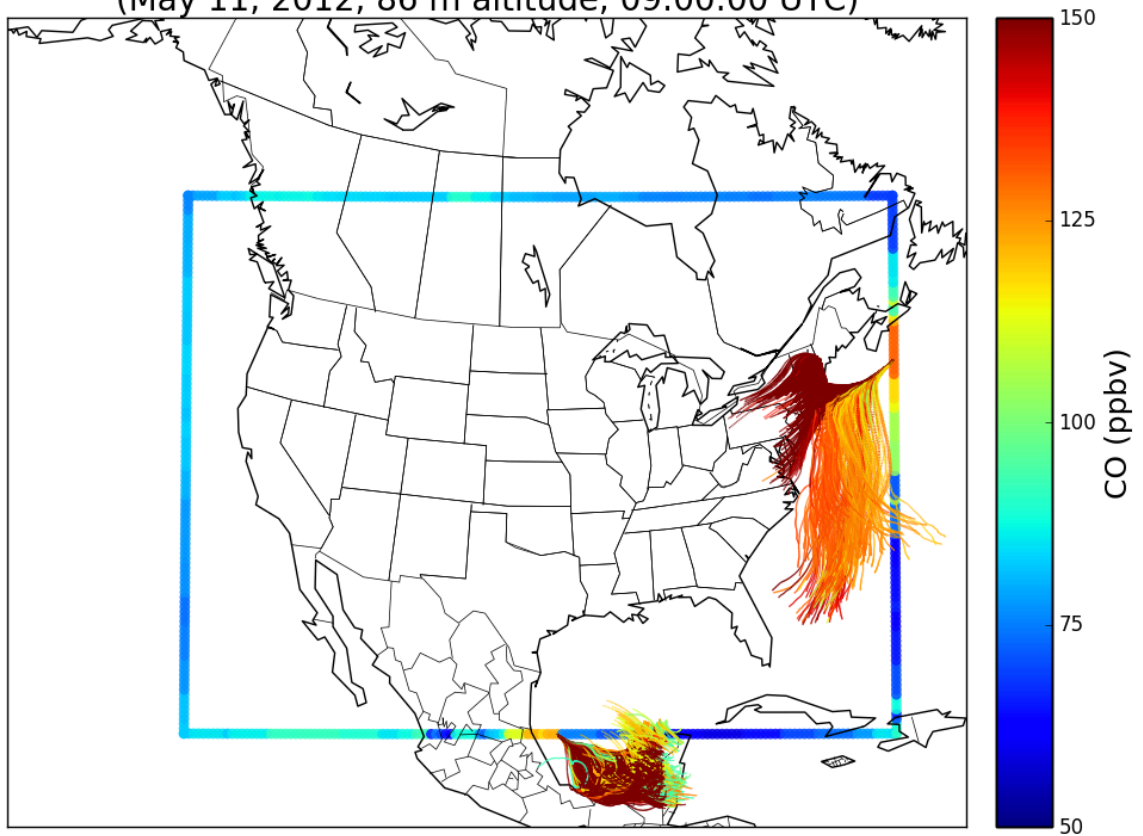


Figure 22. CO along two 2-day STILT-ASP back-trajectory calculations (500 Lagrangian parcels each) overlotted on the GEOS-Chem boundary conditions for May 11, 2012 at 09:00 UTC.

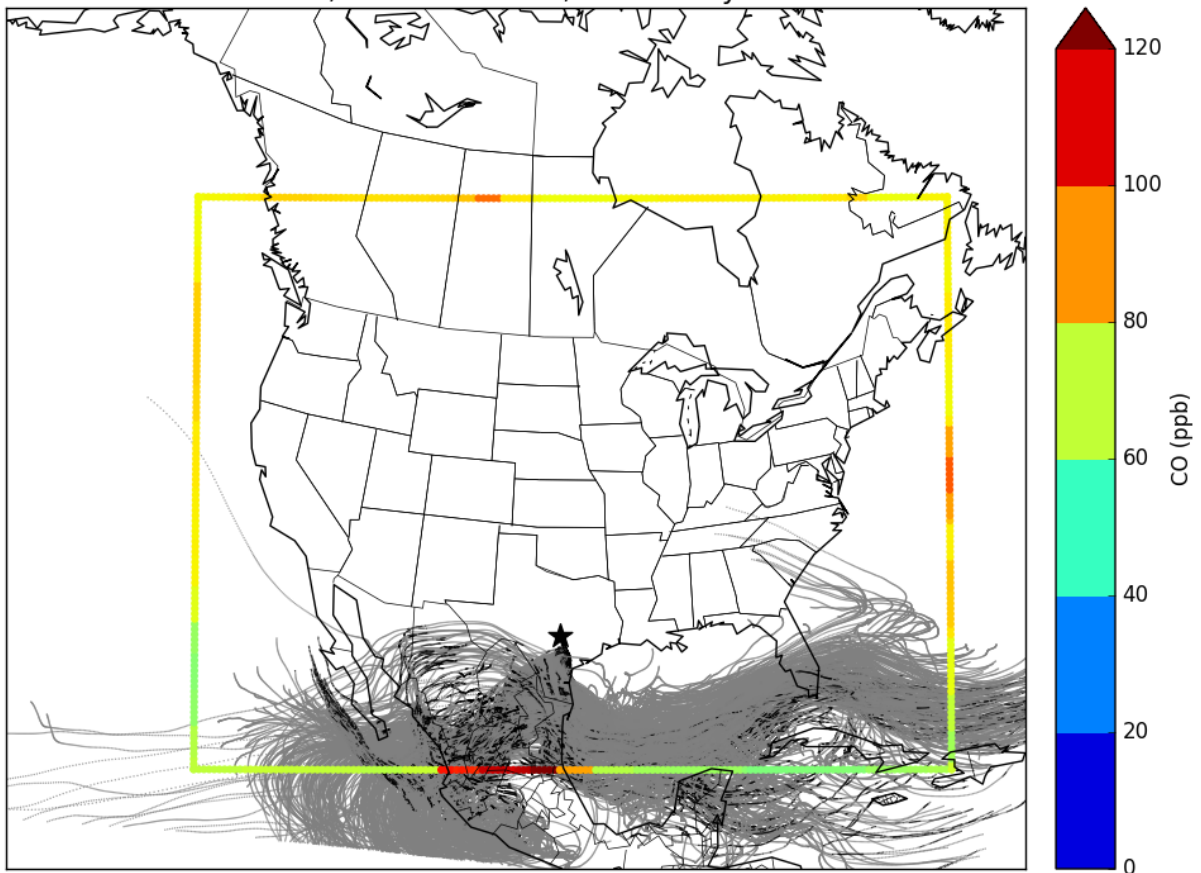


Figure 23. STILT 7-day back trajectory run (500 parcels) for May 5, 2012 for the Austin, TX site. Note the southerly flow, indicating the possibility that wildfires in Mexico may impact the Austin site.

3.2 Examining CAMx Boundary Conditions with STILT-ASP

3.2.1 Impact of Fires on CO

We first analyzed our STILT-ASP simulations for the impacts of fire CO on the boundaries of the TCEQ modeling domain by running STILT-ASP v2.0 *without* gas-phase chemistry (but with all emissions) for each grid box along the southern boundary of the CAMx 36 km domain for our four selected time periods: May 11 at 09:00 UTC (03:00 CST, Figure 24), May 24 at 18:00 UTC (12:00 CST, Figure 25), June 1 at 18:00 UTC (12:00 CST, Figure 26), and June 2 at 12:00 UTC (06:00 CST, Figure 27). STILT-ASP v2.0 was run with 500 Lagrangian parcels for seven-day back-trajectories using NARR meteorology and the NCAR MOZART-4/GEOS-5 chemical forecasts for boundary conditions. Fire emissions were taken from the FINN inventory (Wiedinmyer et al., 2011), biogenic emissions from the MEGAN model (Guenther et al., 2006), and anthropogenic emissions from the TCEQ 2012 modeling episode. Chemistry was not calculated for these simulations to reduce run time and thus increase the number of points that can be calculated.

These results show the same high bias in STILT-ASP v2.0 simulations of CO that was observed during the DISCOVER-AQ period in Houston (Alvarado et al., 2017), as STILT-ASP v2.0 consistently predicts larger CO concentrations than GEOS-Chem. However, the STILT-ASP v2.0 simulations also see a lot of fine scale structure in the impacts of fires on CO along the boundaries that is not captured by the low-resolution boundary conditions from GEOS-Chem. For example, Figure 24 shows that there was a large impact of fires along the southern boundary of the CAMx domain on May 11, 2012, with the CO from fires estimated by the no chemistry STILT-ASP v2.0 runs reaching a peak of about 150 ppbv. In addition, STILT-ASP is able to identify that a related spike in CO to the east of this fire plume is not due to fires, but from other CO sources in the region. The GEOS-Chem results do show an enhancement in CO that appears consistent with the biomass burning impacts predicted by STILT-ASP, but this enhancement is much smaller in magnitude, and does not have the same horizontal extent or peak location as predicted by STILT-ASP. These differences may be due to differences in the fire emission inventory used in GEOS-Chem (i.e., GFED; van der Werf et al., 2010) from the FINN v1.5 inventory used in STILT-ASP v2.0, or due to the large horizontal resolution of GEOS-Chem, such that GEOS-Chem automatically mixes all fire emissions within a given model grid box, whereas STILT-ASP v2.0 simulates each location individually.

Similar results are seen for the other three periods examined. On May 24, STILT-ASP estimated a very sharp spike in biomass burning CO with a peak magnitude of over 30 ppbv (Figure 25). On June 1, four individual fire plumes can be identified, with peak magnitudes of fire CO between 6 and 16 ppbv (Figure 26). On June 2, we see two very narrow fire plumes mixed in with a general enhancement of CO that is reflected in the GEOS-Chem boundary conditions (Figure 27).

3.2.2 Impact of Fires on O₃, NO_x, and PAN

In order to look at the impacts of fires on O₃, NO_x, and PAN along the boundaries, we ran STILT-ASP v2.0 with chemistry for 3-day back-trajectories for seven points with substantial fire CO impacts on May 11, 2012 at 09:00 UTC (03:00 CST) and the three points covering the fire CO peak on May 24, 2012 at 18:00 UTC (12:00 CST). The emissions used were the same as those used for the no-chemistry runs.

3.2.2.1 May 11, 2012 Cases

Figure 28 shows the STILT-ASP v2.0 predictions for O₃ along the southern boundary for the seven May 11, 2012 cases with and without fires. The STILT-ASP v2.0 results suggest that fires are contributing up to 24 ppbv of O₃ along the boundary. However, the modeled impact of fires on CO is also large (up to 141 ppbv, Figure 29), giving an average $\Delta O_3/\Delta CO$ of 0.15 mol/mol (Figure 30). This level of O₃ enhancement relative to CO ($\Delta O_3/\Delta CO$) is consistent with the review of Jaffe and Wigder (2012), which found that the average $\Delta O_3/\Delta CO$ for smoke aged about 1-2 days was 0.2 ± 0.1 mol/mol. However, the absolute O₃ concentrations predicted are much higher than the GEOS-Chem output, and appear high for nighttime conditions such as these, possibly due to an underestimate of O₃ loss at night by STILT-ASP v2.0.

In addition, STILT-ASP v2.0 gives a curious result for the impact of fires on NO_x and PAN concentrations along the southern boundary. Figure 31 shows that adding the fire emissions actually *decreases* the NO_x concentration simulated by STILT-ASP v2.0 for five of the seven cases examined here, and that the estimated NO_x concentrations are about an order of magnitude smaller than the GEOS-Chem values. The estimated PAN concentrations are also smaller than the GEOS-Chem values by a factor of five, and while five cases show an increase in PAN due to fire emission, the other two show a decrease (Figure 32). This appears to be due to the chemistry of the fire S/IVOCs included in ASP v2.1. As described in Alvarado et al. (2015), our assumed chemistry for these lumped, unidentified compounds assumes that for every NO that reacts with the peroxy radicals produced by the S/IVOC + OH reaction, only 0.6 NO₂ molecules are produced, with the rest producing alkyl nitrate S/IVOCs which are assumed to be able to continue to react with OH and consume NO_x indefinitely. This was necessary to prevent the ASP v2.1 model from overestimating the formation of O₃ in the first five hours after plume emission in the study of Alvarado et al. (2015). However, over the seven-day back trajectories simulated here, this chemistry of the biomass burning S/IVOCs not only consumes all the fire NO_x, it consumes some of the anthropogenic NO_x as well that otherwise would be available for O₃ formation, in this case resulting in a net loss of NO_x and PAN when fire emissions are added. This suggests that the S/IVOC chemistry in ASP v2.1 may need to be re-examined for the longer time periods used in STILT-ASP v2.0.

Examination of the concentrations along the back-trajectories for one of these cases supports this explanation. Figure 33 shows the CO concentrations along the 500 back-trajectories for one of the boundary receptors with fire emissions. We can see that the Lagrangian parcels pick up their CO enhancement while passing over the fires in the Yucatan Peninsula. Figure 34 shows that the Lagrangian parcels also pick up NO_x over these fires, but that it is rapidly depleted by the S/IVOC chemistry. The results for PAN are similar (Figure 35), with an enhancement over the Yucatan that is rapidly depleted.

Figure 36 shows the results for O₃. Parcels that pass over the Yucatan from the SE see a rapid increase in their O₃ levels from their initially low values (< 30 ppbv). However, the parcels that start over Mexico within the CAMx domain begin with high O₃ values, which stay high for the entire three-day back-trajectory. This indicates that STILT-ASP v2.0 may have trouble simulating the diurnal cycle of O₃.

3.2.2.2 May 24, 2012 Cases

Figure 37 shows the STILT-ASP v2.0 predictions for O₃ along the southern boundary for the three May 24 cases with and without fires. These results suggest that fires are contributing up to 9.1 ppbv of O₃ along the boundary. However, the modeled impact of fires on CO is also large (up to 35 ppbv, Figure 38), giving an average $\Delta O_3/\Delta CO$ of 0.26 mol/mol, consistent with the average value of 0.2 ± 0.1 mol/mol from the review of Jaffe and Wigder (2012). The absolute O₃ concentrations are again higher than the GEOS-Chem output, but not as dramatically as in the May 11 cases.

For these three fire cases, Figure 39 shows that adding the fire emissions increases the NO_x concentration simulated by STILT-ASP v2.0, and that estimated NO_x concentrations are a factor of two larger than the GEOS-Chem values, in contrast with the May 11 cases. The STILT-ASP v2.0 estimated PAN concentrations are larger than the GEOS-Chem values by an average of 60%, but all three cases show an increase in PAN due to fire emission (Figure 40). Thus the STILT-ASP v2.0 results for these daytime cases appear more consistent with our conceptual model of the impacts of fires on these species than the nighttime May 11 cases.

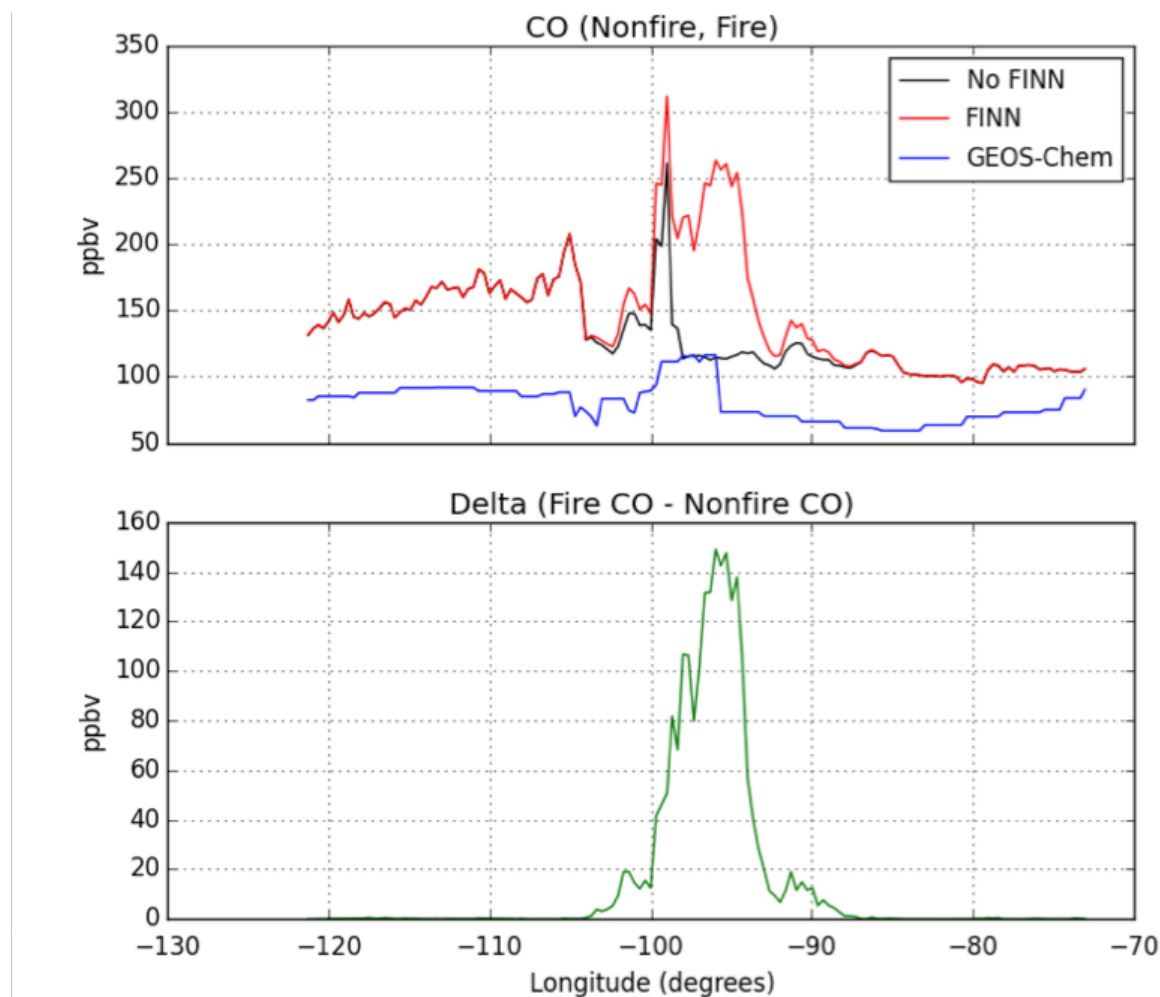


Figure 24. (top panel) Simulated CO mixing ratios (ppbv) from STILT-ASP v2.0 no-chemistry 7-day back-trajectory run results with (red line) and without (black line) FINN fire emissions for

May 11, 2012 at 09:00 UTC (03:00 CST) at 86 m above ground level along the southern boundary of the CAMx 36 km domain. The blue line shows the GEOS-Chem boundary condition results. (bottom panel) Difference between the with-fire and without-fire emissions STILT-ASP simulations.

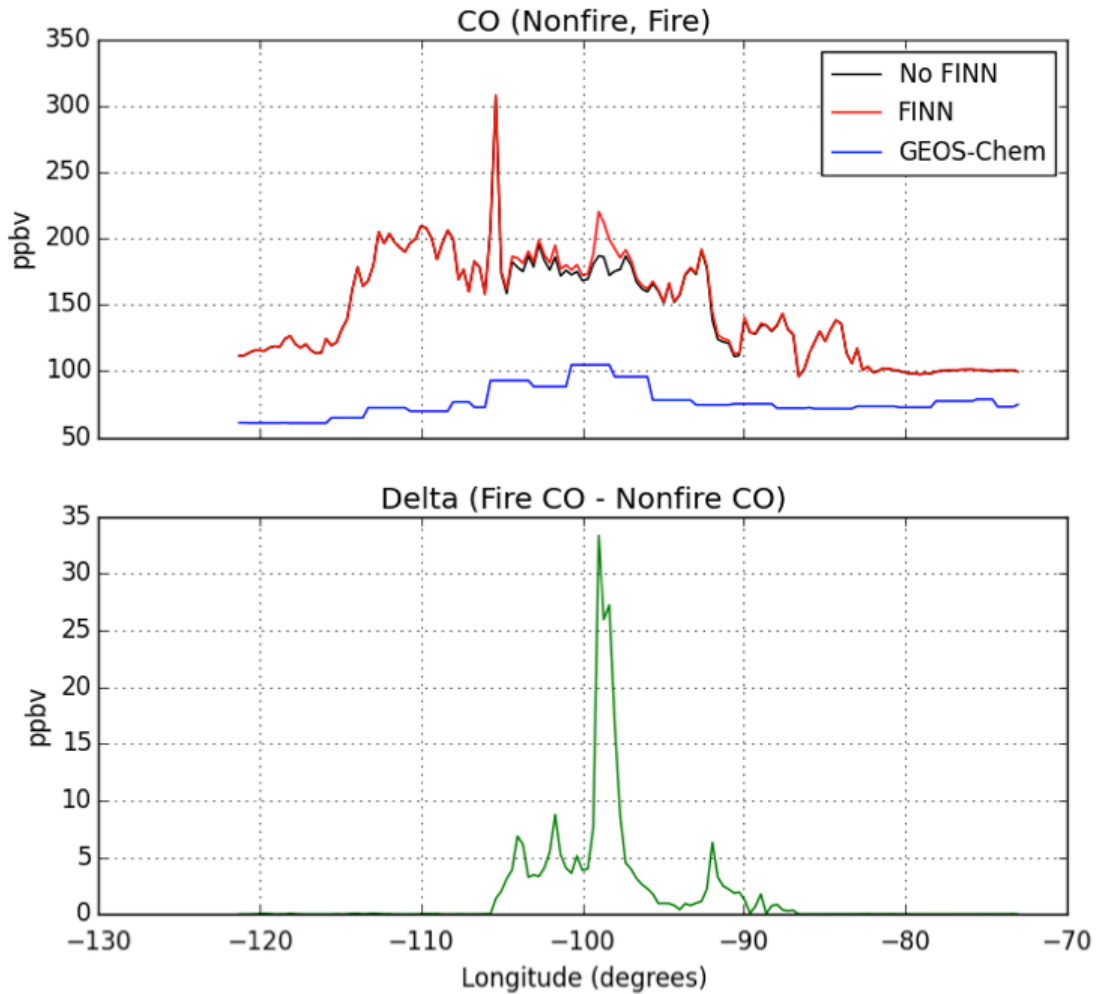


Figure 25. As in Figure 24, but for May 24, 2012 at 18:00 UTC (12:00 CST) at 86 m above ground level.

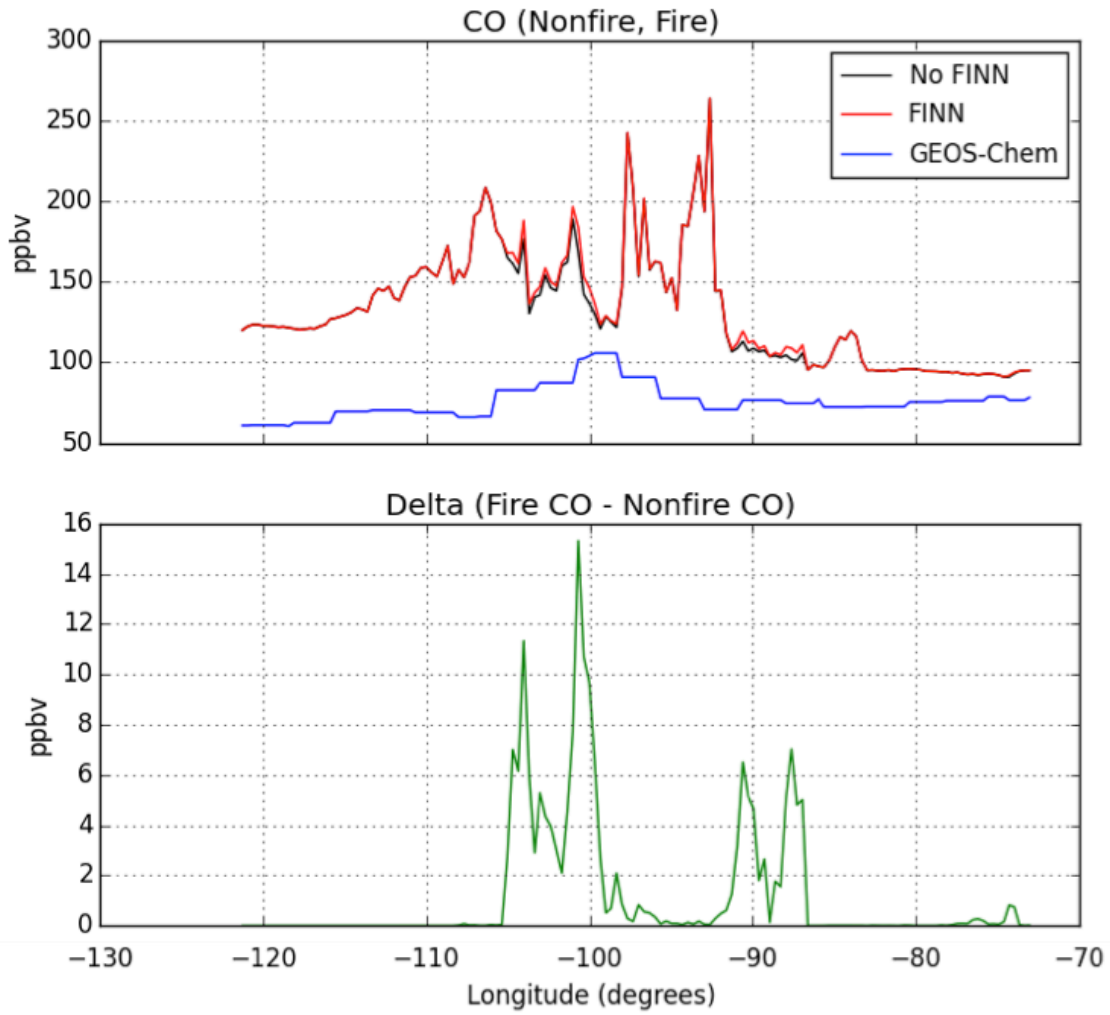


Figure 26. As in Figure 24, but for June 1, 2012 at 18:00 UTC (12:00 CST) at 86 m above ground level.

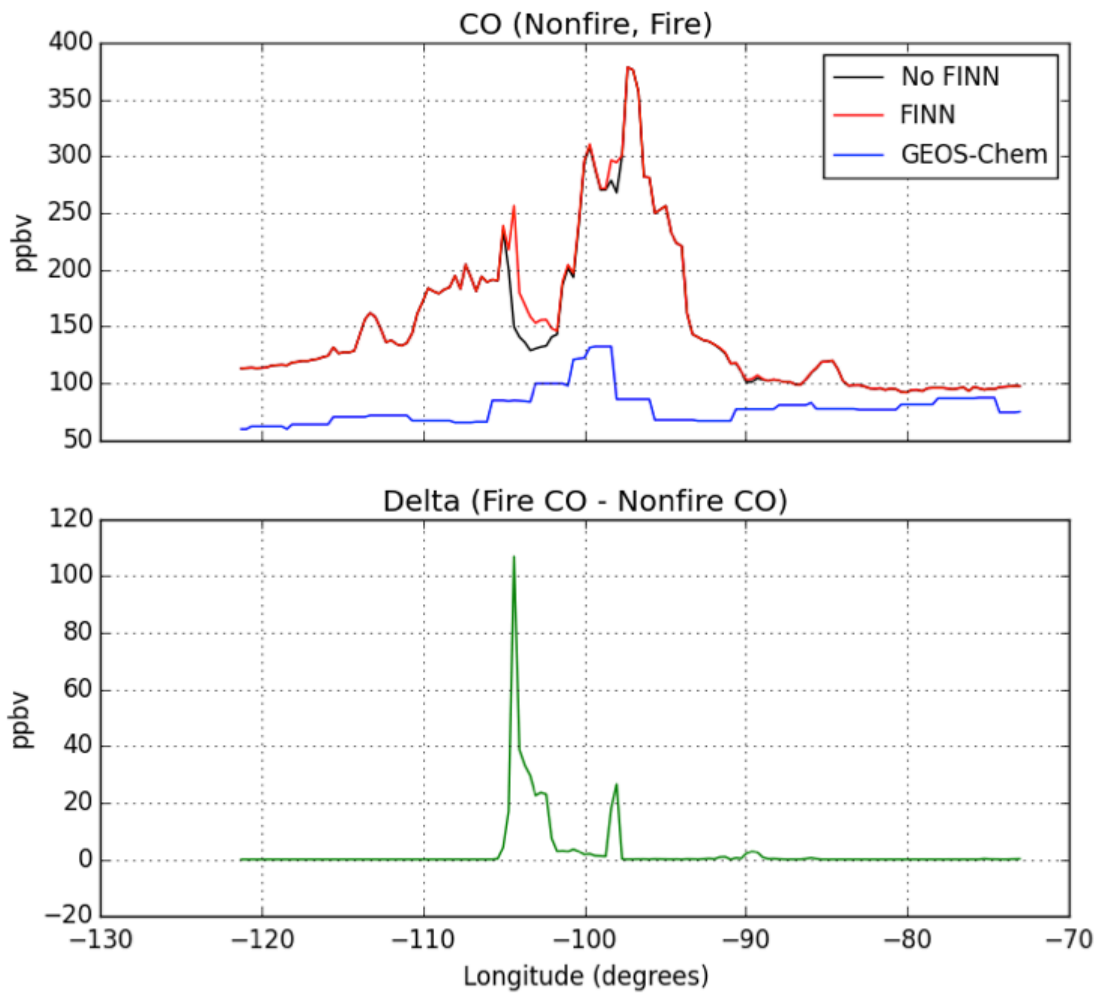


Figure 27. As in Figure 24, but for June 2, 2012 at 12:00 UTC (06:00 CST) at 86 m above ground level.

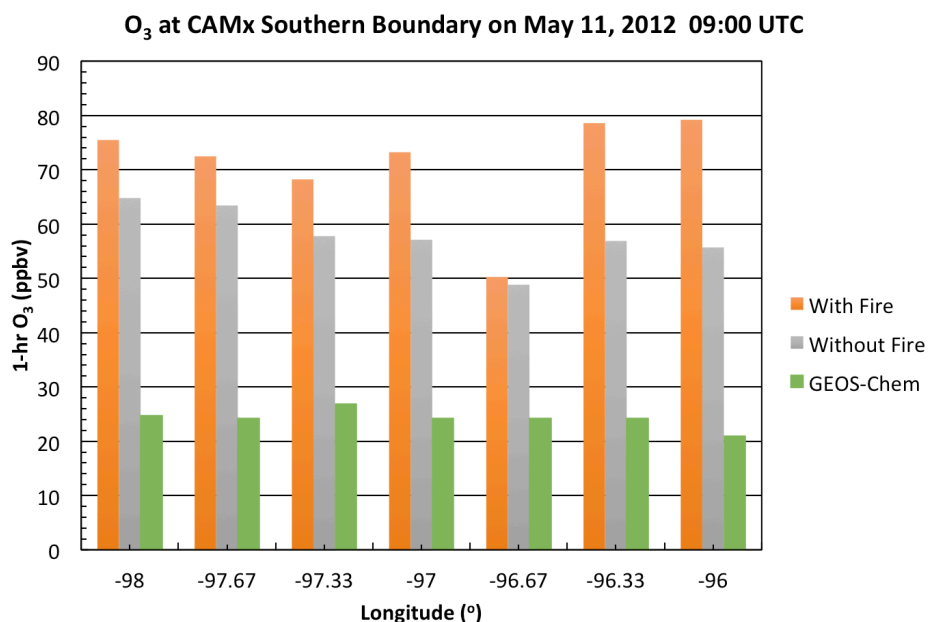


Figure 28. STILT-ASP v2.0 calculations of O₃ (ppbv) along the southern CAMx domain boundary with fire emissions (orange) and without fire emissions (grey) for 09:00 UTC (03:00 CST) on May 11, 2012 compared with the GEOS-Chem derived boundary condition values (green).

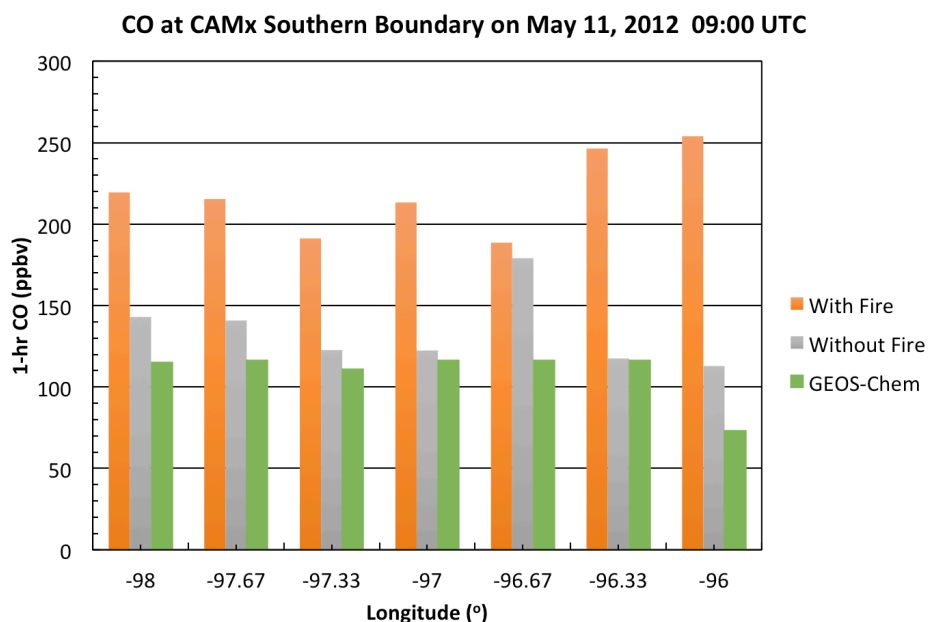


Figure 29. STILT-ASP v2.0 calculations of CO (ppbv) along the southern CAMx domain boundary with fire emissions (orange) and without fire emissions (grey) for 09:00 UTC (03:00 CST) on May 11, 2012 compared with the GEOS-Chem derived boundary condition values (green).

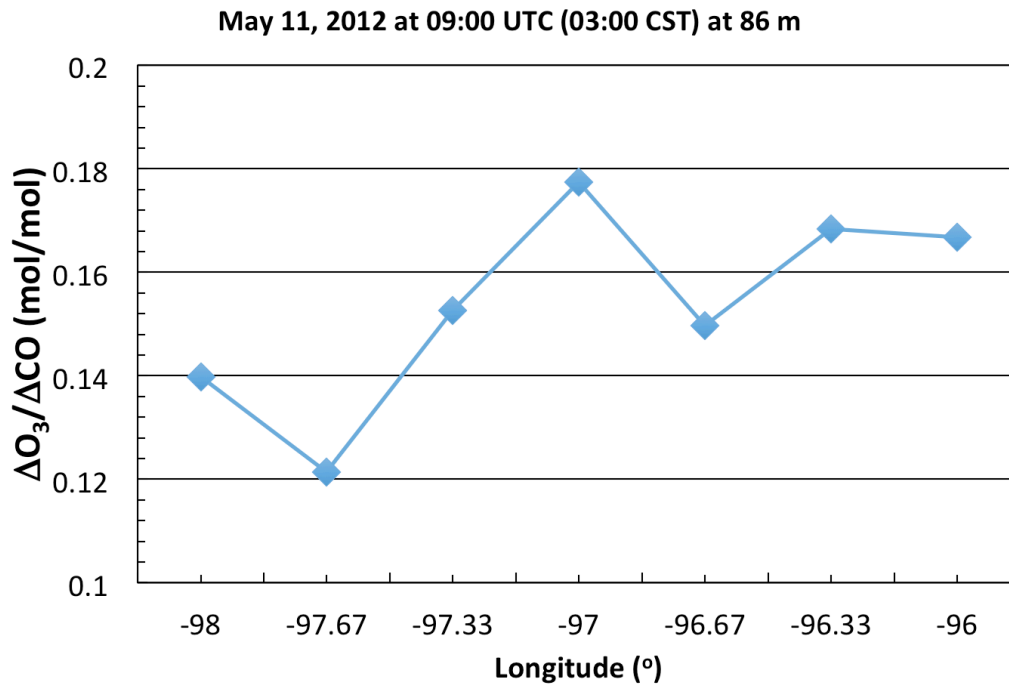


Figure 30. STILT-ASP v2.0 calculations of $\Delta O_3/\Delta CO$ (mol/mol) along the southern CAMx domain boundary for 09:00 UTC (03:00 CST) on May 11, 2012.

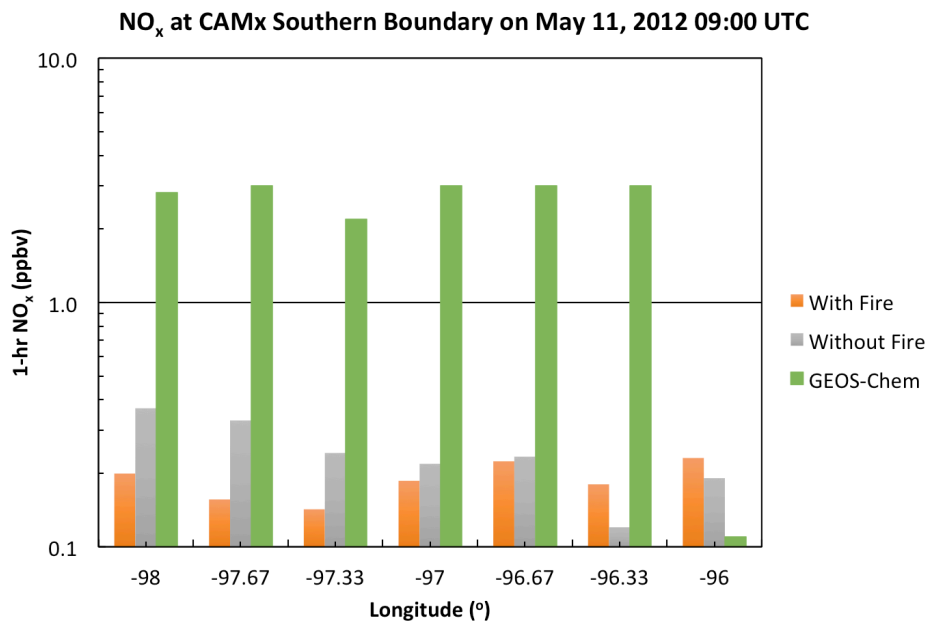


Figure 31. STILT-ASP v2.0 calculations of O_3 (ppbv) along the southern CAMx domain boundary with fire emissions (orange) and without fire emissions (grey) for 09:00 UTC (03:00 CST) on May 11, 2012 compared with the GEOS-Chem derived boundary condition values (green).

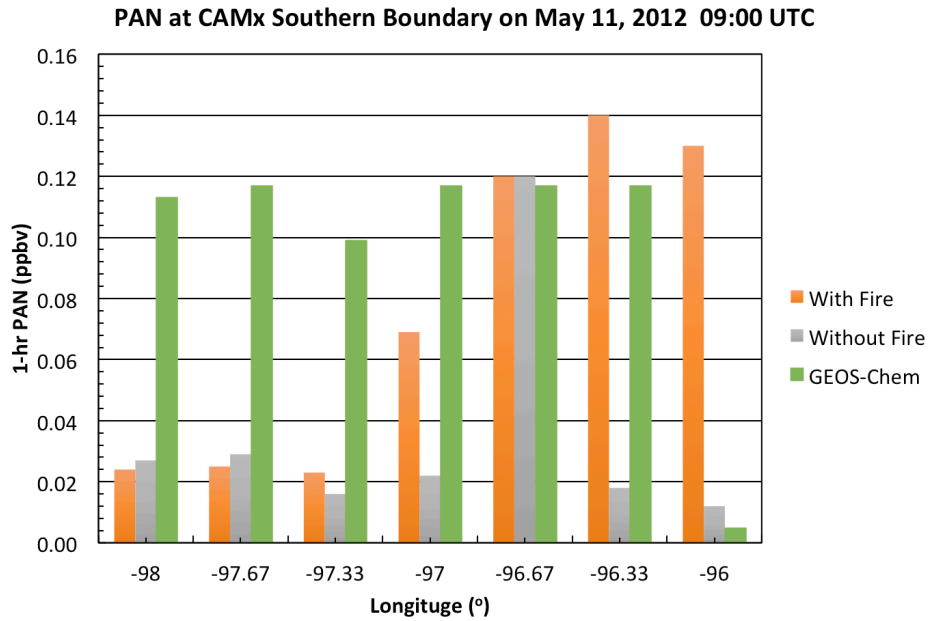


Figure 32. STILT-ASP v2.0 calculations of PAN (ppbv) along the southern CAMx domain boundary with fire emissions (orange) and without fire emissions (grey) for 09:00 UTC (03:00 CST) on May 11, 2012 compared with the GEOS-Chem derived boundary condition values (green).

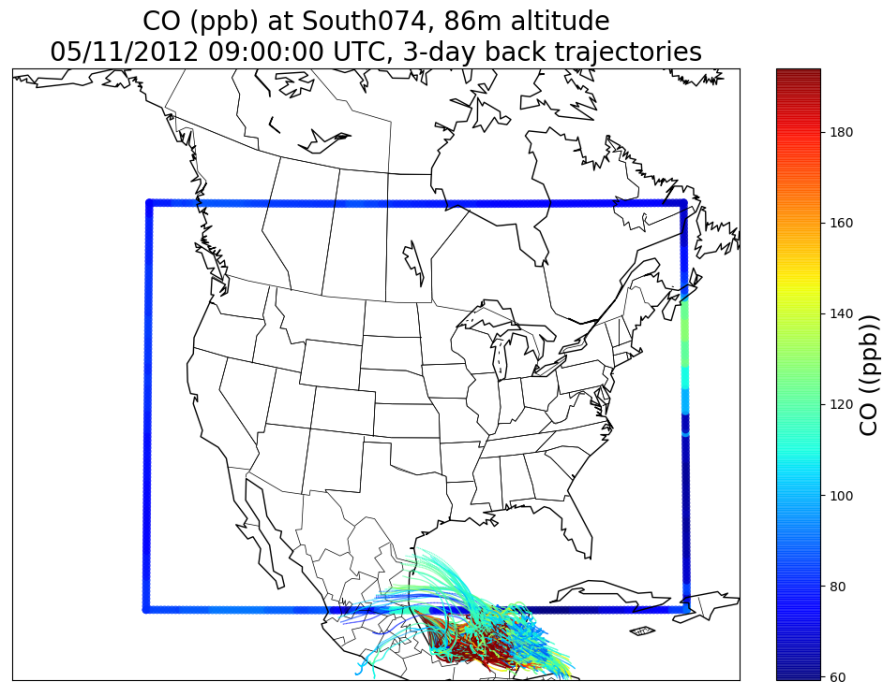


Figure 33. CO (ppbv) from a 3-day back trajectory run of STILT-ASP v2.0 for May 11, 2012 at 09:00 UTC (03:00 CST) for the 74 grid box of the southern boundary of the CAMx modeling domain. The GEOS-Chem boundary conditions are also shown.

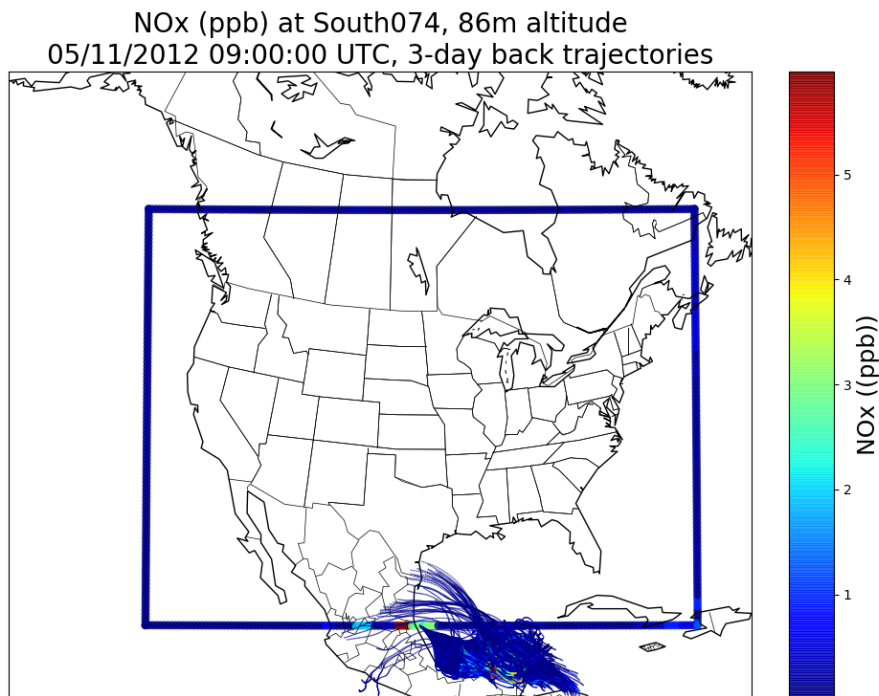


Figure 34. NO_x (ppbv) from a 3-day back trajectory run of STILT-ASP v2.0 for May 11, 2012 at 09:00 UTC (03:00 CST) for the 74 grid box of the southern boundary of the CAMx modeling domain. The GEOS-Chem boundary conditions are also shown.

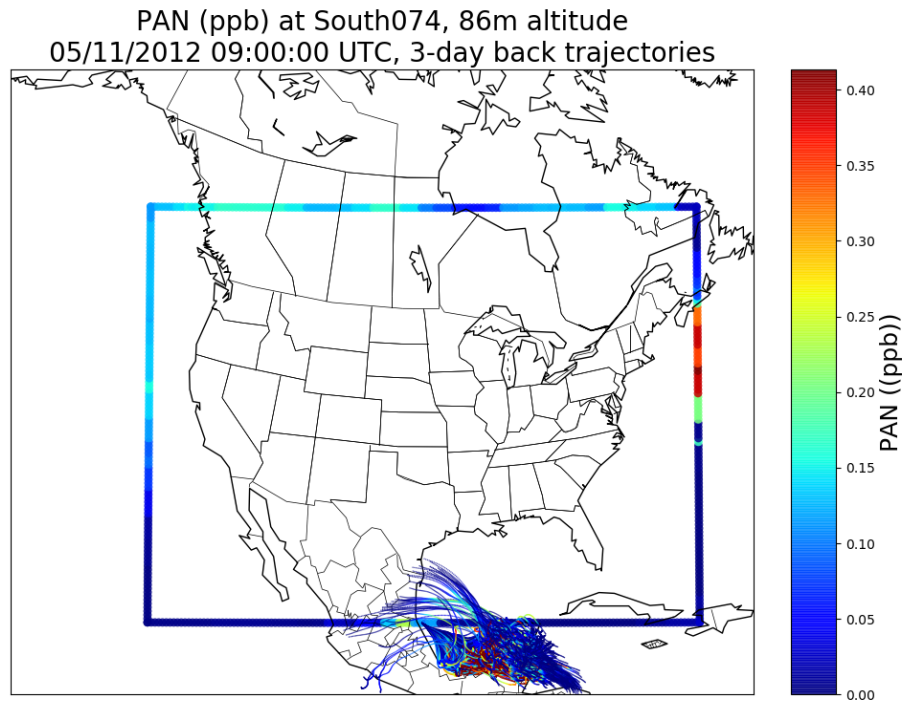


Figure 35. PAN (ppbv) from a 3-day back trajectory run of STILT-ASP v2.0 for May 11, 2012 at 09:00 UTC (03:00 CST) for the 74 grid box of the southern boundary of the CAMx modeling domain. The GEOS-Chem boundary conditions are also shown.

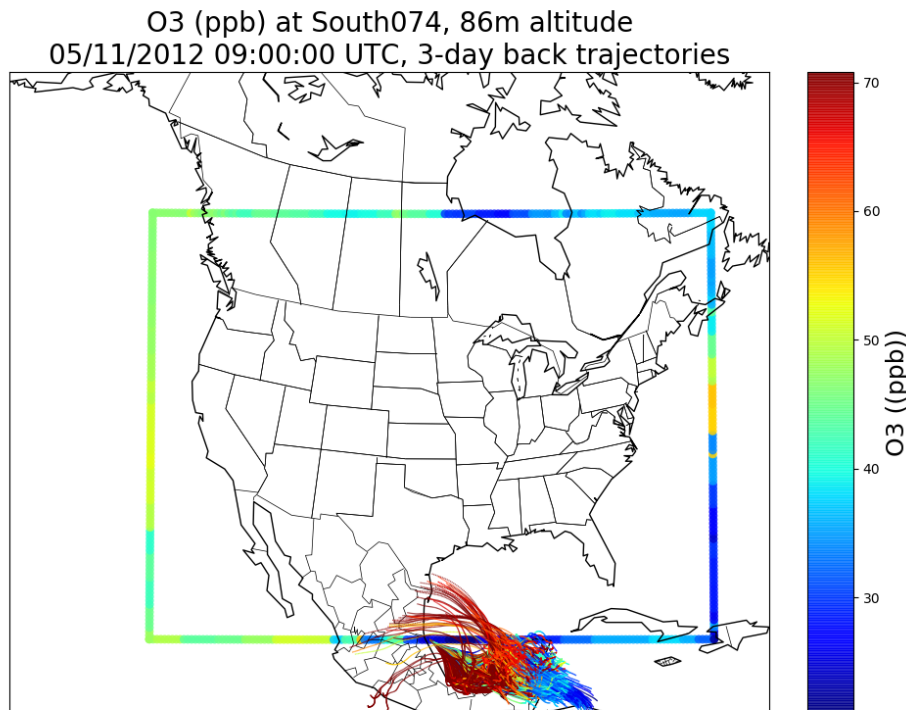


Figure 36. O₃ (ppbv) from a 3-day back trajectory run of STILT-ASP v2.0 for May 11, 2012 at 09:00 UTC (03:00 CST) for the 74 grid box of the southern boundary of the CAMx modeling domain. The GEOS-Chem boundary conditions are also shown.

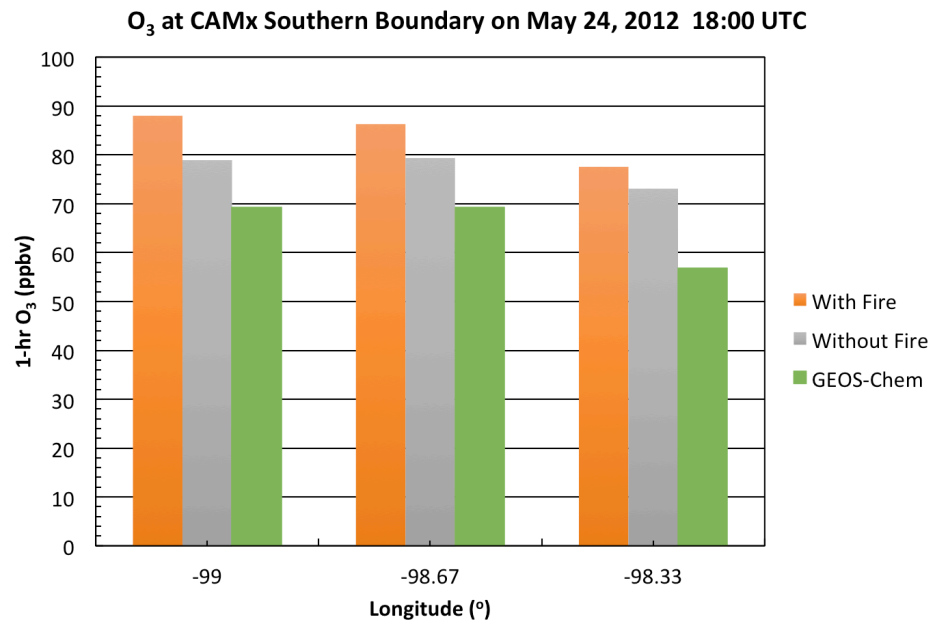


Figure 37. STILT-ASP v2.0 calculations of O₃ (ppbv) along the southern CAMx domain boundary with fire emissions (orange) and without fire emissions (grey) for 18:00 UTC (12:00 CST) on May 24, 2012 compared with the GEOS-Chem derived boundary condition values (green).

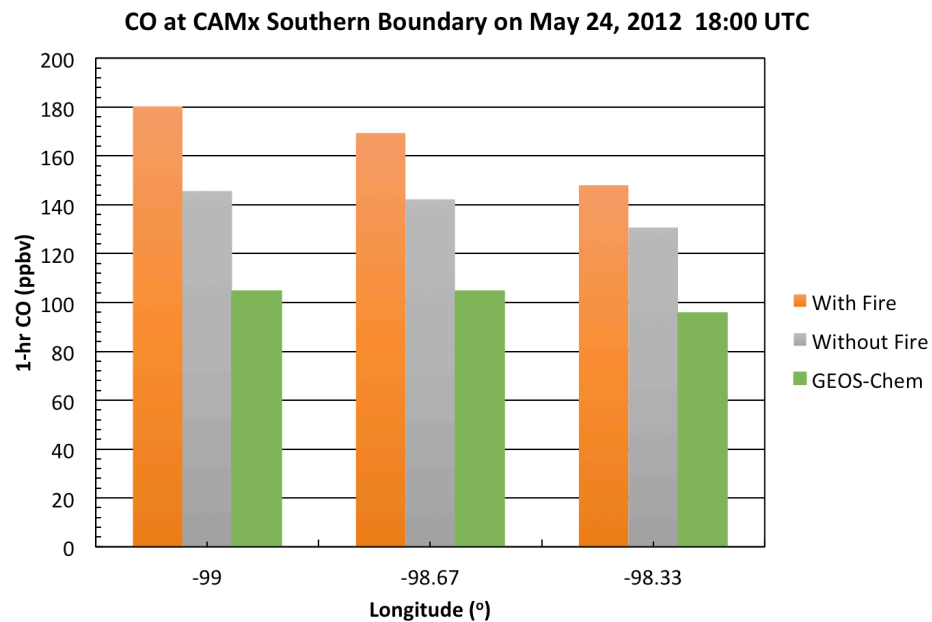


Figure 38. STILT-ASP v2.0 calculations of CO (ppbv) along the southern CAMx domain boundary with fire emissions (orange) and without fire emissions (grey) for 18:00 UTC (12:00 CST) on May 24, 2012 compared with the GEOS-Chem derived boundary condition values (green).

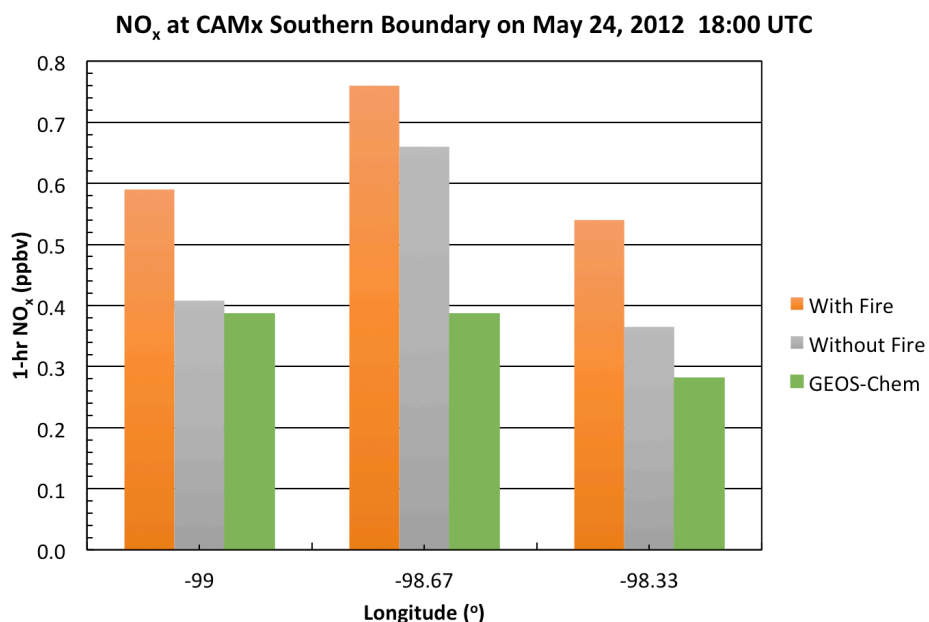


Figure 39. STILT-ASP v2.0 calculations of O₃ (ppbv) along the southern CAMx domain boundary with fire emissions (orange) and without fire emissions (grey) for 18:00 UTC (12:00 CST) on May 24, 2012 compared with the GEOS-Chem derived boundary condition values (green).

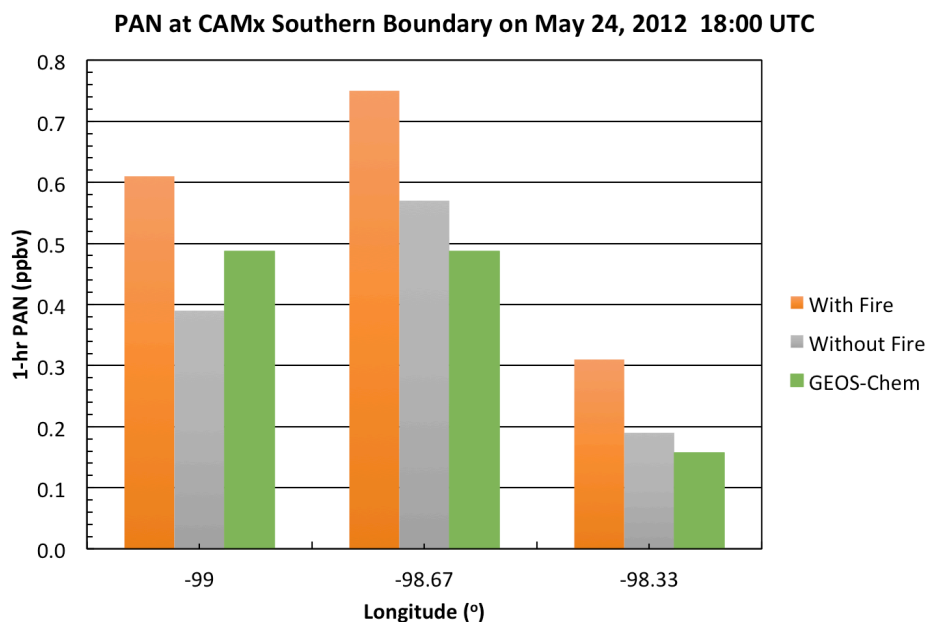


Figure 40. STILT-ASP v2.0 calculations of PAN (ppbv) along the southern CAMx domain boundary with fire emissions (orange) and without fire emissions (grey) for 18:00 UTC (12:00 CST) on May 24, 2012 compared with the GEOS-Chem derived boundary condition values (green).

3.3 Assessing Impact of Remote (out-of-domain) Fires on Texas Air Quality

In order to determine whether or not remote wildfires impacted the grid, the STILT model was then run for a selection of cases to calculate the one-week air flow history for the city of Austin, as shown in Figure 22. We identified three periods where fires were significantly impacting the southern border of the TCEQ modeling domain during the May and June 2012 TCEQ modeling episode: May 5, 11, and 25. We ran STILT-ASP for a receptor in Austin for these periods. STILT-ASP v2.0 was run with full chemistry for 500 Lagrangian parcels on seven-day back-trajectories using NARR meteorology and the NCAR MOZART-4/GEOS-5 chemical forecasts for boundary conditions. Fire emissions were taken from the FINN inventory (Wiedinmyer et al., 2011), biogenic emissions from the MEGAN model (Guenther et al., 2006), and anthropogenic emissions from the TCEQ 2012 modeling episode, as with the boundary condition analysis in Section 3.2. On each day, we ran eight simulations to cover the eight hours included in the Austin/Round Rock CAMS 3 MDA8 on each of the selected days (11:00-18:00 CST on May 5 and 11, 10:00-17:00 CST on May 25).

3.3.1 May 11, 2012

Figure 41 shows the difference in the STILT-ASP v2.0 predictions of CO when fire emissions are included (“With Fire”) and when they are excluded (“Without Fire”). We see a small enhancement of CO from fires of 2.2-4.9 ppbv during this period. Figure 42 shows the seven-day back-trajectories for CO, which show contributions from all over southern North America and the Gulf of Mexico, with some trajectories passing over the Pacific coast of the US. The trajectories are not focused on the Yucatan, which is consistent with the relatively small impact of fires on CO at this site.

The review of Jaffe and Wigder (2012) found that the average $\Delta\text{O}_3/\Delta\text{CO}$ for smoke aged about 1-2 days was 0.2 ± 0.1 , but that negative enhancement ratios have been measured in the past. Thus, based on the modeled CO enhancement from fires, we would expect a small O_3 enhancement of around 0.5-1.0 ppbv. Instead, while the overall O_3 is reasonably close to the observations (MB = +3.6 ppbv, RMSE = 5.9 ppbv), we actually see a small *decrease* in the modeled MDA8 O_3 of 0.9 ppbv when fires are included (Figure 43). Similarly, the overall NO_x concentrations match reasonably well with observations (MB = +0.32 ppbv, RMSE = 1.89 ppbv, Figure 44), but are lower when fire emissions are added. This appears to be due to the chemistry of the fire S/IVOCs included in ASP v2.1, as described in Section 0. Again, the S/IVOC chemistry is leading to an overestimated rapid loss of NO_x , including the anthropogenic NO_x in the Austin/Round Rock area, leading to a slight loss of O_3 and NO_x when fire emissions are added. This also suggests that the S/IVOC chemistry in ASP v2.1 may need to be re-examined for the longer time periods (> 5 hours) used in STILT-ASP v2.0.

Figure 45 shows the results for $\text{PM}_{2.5}$. We see that STILT-ASP v2.0 strongly overestimates $\text{PM}_{2.5}$ concentrations relative to observations on this day (MB = +27.4 $\mu\text{g}/\text{m}^3$, RMSE = 27.8 $\mu\text{g}/\text{m}^3$), as was seen in previous work (Alvarado et al., 2016, 2017). This may be due to the assumption in STILT-ASP v2.0 that all fire and anthropogenic aerosols are emitted with a single, monodisperse size distribution with an average diameter of 0.1 μm , and that deposition only affects the Lagrangian parcels when they are in the surface layer of the input meteorology. Both of these effects tend to underestimate the deposition of $\text{PM}_{2.5}$ to the surface. However, these

results can be used to estimate the relative fraction of $PM_{2.5}$ at the receptor that is due to fires. In this case, we estimate that on average, 12% of the $PM_{2.5}$ measured during this period is due to fires, which when applied to the observed $PM_{2.5}$ values, gives an estimate of $0.9 \mu\text{g}/\text{m}^3$ as the $PM_{2.5}$ contribution from fires for this episode.

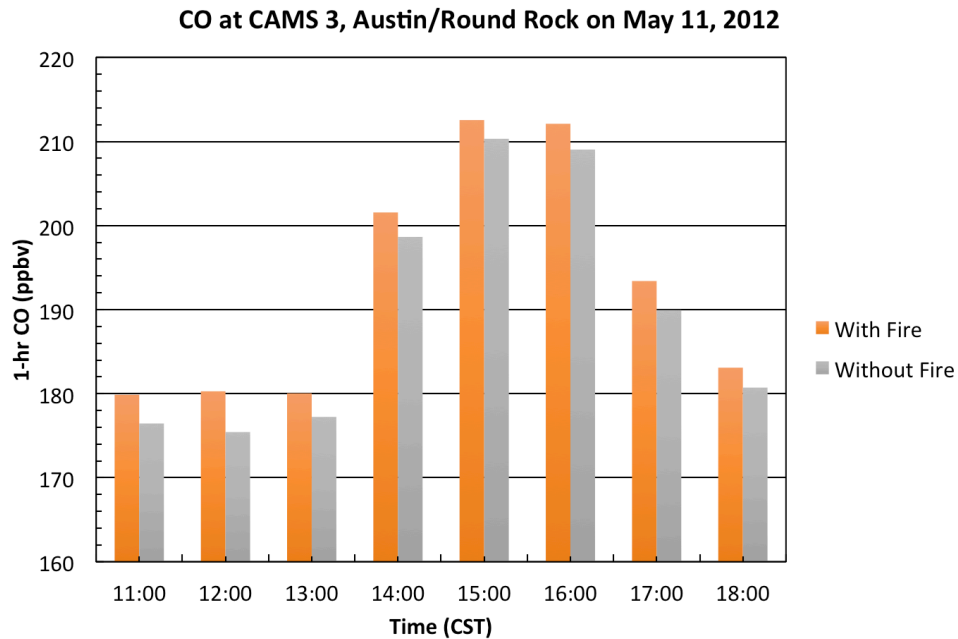


Figure 41. STILT-ASP v2.0 estimates of CO (ppbv) at the Austin/Round Rock CAMS 3 site with fire emissions (orange) and without fire emissions (grey) for 11:00-18:00 CST on May 11, 2012. Note that the CAMS 3 site measured 100 ± 100 ppbv CO during this period.

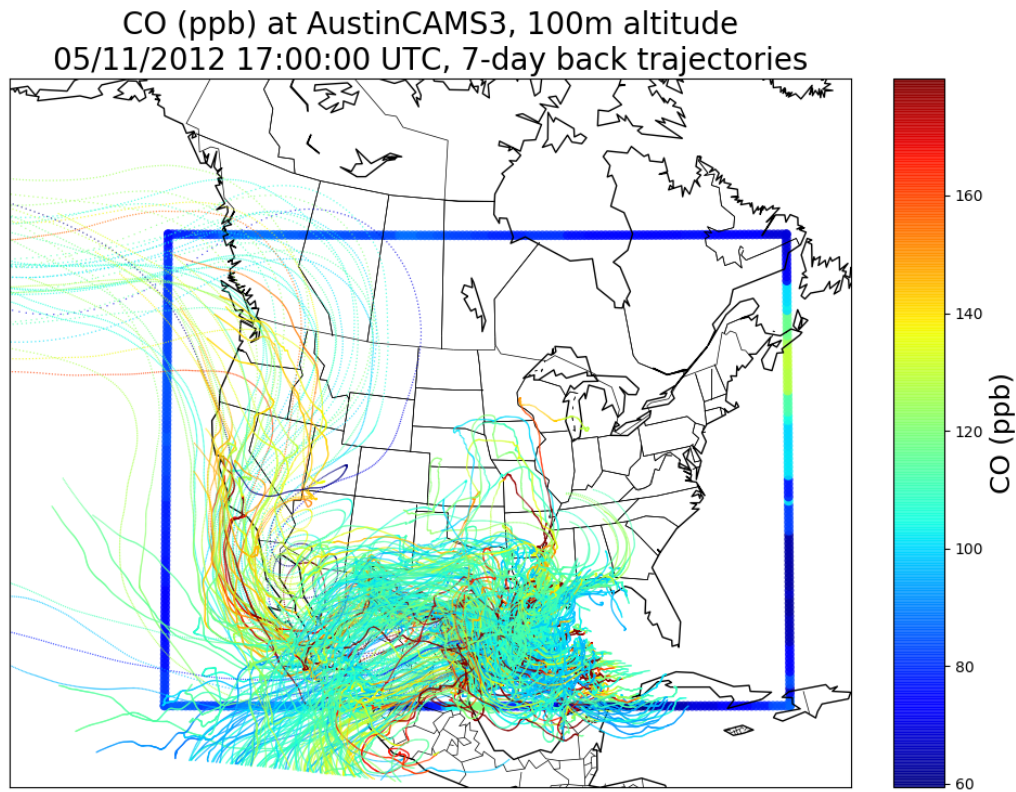


Figure 42. CO (ppbv) from a 7-day back trajectory run of STILT-ASP v2.0 for May 11, 2012 at 17:00 UTC (11:00 CST) for CAMS3 site at Austin/Round Rock. The GEOS-Chem boundary conditions are also shown.

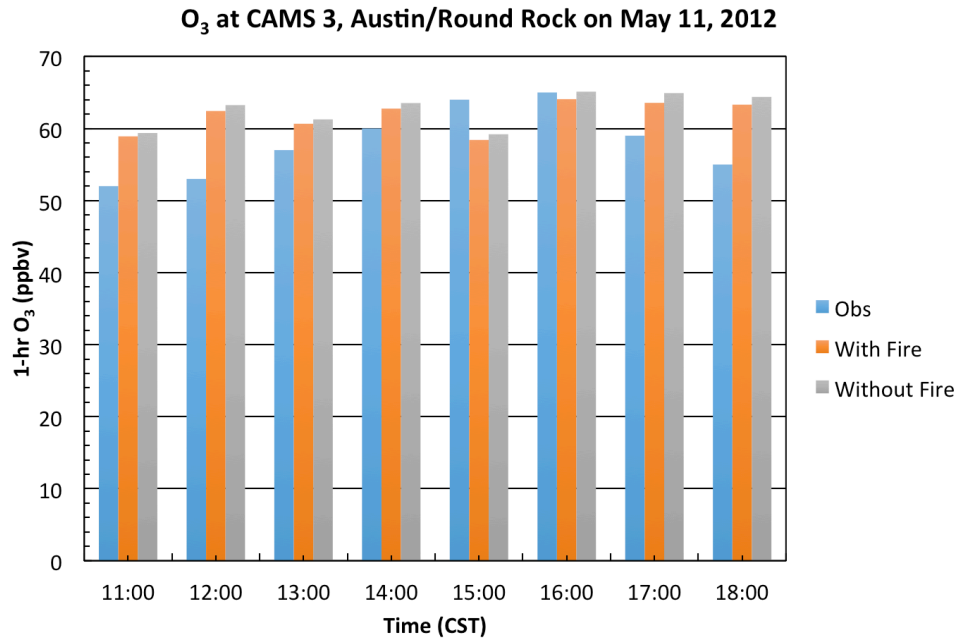


Figure 43. STILT-ASP v2.0 estimates of O₃ (ppbv) at the Austin/Round Rock CAMS 3 site with fire emissions (orange) and without fire emissions (grey) for 11:00-18:00 CST on May 11, 2012 compared with observations (blue).

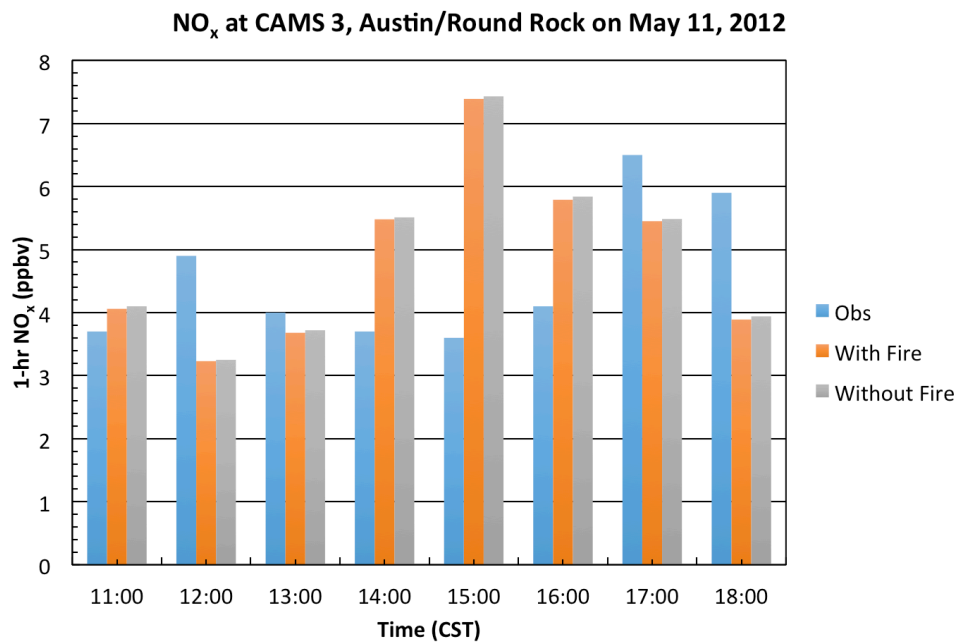


Figure 44. STILT-ASP v2.0 estimates of NO_x (ppbv) at the Austin/Round Rock CAMS 3 site with fire emissions (orange) and without fire emissions (grey) for 11:00-18:00 CST on May 11, 2012 compared with observations (blue).

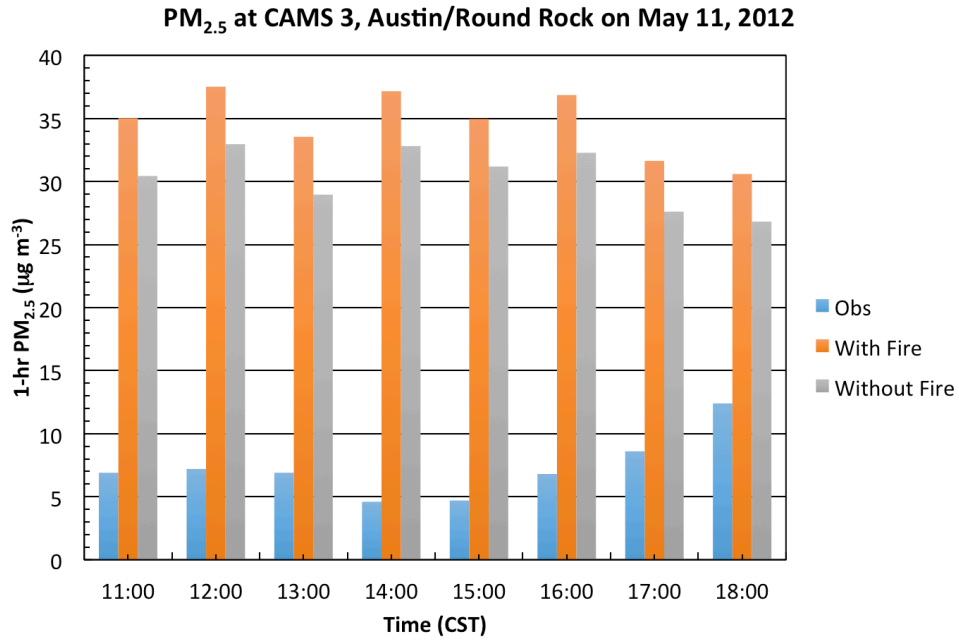


Figure 45. STILT-ASP v2.0 estimates of PM_{2.5} (µg/m³) at the Austin/Round Rock CAMS 3 site with fire emissions (orange) and without fire emissions (grey) for 11:00-18:00 CST on May 11, 2012 compared with observations (blue).

3.3.1 May 5, 2012

Note that, as the TCEQ emissions used in STILT-ASP v2.0 only cover May-September, these May 5 cases were only calculated using a 4-day back-trajectory, unlike the 7-day trajectories used for the other Austin CAMS3 cases. Figure 46 shows the STILT-ASP v2.0 CO concentrations both with and without fire emissions for CAMS 3 of Austin/Round Rock on May 5, 2012. The modeled CO concentrations (124-138 ppbv) are consistent with the values of 100 ± 100 ppbv measured at CAMS 3 during this period. The average fire impact (Δ CO) over the MDA8 O₃ period is 8.1 ppbv, and peaks at a value of 18.3 ppbv at 13:00 CST.

Figure 47 shows the results for O₃. Unlike the results for May 11, on May 5 STILT-ASP v2.0 substantially overestimates the amount of O₃ relative to measurements (MB = +37 ppb, RMSE = 37 ppbv) for this moderate O₃ day and underestimates the NO_x concentration (MB = -2.6 ppbv, RMSE = 2.7 ppbv, Figure 48). The modeled total impact of fires on the MDA8 O₃ is small (0.17 ppbv), with the impact changing from positive to negative depending on the hour, giving a small but not unreasonable value for Δ O₃/ Δ CO (0.021 mol/mol).

While the total PM_{2.5} is still overestimated for this case (MB = +10.2 μ g/m³, RMSE = 10.5 μ g/m³ Figure 49), the overestimate is not as severe as it was on May 11. The model estimates that 17% of the PM_{2.5} came from fires, which given the observed values would translate to 2.6 μ g/m³ over the 8-hour period.

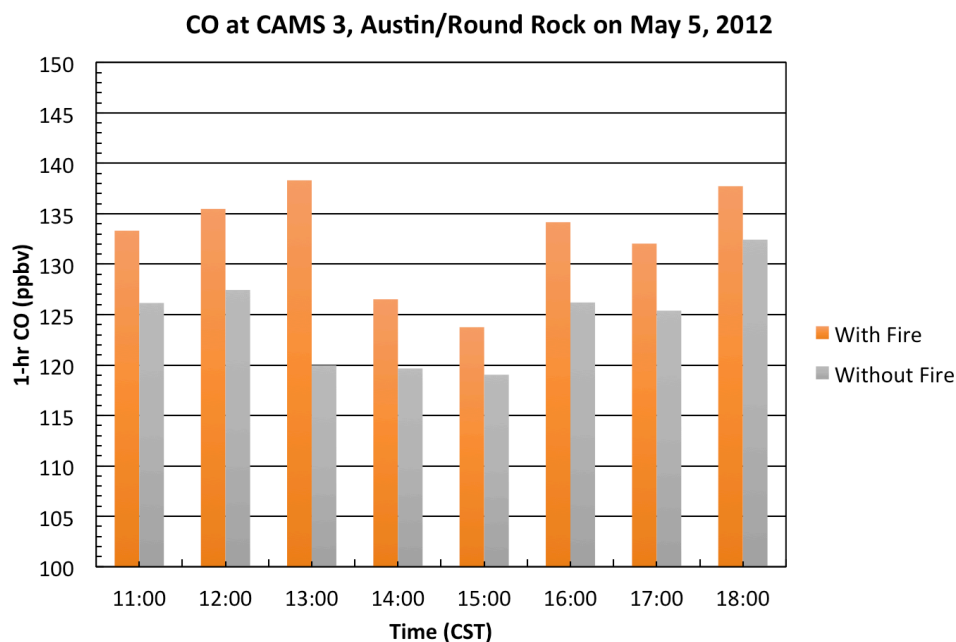


Figure 46. STILT-ASP v2.0 estimates of CO (ppbv) at the Austin/Round Rock CAMS 3 site with fire emissions (orange) and without fire emissions (grey) for 11:00-18:00 CST on May 5, 2012. Note that the CAMS 3 site measured 100 ± 100 ppbv CO during this period.

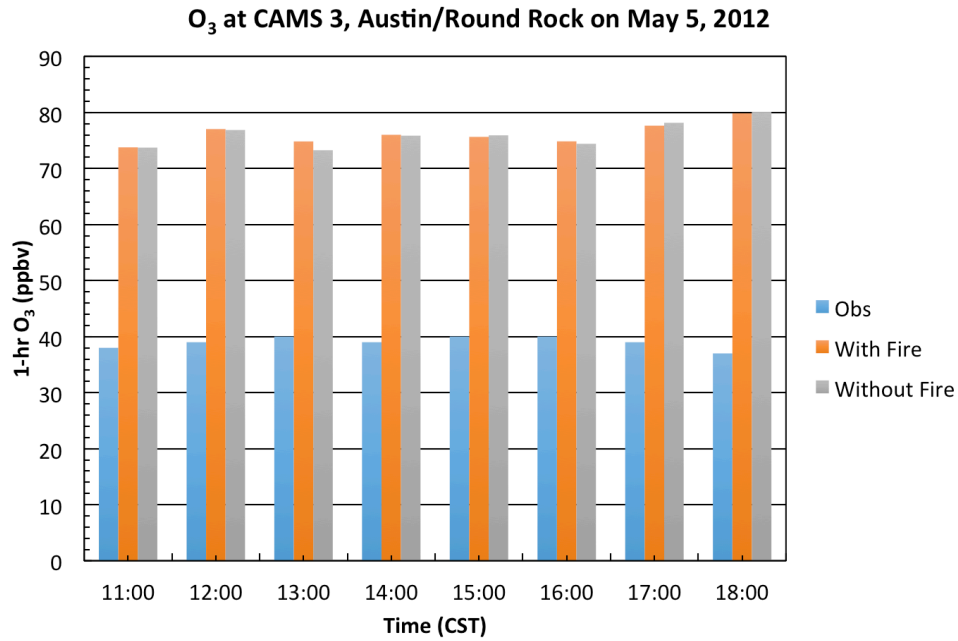


Figure 47. STILT-ASP v2.0 estimates of O₃ (ppbv) at the Austin/Round Rock CAMS 3 site with fire emissions (orange) and without fire emissions (grey) for 11:00-18:00 CST on May 5, 2012 compared with observations (blue).

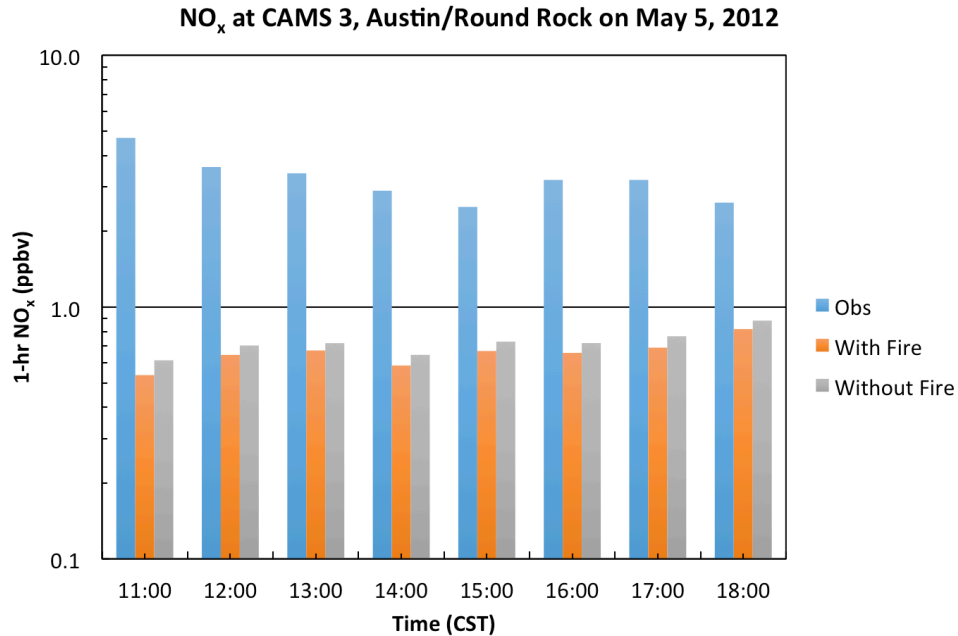


Figure 48. STILT-ASP v2.0 estimates of NO_x (ppbv) at the Austin/Round Rock CAMS 3 site with fire emissions (orange) and without fire emissions (grey) for 11:00-18:00 CST on May 5, 2012 compared with observations (blue).

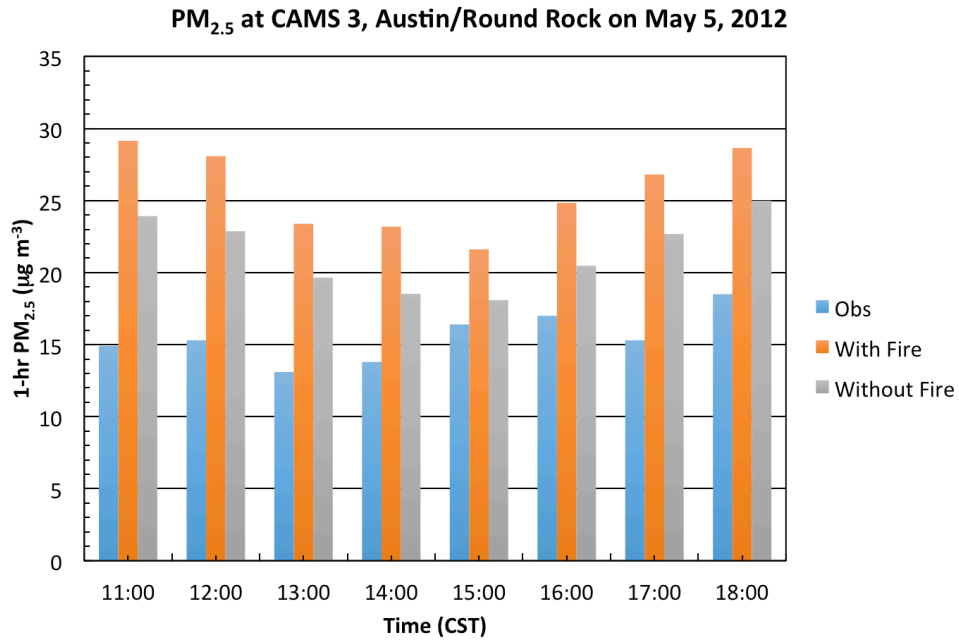


Figure 49. STILT-ASP v2.0 estimates of PM_{2.5} (µg/m³) at the Austin/Round Rock CAMS 3 site with fire emissions (orange) and without fire emissions (grey) for 11:00-18:00 CST on May 5, 2012 compared with observations (blue).

3.3.2 May 25, 2012

Figure 50 shows the STILT-ASP v2.0 CO concentrations both with and without fire emissions for CAMS 3 of Austin/Round Rock on May 25, 2012. The modeled CO concentrations (147-173 ppbv) are consistent with the values of 100 ± 100 ppbv measured at CAMS 3 during this period. The average fire impact (Δ CO) over the MDA8 O₃ period is 5.3 ppbv, and peaks at a value of 9.1 ppbv at 13:00 CST.

Figure 51 shows the results for O₃. Similar to the results on May 5, STILT-ASP v2.0 substantially overestimates the amount of O₃ relative to measurements (MB = +42 ppb, RMSE = 42 ppbv) for this moderate O₃ day and underestimates the NO_x concentration (MB = -2.6 ppbv, RMSE = 2.7 ppbv, Figure 52). The modeled total impact of fires on the MDA8 O₃ is small (0.32 ppbv), with the impact changing from positive to negative depending on the hour, giving a small but not unreasonable value for Δ O₃/ Δ CO (0.035 mol/mol).

While the total PM_{2.5} is still overestimated for this case (MB = +4.9 μ g/m³, RMSE = 5.3 μ g/m³, Figure 53), the overestimate is not as severe as it was on May 11. The model estimates that 21% of the PM_{2.5} came from fires which, given the observed values, would translate to 4.0 μ g/m³ over the 8-hour period.

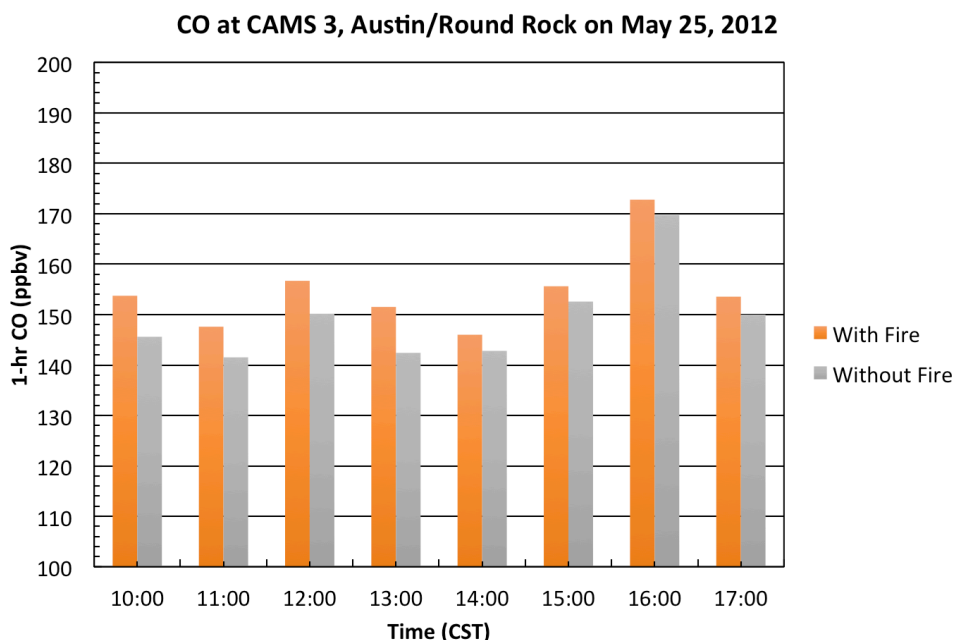


Figure 50. STILT-ASP v2.0 estimates of CO (ppbv) at the Austin/Round Rock CAMS 3 site with fire emissions (orange) and without fire emissions (grey) for 10:00-17:00 CST on May 25, 2012. Note that the CAMS 3 site measured 100 ± 100 ppbv CO during this period.

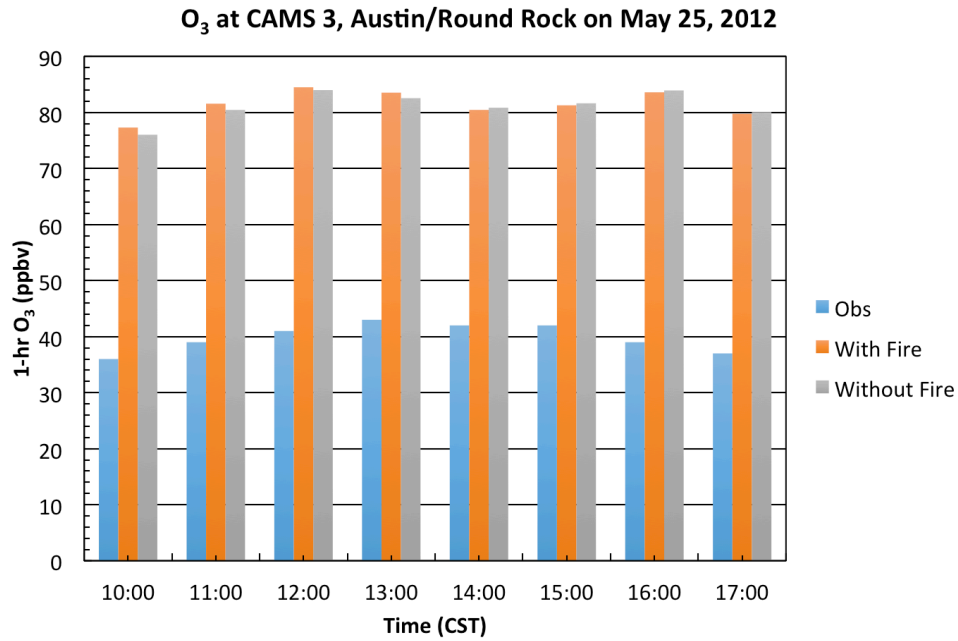


Figure 51. STILT-ASP v2.0 estimates of O₃ (ppbv) at the Austin/Round Rock CAMS 3 site with fire emissions (orange) and without fire emissions (grey) for 10:00-17:00 CST on May 25, 2012 compared with observations (blue).

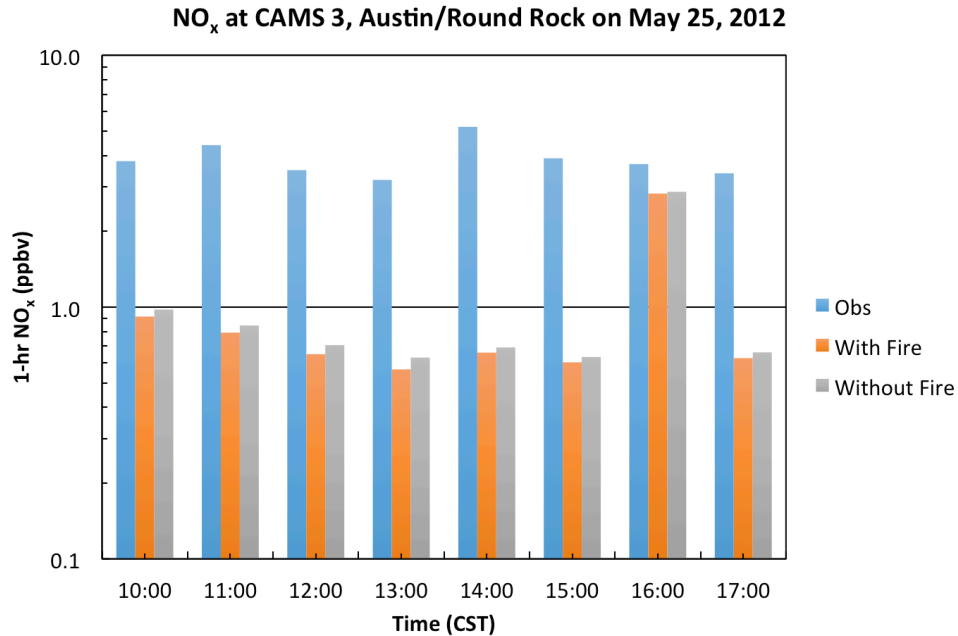


Figure 52. STILT-ASP v2.0 estimates of NO_x (ppbv) at the Austin/Round Rock CAMS 3 site with fire emissions (orange) and without fire emissions (grey) for 10:00-17:00 CST on May 25, 2012 compared with observations (blue).

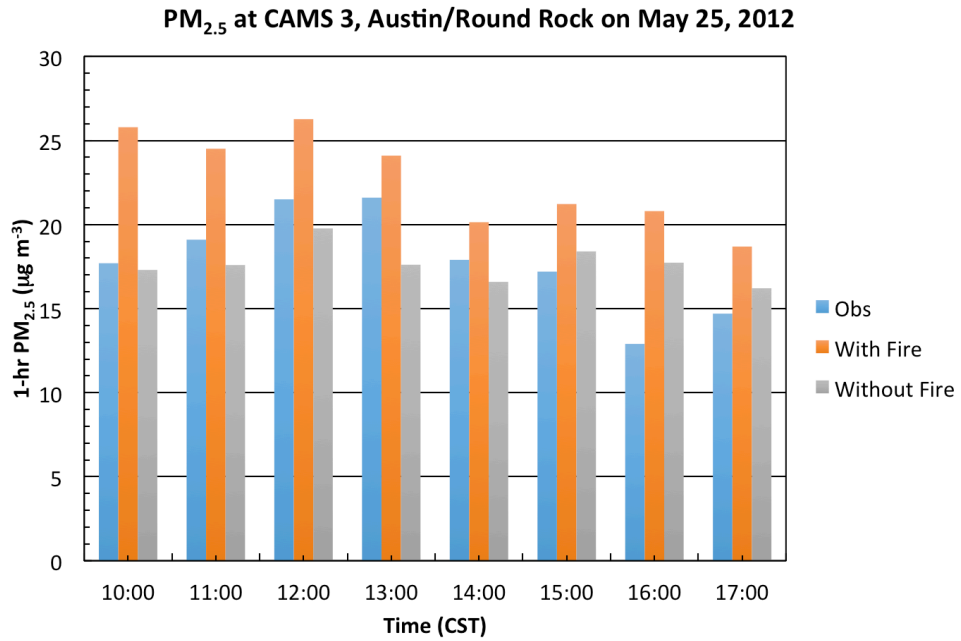


Figure 53. STILT-ASP v2.0 estimates of PM_{2.5} (µg/m³) at the Austin/Round Rock CAMS 3 site with fire emissions (orange) and without fire emissions (grey) for 10:00-17:00 CST on May 25, 2012 compared with observations (blue).

3.4 Assessing the Impact of Close (in-domain) Fires on Texas Air Quality

In order to compare the STILT-ASP v2.0 predictions of the impacts of wildfires on O₃ and PM_{2.5} with the CAMx simulations of McDonald-Buller et al. (2015), we ran STILT-ASP for the CAMS 12 site in El Paso on two dates (June 4 and June 28) that were shown to have significant fire impacts on O₃ in McDonald-Buller et al. (2015). STILT-ASP v2.0 was run with full chemistry for 500 Lagrangian parcels on seven-day back-trajectories using NARR meteorology and the NCAR MOZART-4/GEOS-5 chemical forecasts for boundary conditions. Fire emissions were taken from the FINN inventory (Wiedinmyer et al., 2011), biogenic emissions from the MEGAN model (Guenther et al., 2006), and anthropogenic emissions from the TCEQ 2012 modeling episode. On each day, we ran eight simulations to cover the eight hours included in the El Paso CAMS 12 MDA8 on each day (11:00-18:00 MST on both days).

3.4.1 June 4, 2012

Figure 54 shows the STILT-ASP v2.0 CO concentrations both with and without fire emissions for CAMS 12 of El Paso on June 4, 2012. The modeled CO concentrations (116-130 ppbv) are slightly higher than the values of 0 ± 100 ppbv measured at CAMS 3 during this period. The average fire impact (Δ CO) over the MDA8 O₃ period is 3.4 ppbv, and peaks at a value of 4.5 ppbv at 14:00 MST.

Figure 55 shows the results for O₃. STILT-ASP v2.0 somewhat overestimates the amount of O₃ relative to measurements on this day (MB = +16 ppb, RMSE = 16 ppbv) and strongly underestimates the NO_x concentration (MB = -4.4 ppbv, RMSE = 5.2 ppbv, Figure 56). The modeled total impact of fires on the MDA8 O₃ is small and negative (-0.38 ppbv), giving a value for Δ O₃/ Δ CO of -0.11 mol/mol. This is a much smaller impact than the results of McDonald-Buller et al. (2015) for this period, but their simulation was using CAMx with FINN v2.1 emissions, not the FINN v1.5 emissions used here, and as noted above, STILT-ASP v2.0 may be underestimating the O₃ formation from fire emissions by overestimating the NO_x loss during S/IVOC oxidation. A cleaner comparison is with the results of our implementation of the sub-grid parameterization of Lonsdale et al. (2015) into CAMx (Section 2.6), which used the FINN v1.5 emissions as well. There, CAMx with the parameterization predicted fire impacts on O₃ of 2.1 ppbv at El Paso at 17:00 CST. Thus while both models agree that the impacts of fires on El Paso air quality on this day were small, they disagree on the sign of the impact.

The total PM_{2.5} is overestimated for this case (MB = +7.5 $\mu\text{g}/\text{m}^3$, RMSE = 8.0 $\mu\text{g}/\text{m}^3$, Figure 57), consistent with the results of Section 3.3. The model estimates that 24% of the PM_{2.5} came from fires which, given the observed values, would translate to 1.9 $\mu\text{g}/\text{m}^3$ over the 8-hour period.

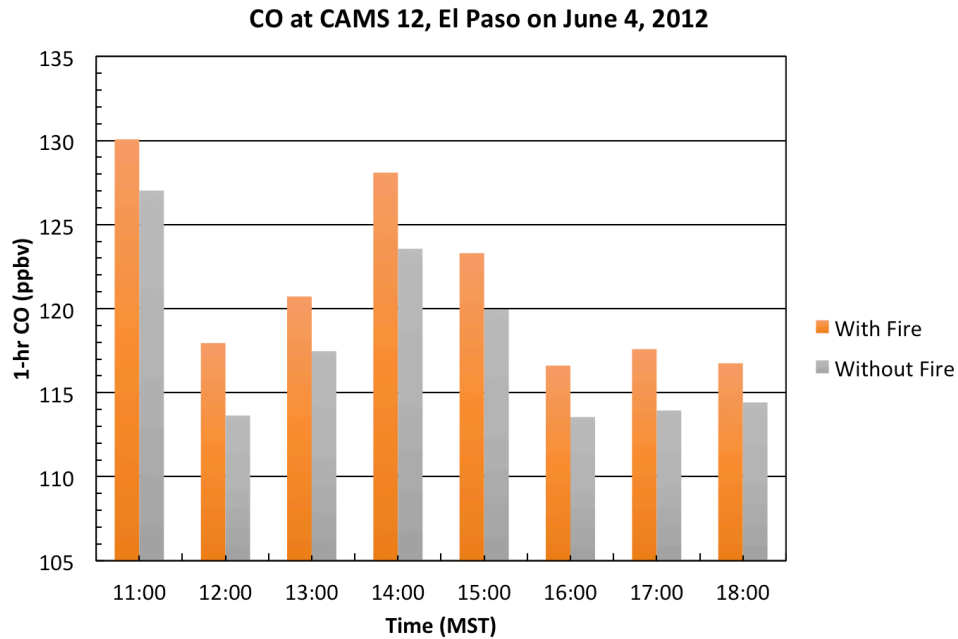


Figure 54. STILT-ASP v2.0 estimates of CO (ppbv) at the El Paso CAMS 12 site with fire emissions (orange) and without fire emissions (grey) for 11:00-18:00 MST on June 4, 2012 compared with observations (blue).

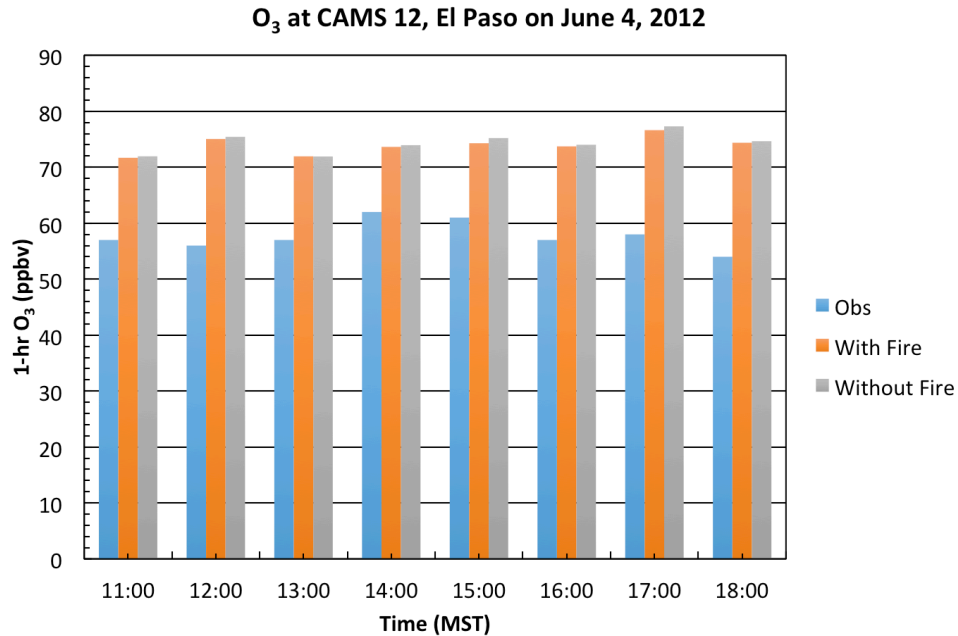


Figure 55. STILT-ASP v2.0 estimates of O₃ (ppbv) at the El Paso CAMS 12 site with fire emissions (orange) and without fire emissions (grey) for 11:00-18:00 MST on June 4, 2012 compared with observations (blue).

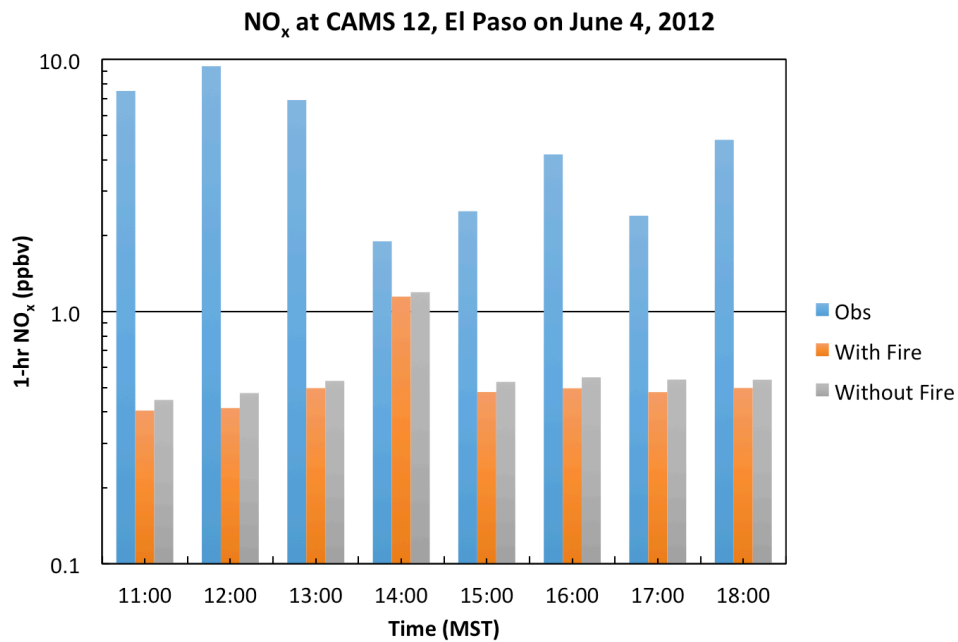


Figure 56. STILT-ASP v2.0 estimates of NO_x (ppbv) at the El Paso CAMS 12 site with fire emissions (orange) and without fire emissions (grey) for 11:00-18:00 MST on June 4, 2012 compared with observations (blue).

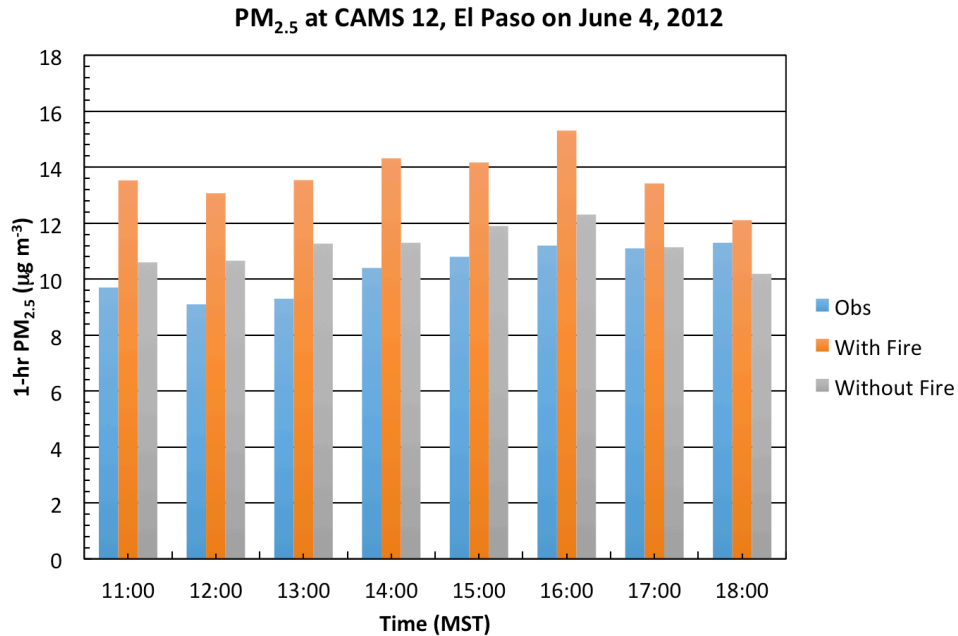


Figure 57. STILT-ASP v2.0 estimates of PM_{2.5} (µg m⁻³) at the El Paso CAMS 12 site with fire emissions (orange) and without fire emissions (grey) for 11:00-18:00 MST on June 4, 2012 compared with observations (blue).

3.4.2 June 28, 2012

Figure 58 shows the STILT-ASP v2.0 CO concentrations both with and without fire emissions for CAMS 12 of El Paso on June 28, 2012. The modeled CO concentrations (106-118 ppbv) are slightly higher than the values of 100 ± 100 ppbv and 0 ± 100 ppbv measured at CAMS 3 during this period. The average fire impact (Δ CO) over the MDA8 O₃ period is 2.2 ppbv, and peaks at a value of 3.1 ppbv at 11:00 MST.

Figure 59 shows the results for O₃. STILT-ASP v2.0 somewhat overestimates the amount of O₃ relative to measurements on this day (MB = +20 ppb, RMSE = 21 ppbv) and strongly underestimates the NO_x concentration (MB = -4.3 ppbv, RMSE = 4.8 ppbv, Figure 56). The modeled total impact of fires on the MDA8 O₃ is small and negative (-0.05 ppbv), giving a value for Δ O₃/ Δ CO of -0.016 mol/mol. This is in contrast to our results with CAMx and the sub-grid parameterization (Section 2.6), which suggest that the impact of fires was 1.2 ppbv at 17:00 CST. As noted above, STILT-ASP v2.0 may be underestimating the O₃ formation from fire emissions by overestimating the NO_x loss during S/IVOC oxidation.

The total PM_{2.5} is overestimated for this case (MB = +3.3 μ g/m³, RMSE = 3.5 μ g/m³, Figure 61), consistent with the results of Section 3.3. The model estimates that 18% of the PM_{2.5} came from fires which, given the observed values, would translate to 1.9 μ g/m³ over the 8-hour period.

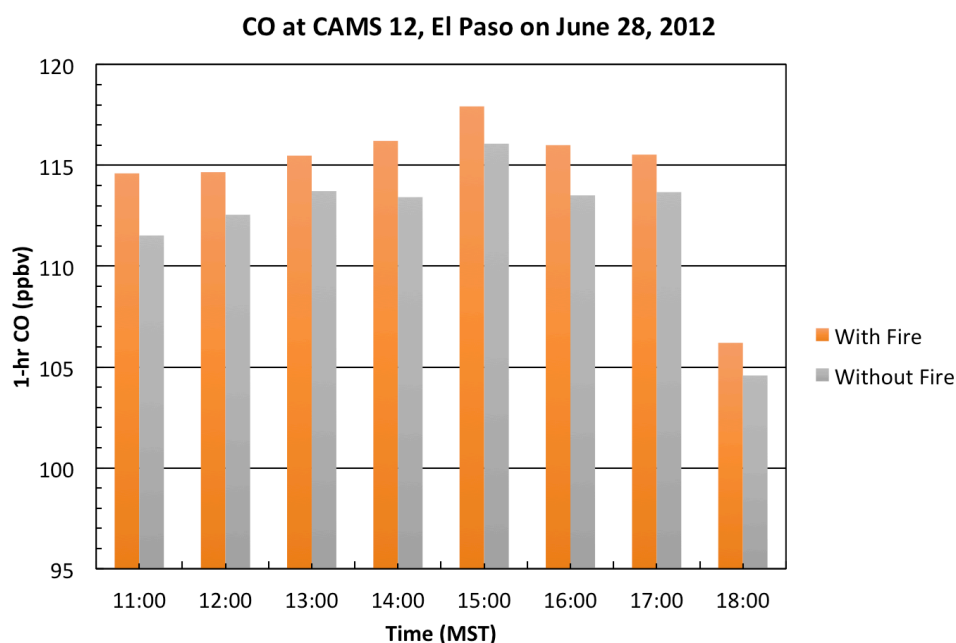


Figure 58. STILT-ASP v2.0 estimates of CO (ppbv) at the El Paso CAMS 12 site with fire emissions (orange) and without fire emissions (grey) for 11:00-18:00 MST on June 28, 2012 compared with observations (blue).

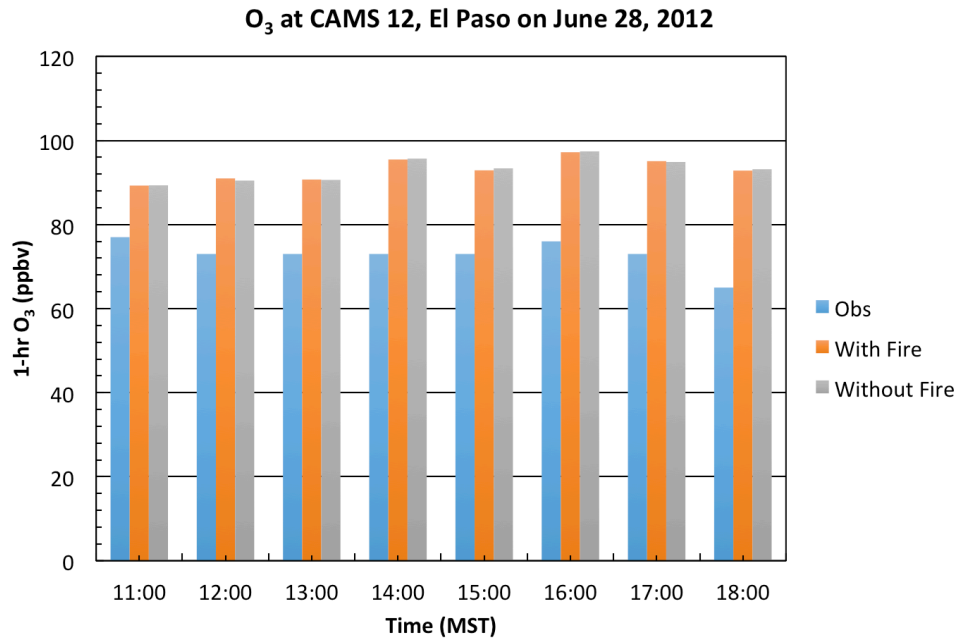


Figure 59. STILT-ASP v2.0 estimates of O₃ (ppbv) at the El Paso CAMS 12 site with fire emissions (orange) and without fire emissions (grey) for 11:00-18:00 MST on June 28, 2012 compared with observations (blue).

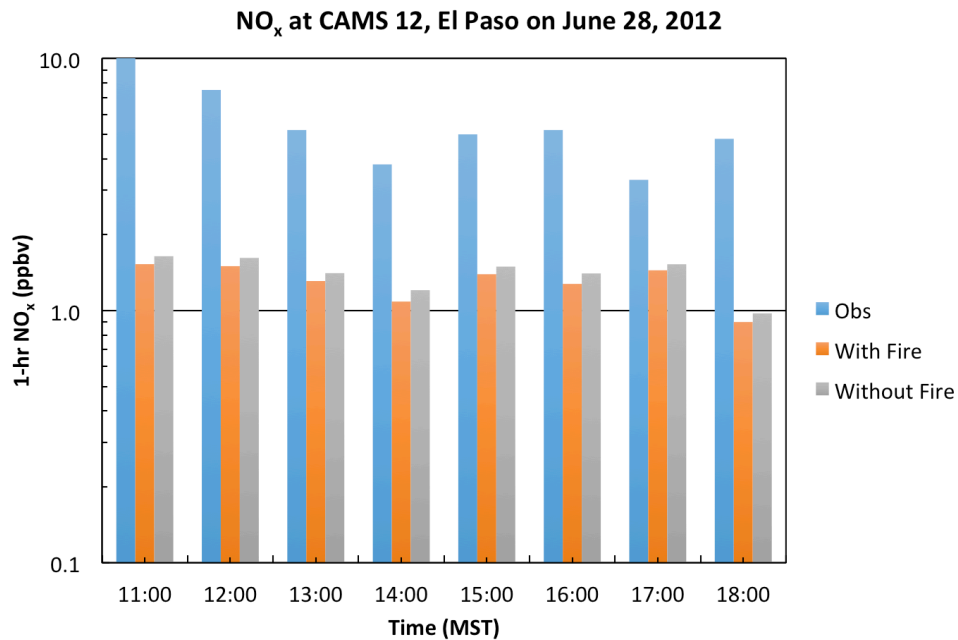


Figure 60. STILT-ASP v2.0 estimates of NO_x (ppbv) at the El Paso CAMS 12 site with fire emissions (orange) and without fire emissions (grey) for 11:00-18:00 MST on June 28, 2012 compared with observations (blue).

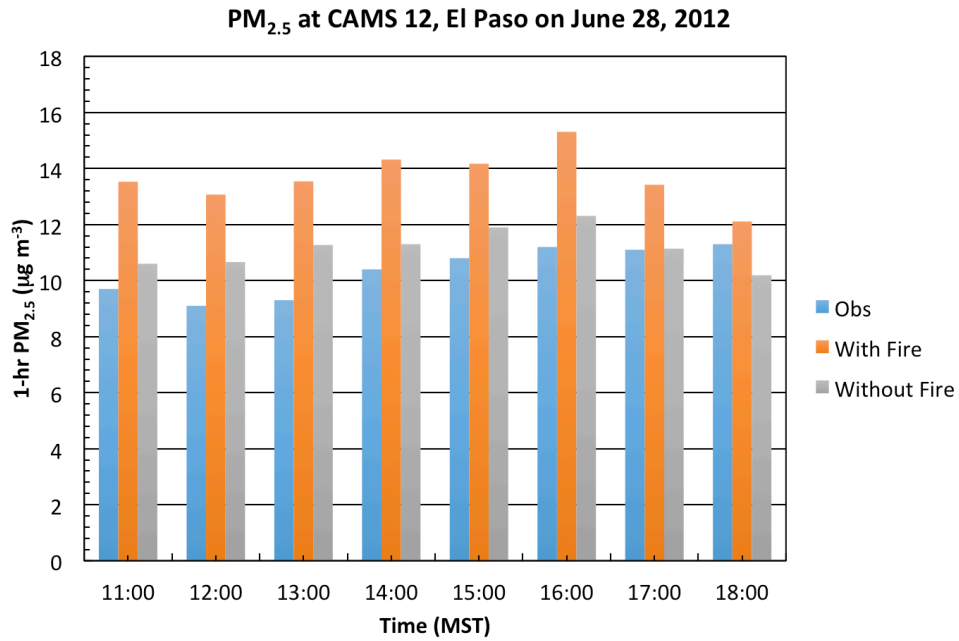


Figure 61. STILT-ASP v2.0 estimates of PM_{2.5} (µg m⁻³) at the El Paso CAMS 12 site with fire emissions (orange) and without fire emissions (grey) for 11:00-18:00 MST on June 28, 2012 compared with observations (blue).

4 Audits of Data Quality and Reconciliation with User Requirements

4.1 SAM-ASP and Parameterization Development

Our evaluation of the SAM-ASP model against our conceptual models of the chemistry of biomass burning plumes, as well as the observations from the Williams Fire (Alvarado et al., 2015) is discussed in Section 2.2. As noted there, we find that SAM-ASP does a reasonable job of simulating CO, PAN, HONO, and NO_x within biomass burning plumes, but that the formation of O₃ is underestimated.

In addition, we carefully examined over 10% of the SAM-ASP outputs for the 400 cases simulated to ensure that they were consistent with our expectations and with literature estimates for these parameters, thus satisfying the Audits of Data Quality requirement for this project. This evaluation process uncovered several coding errors in the coupled model that were corrected in the course of this project, and the corrected SAM-ASP model was used to rerun the 400 simulations. These results appear consistent with our understanding of biomass burning chemistry, and the output from these runs will be delivered to TCEQ along with the final report.

We also examined over 10% of the output of the GEM parameterization to ensure that they were consistent with our expectations and with literature estimates for these parameters. Our initial evaluation showed that each fuel type needs to have its own GEM trained separately from the others, as combining all fuel types gave unphysical results. We also compared the GEM results to the output of the original SAM-ASP model for cases that the GEM parameterization was not trained on.

The results of this evaluation of the GEM parameterization are given in Section 2.4, and satisfies the Audits of Data Quality requirement for this project. We found that our current GEM training approach does *not* result in a parameterization of sufficient quality for use in regional air quality modeling. For O₃, the dependence on fuel type, temperature, day of year, and latitude in the GEM parameterization appeared reasonable, but the dependence on time of day was unrealistic. For NO_y species, mass conservation was not obeyed for points outside of the training set and the dependence on the input variables was unreasonable.

Thus, for implementation into CAMx we instead shifted back to the earlier look-up table parameterization of Lonsdale et al. (2015). Over 10% of the outputs of this parameterization were examined, thus satisfying the Audits of Data Quality requirement for this project, and this parameterization was found to be of sufficient quality to be used in regional air quality modeling. As expected, the parameterization reduced the modeled O₃ formation near the fire sources, making the results more consistent with our knowledge of biomass-burning chemistry. However, we have not been able to sufficiently evaluate the implementation of the parameterization of Lonsdale et al. (2015) within the CAMx model against surface observations. Thus the current implementation of the sub-grid scale parameterization of fire chemistry in CAMx, as part of Task 1, should be considered an experimental, preliminary version that still needs further evaluation and improvement before it is ready for use in regulatory modeling applications.

In addition, the QAPP listed the following assessment questions for Task 1:

- *What are the software and hardware requirements for the updated CAMx model using the new sub-grid scale parameterization? How long should a reference model run take?*

Our new CAMx source code requires the use of NetCDF, as we make output files in that format. In addition, currently our parameterization only works using OpenMP parallelization, thus MPI runs cannot be done when the parameterization is on, and the parameterization has not been tested on nested grids.

Adding the plume-in-grid puffs for the fires does increase the memory requirement of the software. We currently limit the number of fire puffs to 106, and each puff tracks $O(100)$ species as double-precision floating point variables of 8 bytes each, so the parameterization requires approximately 800 MB of RAM. In addition, we currently load all of the ASP parameterization files into memory at the start of the model run, which requires 4 GB of RAM. Thus the total memory increase is about 5 GB, which should be negligible for most applications.

When the puffs are forced to dump to the grid immediately, the parameterization has a negligible impact on the timing of the simulation (~ 10 min to run one model day of the 36 km resolution grid on 32 threads on an Amazon Web Services m4.16xlarge instance using OpenMP). When the puffs are tracked for 5 hours, the runtime is doubled to ~ 20 min.

- *What is the magnitude of the change in the model simulations when the sub-grid scale parameterization is used? Do these changes improve the agreement of the simulations with observations from EPA (e.g., CASTNET for O_3 , IMPROVE for OA) and TCEQ (e.g., monitor data on O_3 , NO_x , and $PM_{2.5}$).*

As shown in Section 2.6, adding the sub-grid parameterization to CAMx can reduce the modeled impact of fires on O_3 near the source significantly ($\sim 30\%$). However, we have not been able to sufficiently evaluate the implementation of the parameterization of Lonsdale et al. (2015) within the CAMx model against surface observations. Thus the current implementation of the sub-grid scale parameterization of fire chemistry in CAMx, as part of Task 1, should be considered an experimental, preliminary version that still needs further evaluation and improvement before it is ready for use in regulatory modeling applications.

- *Is the simulated chemical formation of O_3 , $PM_{2.5}$, and other chemical species in the PiG module reasonable? Are these predictions consistent with the original SAM-ASP model? Are these predictions consistent with the scientific literature on the impacts of wildfires on O_3 and $PM_{2.5}$?*

The simulated chemical formation of O_3 and other species within SAM-ASP appears reasonable and consistent with the scientific literature on the impacts of wildfires on O_3 and $PM_{2.5}$, as discussed in Section 2.2.

However, our evaluation of the GEM parameterization showed that these results are not consistent with the original SAM-ASP model or the scientific literature on the impacts of wildfires on O_3 . Thus we instead used the sub-grid parameterization of Lonsdale et al. (2015) within a copy of the PiG module in CAMx. The model predictions with this parameterization are consistent with the scientific literature on the impacts of wildfires on O_3 .

CAMx using the Lonsdale et al. (2015) parameterization in the PiG module appears consistent with the scientific literature on the formation of O₃ from biomass burning emissions, but we have not been able to sufficiently evaluate it against surface observations.

- *Under what conditions is the updated model expected to be valid?*

The SAM-ASP coupled model is expected to be valid for simulating the chemistry in wildfire plumes within the conditions discussed in Section 2.2 and 2.3.

The GEM parameterization does not appear consistent with the original SAM-ASP model or the scientific literature on the impacts of wildfires on O₃. Thus the GEM parameterization should *not* be considered valid.

CAMx using the Lonsdale et al. (2015) parameterization in the PiG module is expected to be valid under many conditions, but we have not been able to sufficiently evaluate it against surface observations. Thus the current implementation of the sub-grid scale parameterization of fire chemistry in CAMx, as part of Task 1, should be considered an experimental, preliminary version that still needs further evaluation and improvement before it is ready for use in regulatory modeling applications.

4.2 STILT-ASP Examination of the Impacts of Long-Range BB Transport

The performance of the STILT-ASP v2.0 model used in this task had been previously evaluated against observations from the 2013 DISCOVER-AQ campaign in Houston (Alvarado et al., 2017). In this project, over 10% of the outputs of the STILT-ASP v2.0 model were evaluated for consistency with our conceptual understanding of the chemistry of biomass burning, with the GEOS-Chem derived boundary conditions for the 2012 TCEQ CAMx modeling episode (Section 0), and with surface monitor observations where available (Sections 3.3 and 3.4), thus satisfying the Audits of Data Quality requirement for this project.

As discussed above, the STILT-ASP v2.0 runs along the southern CAMx boundary gave significantly higher CO than the GEOS-Chem boundary conditions, consistent with the high CO bias in STILT-ASP v2.0 observed in Alvarado et al. (2017), but may also be due to differences in the fire emission inventories used. The STILT-ASP v2.0 prediction of O₃ was also high relative to GEOS-Chem, which appears to be due to an error in the simulation of the diurnal cycle of O₃, especially at night. However, the predicted impact of fires on O₃ relative to CO is consistent with the scientific literature. Predictions of NO_x and PAN were both much lower than the GEOS-Chem values, and this appears to be due to the chemistry of S/IVOCs used in ASP v2.1, which were derived from measurements of a biomass burning plume for the first 0 to 5 hours of aging. Thus the chemical mechanism of ASP v2.1 may need to be re-examined for the longer runs of STILT-ASP v2.0.

We also compared our STILT-ASP v2.0 predictions with observations from the Austin CAMS 3 site during the MDA8 O₃ period on three days (May 5, May 11, and May 25, 2012). On the day with the highest MDA8 O₃ (May 11), the model predictions of O₃, CO, and NO_x were all consistent with the observations, with O₃ slightly overestimated (MB of +3.6 ppbv, RMSE of 5.9 ppbv) and NO_x slightly overestimated (MB of +0.3 ppbv, RMSE of 1.9 ppbv). However, PM_{2.5} was substantially overestimated, likely due to an underestimation of PM_{2.5} deposition. However,

as deposition should affect all aerosol sources relatively evenly, so the STILT-ASP v2.0 results can be used to estimate the relative fraction of PM_{2.5} at the receptor that is due to fires. However, the results for May 5 and May 25 Austin cases were very different, with STILT-ASP v2.0 strongly overestimating O₃ (MB = +40 ppbv) and underestimating NO_x (MB = -2.6 ppbv) on these days, but with less severe overestimates of PM_{2.5}.

We also ran STILT-ASP for the CAMS 12 site in El Paso on two dates (June 4 and June 28) that were shown to have significant fire impacts on O₃ in McDonald-Buller et al. (2015). STILT-ASP v2.0 somewhat overestimated the amount of O₃ relative to measurements on June 5 (MB = +16 ppb, RMSE = 16 ppbv) and strongly underestimated the NO_x concentration (MB = -4.4 ppbv, RMSE = 5.2 ppbv). The performance on June 28 was similar with O₃ overestimated (MB = +20 ppb, RMSE = 21 ppbv) and NO_x underestimated (MB = -4.3 ppbv, RMSE = 4.8 ppbv).

In addition, the QAPP listed the following assessment questions for Task 2:

- *What is the impact on CAMx simulations of Texas and North American air quality of perturbing boundary concentrations impacted by BB by ~20%? Is this simulated impact consistent with the scientific literature?*

We did not evaluate the impact of a 20% perturbation in the CAMx boundary conditions on Texas air quality in this project, as our evaluation of the CAMx boundary conditions from GEOS-Chem with the STILT-ASP model suggested that the difference between the STILT-ASP v2.0 calculation of fire impacts and the GEOS-Chem derived boundary conditions was so large that such a sensitivity study was unlikely to correctly represent the sensitivity of Texas air quality to remote fires (Section 0).

- *How does the “Lagrangian” estimate of the impact of fires on the boundary conditions for CO, O₃, NO_y species, OA, etc., from STILT-ASP differ from the “Eulerian” estimate from GEOS-Chem? Is this difference consistent with our understanding of the impact of numerical diffusion on the transport of biomass burning plumes in Eulerian models?*

As discussed above, the STILT-ASP v2.0 runs along the southern CAMx boundary gave significantly higher CO than the GEOS-Chem boundary conditions, consistent with the high CO bias in STILT-ASP v2.0 observed in Alvarado et al. (2017), but may also be due to differences in the fire emission inventories used. The STILT-ASP v2.0 prediction of O₃ was also high relative to GEOS-Chem, which appears to be due to an error in the simulation of the diurnal cycle of O₃, especially at night. However, the predicted impact of fires on O₃ relative to CO is consistent with the scientific literature. Predictions of NO_x and PAN were both much lower than the GEOS-Chem values, and this appears to be due to the chemistry of S/IVOCs used in ASP v2.1, which were derived from measurements of a biomass burning plume for the first 0 to 5 hours of aging. Thus the chemical mechanism of ASP v2.1 may need to be re-examined for the longer runs of STILT-ASP v2.0.

- *How consistent are the CAMx (Eulerian) and STILT-ASP (Lagrangian) estimated impacts of remote North American biomass burning on Texas air quality? Is this difference consistent with our understanding of the impact of numerical diffusion on the transport of biomass burning plumes in Eulerian models?*

In order to compare the STILT-ASP v2.0 predictions of the impacts of wildfires on O₃ and PM_{2.5} with the CAMx simulations of McDonald-Buller et al. (2015), we ran STILT-ASP for the CAMS 12 site in El Paso on two dates (June 4 and June 28) that were shown to have significant fire impacts on O₃ in McDonald-Buller et al. (2015). However, the STILT-ASP v2.0 estimates of the impacts of fires on CO were small (2-3 ppbv), likely due to the use of the FINN v1.5 emissions rather than the FINN v2.1 emissions used by McDonald-Buller et al. (2015). Furthermore, the STILT-ASP v2.0 estimate of the impact of fires on MDA8 O₃ on these days is small and negative (-0.1 to -0.4 ppbv), unlike the small but positive impacts predicted by CAMx with the biomass burning parameterization (2.1 and 1.2 ppbv), but this may be due to errors in the S/IVOC chemistry as discussed above.

5 Conclusions

Here we summarize the conclusions of our project, with reference to the corresponding report section.

- The revised SAM-ASP model is able to correctly simulate the dilution of CO in the Williams Fire smoke plume, as well as the chemical loss of NO_x, HONO, NH₃ and chemical formation of PAN within the plume. The formation of O₃ in the model is underestimated (model value of $\Delta O_3/\Delta CO$ of 0.05 mol/mol at 4.5 hr downwind, rather than the measured value of 0.10 mol/mol). Thus we conclude that SAM-ASP does a reasonable job of simulating CO, HONO, PAN, and NO_x within biomass burning plumes, but currently underestimates the formation of O₃ (Section 2.2)
- We ran the coupled SAM-ASP model for 100 simulations per fire fuel type and developed a Gaussian Emulator Machine (GEM) to predict the NMER of O₃, NO_x, PAN, and other species in terms of the fuel type, temperature, latitude, day of year, and starting hour of emission. However, our evaluation of the GEM parameterization showed it is not of sufficient quality for use in regional air quality modeling (Section 2.4). While the GEM parameterization is able to represent the dependence of O₃ formation in the plume on fuel type, temperature, day of year, and latitude reasonably well, the dependence on time of day is unrealistic. The GEM predictions for NO_x and other NO_y species have more serious deficiencies, with the GEM parameterization overestimating the NO_x downwind in the Williams Fire relative to both observations and SAM-ASP simulations, and GEM predictions of the formation of PAN and HNO₃ being inconsistent with the GEM predictions of the loss rate of NO_x. Thus, for now we recommend using the parameterization of Lonsdale et al. (2015) in CAMx instead (Section 2.5).
- We implemented the Lonsdale et al. (2015) into CAMx via the PiG module. The parameterization reduced the predicted impacts of fires on O₃ near the sources by ~30%, as expected (Section 2.6).
- The STILT-ASP v2.0 simulations show a lot of fine structure in the impacts of fires on CO along the southern boundary of the TCEQ CAMx modeling domain that is not captured by the boundary conditions from GEOS-Chem. In addition, the STILT-ASP v2.0 estimate of the $\Delta O_3/\Delta CO$ ratio during these events (mean of 0.15 mol/mol) is consistent with the review of Jaffe and Wigder (2012), which found that the average $\Delta O_3/\Delta CO$ for smoke aged about 1-2 days was 0.2 ± 0.1 mol/mol. However, the STILT-ASP v2.0 prediction of O₃ was high relative to GEOS-Chem, which appears to be due to an error in the simulation of the diurnal cycle of O₃, especially at night. Predictions of NO_x and PAN were both much lower than the GEOS-Chem values, and this appears to be due to the chemistry of S/IVOCs used in ASP v2.1. Thus the S/IVOC chemical mechanism of ASP v2.1 may need to be re-examined for the longer one to seven day runs of STILT-ASP v2.0 (Section 0).
- We used STILT-ASP v2.0 to examine the impact of fires on CO, O₃, NO_x, and PM_{2.5} during three days where the Austin/Round Rock urban area was impacted by fires from Central Mexico and the Yucatan. On the day with the highest MDA8 O₃ (May 11), the model predictions of O₃, CO, and NO_x were all consistent with the observations, with O₃ slightly overestimated (MB of +3.6 ppbv, RMSE of 5.9 ppbv) and NO_x slightly overestimated (MB of +0.3 ppbv, RMSE of 1.9 ppbv). However, due to the loss of NO_x

during S/IVOC oxidation, the impact of fire emissions was a decrease of -0.9 ppbv of the MDA8 O₃ (Section 3.3). However, the STILT-ASP v2.0 results for May 5 and May 25 Austin cases were very different, with STILT-ASP v2.0 strongly overestimating O₃ (MB = +40 ppbv) and underestimating NO_x (MB = -2.6 ppbv) on these days, but with less severe overestimates of PM_{2.5}. The model suggests that fires had small but positive impacts on MDA8 O₃ on these days (0.2 and 0.3 ppbv, respectively, Section 3.3).

- PM_{2.5} was generally overestimated by STILT-ASP v2.0, likely due to an underestimate of aerosol deposition (Section 3.3). However, the model results can be used to estimate the relative fraction of PM_{2.5} at the receptor that is due to fires. Fires had noticeable impacts on PM_{2.5} on all three of the Austin days (0.9 µg/m³ on May 11, 2.6 µg/m³ on May 5, and 4.0 µg/m³ on May 25, Section 3.3).
- In order to compare the STILT-ASP v2.0 predictions of the impacts of wildfires on O₃ and PM_{2.5} with the CAMx simulations of McDonald-Buller et al. (2015), we ran STILT-ASP for the CAMS 12 site in El Paso on two dates (June 4 and June 28) that were shown to have significant fire impacts on O₃ in McDonald-Buller et al. (2015). However, the STILT-ASP v2.0 estimates of the impacts of fires on CO were small (2-3 ppbv), likely due to the use of the FINN v1.5 emissions rather than the FINN v2.1 emissions used by McDonald-Buller et al. (2015). Furthermore, the STILT-ASP v2.0 estimate of the impact of fires on MDA8 O₃ on these days is small and negative (-0.1 to -0.4 ppbv), unlike the small but positive impacts predicted by CAMx with the biomass burning parameterization (2.1 and 1.2 ppbv), but this may be due to errors in the S/IVOC chemistry as discussed above (Section 3.4).

6 Recommendations for Further Study

We recommend that future work on assessing the impact of wildfires on air quality in Texas focus on:

- *Continued Development of SAM-ASP*
 - Evaluation and improvement of the coupled SAM-ASP model using data from the upcoming NOAA FIREX campaign. (Note we already plan to perform this work in the future as part of our NOAA-funded FIREX projects.)
 - Explore ways to parallelize and otherwise reduce the computation time of the model, thus allowing more cases to be run.
 - Integrating the TUV or FAST-JX photolysis models into SAM-ASP to improve the simulation of photolysis rates in the model, including interactions with biomass burning aerosols.
- *Exploring Novel Parameterization Approaches*
 - Further refinement of the implementation of the Lonsdale et al. (2015) parameterization within CAMx, including better approaches to account for plume rise and diurnal distribution of FINN emissions, and accounting for the loss of VOCs due to sub-grid scale chemistry.
 - Explore ways of revising the GEM training approach to enforce the conservation of NO_y species and improve the performance for periodic variables.
 - Using different numerical and machine learning methods (e.g., generalized additive models, Random Forest methods) to develop a physically realistic parameterization from a small number of SAM-ASP runs.
 - Adding the effects of fire size, fire radiative power, etc., as input variables for the parameterization.
- *Continued Development of STILT-ASP*
 - Revision of the chemical mechanism of ASP v2.1 to better represent the long-term (1-7 day) chemistry of S/IVOCs and their impacts on NO_x.
 - Adjusting the deposition rate of aerosols within STILT-ASP v2.0 to better reflect ambient observations.
 - Using WRF cloud fields and the TUV or FAST-JX photolysis models into STILT-ASP to calculate photolysis rates, instead of the current approximate RH-profile based approach.
 - Exploring the impact of including grid-scale mixing between Lagrangian parcels on model results and determining appropriate mixing timescales.
 - Exploring methods to improve the speed of the STILT-ASP model through code parallelization and other techniques. This would both make the tool easier to use and would allow more sensitivity cases to be evaluated, allowing improvements to the model to be tested more quickly than is currently possible.

7 References

- Akagi, S. K., R. J. Yokelson, C. Wiedinmyer, M. J. Alvarado, J. S. Reid, T. Karl, J. D. Crouse, and P. O. Wennberg (2011), Emission factors for open and domestic biomass burning for use in atmospheric models, *Atmos. Chem. Phys.*, 11, 4039–4072, doi:10.5194/acp-11-4039-2011.
- Akagi, S. K., J. S. Craven, J. W. Taylor, G. R. McMeeking, R. J. Yokelson, I. R. Burling, S. P. Urbanski, C. E. Wold, J. H. Seinfeld, H. Coe, M. J. Alvarado, and D. R. Weise (2012), Evolution of trace gases and particles emitted by a chaparral fire in California, *Atmos. Chem. Phys.*, 12, 1397–1421, doi:10.5194/acp-12-1397-2012.
- Alvarado, M. J., and R. G. Prinn (2009), Formation of ozone and growth of aerosols in young smoke plumes from biomass burning, Part 1: Lagrangian parcel studies, *J. Geophys. Res.*, 114, D09306, doi:10.1029/2008JD011144.
- Alvarado, M. J., C. Wang, and R. G. Prinn (2009), Formation of ozone and growth of aerosols in young smoke plumes from biomass burning, Part 2: 3D Eulerian studies, *J. Geophys. Res.*, 114, D09307, doi:10.1029/2008JD011186.
- Alvarado, M. J., J. A. Logan, J. Mao, *et al.* (2010), Nitrogen oxides and PAN in plumes from boreal fires during ARCTAS-B and their impact on ozone: an integrated analysis of aircraft and satellite observations, *Atmos. Chem. Phys.*, 10, 9739–9760, doi:10.5194/acp-10-9739-2010.
- Alvarado, M. J., C. R. Lonsdale, R. J. Yokelson, S. K. Akagi, H. Coe, J. S. Craven, E. V. Fischer, G. R. McMeeking, J. H. Seinfeld, T. Soni, J. W. Taylor, D. R. Weise, and C. E. Wold (2015), Investigating the Links Between Ozone and Organic Aerosol Chemistry in a Biomass Burning Plume from a Prescribed Fire in California Chaparral, *Atmos. Chem. Phys.*, 15, 6667–6688, doi:10.5194/acp-15-6667-2015.
- Alvarado, M. J., C. M. Brodowski, and C. R. Lonsdale (2016), *An Analysis of Biomass Burning Impacts on Texas*, Final Report to Texas Commission on Environmental Quality (TCEQ) for Work Order No. 582-16-62311-03 under TCEQ Contract No. No. 582-15-50414, June 30.
- Alvarado, M. J., C. M. Brodowski, and J. D. Hegarty (2017), *STILT-ASP Model Performance Improvement Using DISCOVER-AQ Data*, Final Report to Texas Commission on Environmental Quality (TCEQ) for Work Order No. 582-17-71989-06 under TCEQ Contract No. No. 582-15-50414, June 30.
- Andreae, M. O., and P. Merlet (2001), Emission of trace gases and aerosols from biomass burning, *Global Biogeochem. Cycles*, 15, 955–966, doi:10.1029/2000GB001382.
- Baker, K. (2015), Simulating Fire Event Impacts on Regional O₃ and PM_{2.5} and Looking Forward toward Evaluation, presented at the 14 annual CMAS conference, UNC-Chapel Hill, 5-7 October.
- Goliff, W. S., W. R. Stockwell, and C. V. Lawson (2013), The regional atmospheric chemistry mechanism, version 2, *Atmos. Environ.*, 68, 174–185.

- Guenther, A., T. Karl, P. Harley, C. Wiedinmyer, P. I. Palmer, and C. Geron (2006), Estimates of global terrestrial isoprene emissions using MEGAN (Model of Emissions of Gases and Aerosols from Nature), *Atmos. Chem. Phys.*, 3181–3210, doi:10.5194/acp-6-3181-2006.
- Hegarty, J., R. R. Draxler, A. F. Stein, J. Brioude, M. Mountain, J. Eluszkiewicz, T. Nehr Korn, F. Ngan, and A. Andrews (2013), Evaluation of Lagrangian particle dispersion models with measurements from controlled tracer releases. *J. Appl. Meteor. Climatol.*, 52, 2623–2637, doi: 10.1175/JAMC-D-13-0125.1.
- Henderson, J. M., J. Eluszkiewicz, M. E. Mountain, T. Nehr Korn, R. Y.-W. Chang, A. Karion, J. B. Miller, C. Sweeney, N. Steiner, S. C. Wofsy, and C. E. Miller (2015), Atmospheric transport simulations in support of the Carbon in Arctic Reservoirs Vulnerability Experiment (CARVE), *Atmos. Chem. Phys.*, 15, 4093–4116, doi:10.5194/acp-15-4093-2015.
- Jacob, D. J. (2000), Heterogeneous chemistry and tropospheric ozone, *Atmos. Environ.*, 34, 2131–2159.
- Jacobson, M. Z. (2005), *Fundamentals of Atmospheric Modeling*, 2nd ed., Cambridge University Press, 2005.
- Jaffe, D. A., and N. L. Wigder (2012), Ozone production from wildfires: A critical review, *Atmos. Environ.*, 51, 1–10.
- Jenkin, M. E., S. M. Saunders, V. Wagner, and M. J. Pilling (2003), Protocol for the development of the Master Chemical Mechanism, MCM v3 (Part B): tropospheric degradation of aromatic volatile organic compounds, *Atmos. Chem. Phys.*, 3, 181–193, doi:10.5194/acp-3-181-2003.
- Karamchandani, P., K. Vijayaraghavan, and G. Yarwood (2011), Sub-grid scale plume modeling, *Atmosphere*, 2, 389–406, doi:10.3390:atmos2030389.
- Khairoutdinov, M. F., and D. A. Randall (2003), Cloud resolving modeling of the ARM summer 1997 IOP: Model formulation, results, uncertainties, and sensitivities, *J. Atmos. Sci.*, 60, 607–625.
- Lin, J. C., C. Gerbig, S. C. Wofsy, A. E. Andrews, B. C. Daube, K. J. Davis, and C. A. Grainger (2003), A near-field tool for simulating the upstream influence of atmospheric observations: the Stochastic Time-inverted Lagrangian Transport (STILT) model, *J. Geophys. Res.*, 108, 4493, doi:10.1029/2002JD003161.
- Lonsdale, C. R., R. G. Stevens, C. A. Brock, P. A. Makar, E. M. Knipping, and J. R. Pierce (2012), The effect of coal-fired power-plant SO₂ and NO_x control technologies on aerosol nucleation in the source plumes, *Atmos. Chem. Phys.*, 12, 11519–11531 doi:10.5194/acp-12-11519-2012.
- Lonsdale, C. R., Alvarado, M. J., R. J. Yokelson, K. R. Travis, and E. V. Fischer (2014), A sub-grid scale parameterization of biomass burning plume chemistry for global and regional air quality models, presented at the 2014 Community Modeling and Analysis System (CMAS) Conference, Chapel Hill, NC, 27-29 Oct.
- Lonsdale, C. R., M. J. Alvarado, R. J. Yokelson, S. K. Akagi, E. Fischer, K. Travis, T. Soni, J. S. Craven, J. W. Taylor, G. R. McMeeking, I. R. Burling, S. P. Urbanski, C. E. Wold, J. H. Seinfeld, H. Coe, and D. R. Weise (2015), Using the Aerosol Simulation Program to

- parameterize biomass-burning plumes for global air quality models, American Association for Aerosol Research, Minneapolis, MN, October 12-16.
- Lonsdale, C. R., C. Brodowski, M. Alvarado, J. Henderson, J. R. Pierce, and J. Lin (2016), Regional Modeling of Biomass-Burning Aerosol Impacts, Abstract GC51E-1225, presented at the 2016 AGU Fall Meeting, San Francisco, CA, Dec. 12-16.
- McDonald-Buller, E., Y. Kimura, C. Wiedinmyer, C. Emery, Z. Liu, and G. Yarwood (2015), *Targeted Improvements in the Fire Inventory from NCAR (FINN) Model for Texas Air Quality Planning*, Final Report to Texas Air Quality Research Program (AQR) for Project 14-011, December 2015.
- McKain, K., S. C. Wofsy, T. Nehr Korn, J. Eluszkiewicz, J. R. Ehleringer, and B. B. Stephens (2012), Assessment of ground-based atmospheric observations for verification of greenhouse gas emissions from an urban region, *PNAS*, 109, 8423–8428.
- McKain, K., A. Down, S. M. Raciti, J. Budney, L. R. Hutyr, C. Floerchinger, S. C. Herndon, T. Nehr Korn, M. S. Zahniser, R. B. Jackson, N. Phillips, and S. C. Wofsy (2015), Methane emissions from natural gas infrastructure and use in the urban region of Boston, Massachusetts, *PNAS*, 112, 1941–1946.
- Mesinger, F., G. DiMego, E. Kalnay, K. Mitchell, P. C. Shafran, W. Ebisuzaki, D. Jović, J. Woollen, E. Rogers, E. H. Berbery, and M. B. Ek (2006), North American regional reanalysis, *Bull. Am. Meteorol. Soc.*, 87, 343–360.
- Nehr Korn, T., J. Eluszkiewicz, S. C. Wofsy, J. C. Lin, C. Gerbig, M. Longo, and S. Freitas (2010), Coupled weather research and forecasting–stochastic time-inverted lagrangian transport (WRF–STILT) model, *Meteorol. Atmos. Phys.*, 107, 51–64, doi: 10.1007/s00703-010-0068-x.
- O'Hagan, A. (2006), Bayesian analysis of computer code outputs: a tutorial, *Reliability Engineering and System Safety*, 91, 1290–1300.
- Rastigejev, Y., R. Park, M. P. Brenner, and D. J. Jacob (2010), Resolving intercontinental pollution plumes in global models of atmospheric transport, *J. Geophys. Res.*, 115, D02302, doi:[10.1029/2009JD012568](https://doi.org/10.1029/2009JD012568).
- Robinson, A. L., N. M. Donahue, M. K. Shrivastava, E. A. Weitkamp, A. M. Sage, A. P. Grieshop, T. E. Lane, J. R. Pierce, and S. N. Pandis (2007), Rethinking organic aerosols: semivolatile emissions and photochemical aging, *Science*, 315, 1259–1262.
- Sakamoto, K. M., J. D. Allan, H. Coe, J. W. Taylor, T. J. Duck, and J. R. Pierce (2015), Aged boreal biomass burning aerosol size distributions from BORTAS 2011, *Atmos. Chem. Phys.*, 15, 1633–1646, doi:10.5194/acp-15-1633-2015.
- Sakamoto, K. M., Laing, J. R., Stevens, R. G., Jaffe, D. A., and Pierce, J. R.: The evolution of biomass-burning aerosol size distributions due to coagulation: dependence on fire and meteorological details and parameterization, *Atmos. Chem. Phys.*, 16, 7709–7724, <https://doi.org/10.5194/acp-16-7709-2016>, 2016.
- Stevens, R. G., J. R. Pierce, C. A. Brock, M. K. Reed, J. H. Crawford, J. S. Holloway, T. B. Ryerson, L. G. Huey, and J. B. Nowak (2012), Nucleation and growth of sulfate aerosol in coal-fired power plant plumes: sensitivity to background aerosol and meteorology, *Atmos. Chem. Phys.*, 12, 189–206.

- van der Werf, G. R., J. T. Randerson, L. Giglio, G. J. Collatz, M. Mu, P. S. Kasibhatla, D. C. Morton, R. S. DeFries, Y. Jin, and T. T. van Leeuwen (2010), Global fire emissions and the contribution of deforestation, savanna, forest, agricultural, and peat fires (1997–2009), *Atmos. Chem. Phys.*, 10, 11707–11735, doi:10.5194/acp-10-11707-2010.
- Vinken, G. C. M., K. F. Boersma, D. J. Jacob, and E. W. Meijer (2011), Accounting for non-linear chemistry of ship plumes in the GEOS-Chem global chemistry transport model, *Atmos. Chem. Phys.*, 11, 11707–11722, doi:10.5194/acp-11-11707-2011.
- Wen, D., J. C. Lin, L. Zhang, R. Vet, and M. D. Moran (2013), Modeling atmospheric ammonia and ammonium using a stochastic Lagrangian air quality model (STILT-Chem v0.7), *Geosci. Model Dev.*, 6, 327–344, doi:10.5194/gmd-6-327-2013.
- Wen, D., L. Zhang, J. C. Lin, R. Vet, and M. D. Moran (2014), An evaluation of ambient ammonia concentrations over southern Ontario simulated with different dry deposition schemes within STILT-Chem v0.8, *Geosci. Model Dev.*, 7, 1037–1050, doi:10.5194/gmd-7-1037-2014.
- Wiedinmyer, C., S. K. Akagi, R. J. Yokelson, L. K. Emmons, J. A. Al-Saadi, J. J. Orlando, and A. J. Soja (2011), The Fire Inventory from NCAR (FINN), A high resolution global model to estimate the emissions from open burning, *Geosci. Model Dev.*, 4, 625–641.